THE EUROPEAN
PHYSICAL JOURNAL C

Rare top-quark decays $t \rightarrow cg(g)$ in the aligned two-Higgs-doublet model

Fang-Min Cai[1,a], Shuichiro Funatsu[1,b], Xin-Qiang Li[1,c], Ya-Dong Yang[2,d]

[1] Institute of Particle Physics and Key Laboratory of Quark and Lepton Physics (MOE), Central China Normal University, Wuhan 430079, Hubei, China

[2] School of Physics and Microelectronics, Zhengzhou University, Zhengzhou 450001, Henan, China

Abstract We update the Standard Model (SM) predictions for the branching ratios of the rare top-quark decays $t \rightarrow cg(g)$, and evaluate the maximum rates that can be reached in the aligned as well as in the four conventional two-Higgs-doublet models (2HDMs) with $\mathcal{Z}_2$ symmetries. Taking into account the relevant constraints on the model parameters resulting from a global fit obtained at the 95.5% confidence level, we find that the branching ratios of $t \rightarrow cg$ and $t \rightarrow cgg$ decays can reach up to 3.36×10^{-9} and 2.95×10^{-9} respectively, being therefore of the same order, in the aligned 2HDM (A2HDM). This is obviously different from the SM case, where the predicted branching ratio of the three-body decay $t \rightarrow cgg$ is about two orders of magnitude larger than that of the two-body decay $t \rightarrow cg$. On the other hand, compared with the SM predictions, no significant enhancements are observed in the four conventional 2HDMs with $\mathcal{Z}_2$ symmetries for the branching ratios of these two decays. Nevertheless, the predicted branching ratios of $t \rightarrow cg$ and $t \rightarrow cgg$ decays in the A2HDM are still out of the expected sensitivities of the future high-luminosity Large Hadron Collider and the Future Circular Collider in hadron-hadron mode.

Contents

[a] e-mail: caifangmin@mails.ccnu.edu.cn

[b] e-mail: funatsu@mail.ccnu.edu.cn

[c] e-mail: xqli@mail.ccnu.edu.cn (corresponding author)

[d] e-mail: yangyd@mail.ccnu.edu.cn

1 Introduction

The top quark, as the heaviest elementary particle in the Standard Model (SM), can decay into other light quarks associated with gauge or scalar bosons. Among all the possible decay modes, the flavour-changing neutral-current (FCNC) decays of the top quark, which are absent at tree level and suppressed at loop level by the Glashow–Iliopoulos–Maiani (GIM) mechanism [1] in the SM, are very sensitive to contributions from new physics (NP) [2–36]. For the two-body FCNC top-quark decays $t \rightarrow qV$ and $t \rightarrow qh$, with $q = c, u$, $V = \gamma, Z, g$, and h the SM Higgs, their branching ratios are predicted to be of the orders of 10^{-17} to 10^{-12} within the SM, but could be enhanced by several orders of magnitude in many NP scenarios (see, e.g., Refs. [35,36] and references therein). Among the three-body loop-induced top-quark decays $t \rightarrow cVV$ and $t \rightarrow u_1\bar{u}_2u_2$ with $u_i = u, c$, the decay $t \rightarrow cgg$ has the largest branching ratio, reaching up to about 1.02×10^{-9} within the SM [37–39]. Interestingly, it is found that the branching ratio of the three-body

Springer

decay $t \to cgg$ is about two orders of magnitude larger than that of the two-body decay $t \to cg$ within the SM [39], a phenomenon that will be dubbed "higher-order dominance" and has also been revealed in the bottom- and charm-quark decays [40–46]. Although their SM rates are predicted to be far below the detectable level of present and future colliders, these rare FCNC top-quark decays have been widely studied in various NP models, and significant enhancements are observed relative to the SM expectations; the most prominent examples are the two-Higgs-doublet model (2HDM) [2–14] and the supersymmetry [15–25], within which these rare top-quark decays might be even detectable at the future colliders. Especially, it is interesting to check if the "higher-order dominance" phenomenon observed in $t \to cg(g)$ decays within the SM [39] is still valid for a viable NP model.

Among the various NP scenarios, the 2HDM [47] provides a minimal extension of the SM scalar sector by adding a second scalar doublet with hypercharge $Y = 1/2$, and can naturally satisfy the electroweak precision tests, giving rise at the same time to a very rich phenomenology [48,49]. In a generic 2HDM, the non-diagonal couplings of the neutral scalars to the SM fermions would unavoidably lead to non-vanishing tree-level FCNC interactions. To avoid these unwanted tree-level FCNC couplings, an *ad-hoc* discrete $\mathcal{Z}_2$ symmetry is often imposed on the Yukawa sector of the model [50]. Depending on the $\mathcal{Z}_2$ charge assignments to the scalars and fermions, this results in four types of 2HDMs (types I, II, X, Y) [48,49] under the hypothesis of natural flavour conservation [50]. In the aligned 2HDM (A2HDM) [51], on the other hand, the absence of tree-level FCNC interactions is automatically guaranteed by assuming the alignment in flavour space of the two Yukawa matrices for each type of the right-handed fermions. Interestingly, the A2HDM can recover, as particular cases, all the known specific implementations of the conventional 2HDMs based on $\mathcal{Z}_2$ symmetries. The model is also featured by possible new sources of CP violation beyond that of the Cabibbo–Kobayashi–Maskawa (CKM) quark-mixing matrix [52,53]. Thus, the A2HDM has been widely studied from the various theoretical points of view [54–59], as well as for its phenomenologies in the low-energy flavour physics [60–75], the electric dipole moments of the leptons, the neutron and various atoms [76–79], the anomalous magnetic moment of the muon [80–85], and the high-energy collider physics [12,86–101]. Recently, assuming that there are no new sources of CP violation beyond the CKM quark-mixing matrix, and taking into account the most constraining processes and observables mentioned above, together with the theoretical requirements of perturbativity and positivity of the scalar potential, a detailed global fit has been performed to the A2HDM [75].

In this paper, we shall perform a detailed study of the rare top-quark decay $t \to cgg$ and its comparison with the two-body decay $t \to cg$ in the A2HDM as well as in the four conventional 2HDMs with $\mathcal{Z}_2$ symmetries. Taking into account the relevant constraints on the model parameters from a global fit obtained at the 95.5% confidence level (CL) [75], we find that the branching ratios of $t \to cg$ and $t \to cgg$ decays can reach up to 3.36×10^{-9} and 2.95×10^{-9} respectively, being therefore of the same order, in the A2HDM. This is obviously different from the SM case, where the predicted branching ratio of $t \to cgg$ is about two orders of magnitude larger than that of $t \to cg$ [39]. On the other hand, compared with the SM predictions, no significant enhancements are observed in the four conventional 2HDMs with $\mathcal{Z}_2$ symmetries for the branching ratios of these two decays. Searches for the decay $t \to cg$ have been performed at the Large Hadron Collider (LHC), with the upper limit on its branching ratio being of $\mathcal{O}(10^{-4})$ [102,103], which is still much higher than the model predictions. These rare FCNC decays will also be studied at the future experiments, such as the high-luminosity LHC (HL-LHC) [104–108] and the Future Circular Collider (FCC) [109–112]. For example, the 95%-CL limit on the branching ratio of $t \to cg$ at the 100-TeV FCC in hadron-hadron mode (FCC-hh) with an integrated luminosity of 10 ab^{-1} is estimated to be of $\mathcal{O}(10^{-7}–10^{-8})$ [113,114], which is at least one order of magnitude higher than the maximum value predicted in the A2HDM. As a consequence, the predicted branching ratios of $t \to cg$ and $t \to cgg$ decays in the A2HDM are still out of the expected sensitivities of the future HL-LHC and FCC-hh.

This paper is organized as follows. In Sect. 2, we recapitulate the A2HDM, focusing only on the scalar and Yukawa sectors that are most relevant to us. In Sect. 3, we present our calculation of the decay rates of $t \to cg(g)$ decays, with the resulting R functions present in the $t \to cgg$ decay supplemented in Appendix A. Our numerical results are then given in Sect. 4, where we show the maximum branching ratios of $t \to cg(g)$ decays that can be reached in the A2HDM, and give also a simple analysis of these two decays in the four conventional 2HDMs with $\mathcal{Z}_2$ symmetries. Our conclusion is finally made in Sect. 5.

2 Aligned two-Higgs-doublet model

As a simple extension of the SM, the 2HDM is invariant under the SM gauge group and includes, besides the SM matter and gauge fields, two complex scalar $SU(2)_L$ doublets,

$$\phi_a = e^{i\theta_a} \left[\begin{array}{c} \phi_a^+ \\ \frac{1}{\sqrt{2}} (v_a + \rho_a + i\eta_a) \end{array} \right], \tag{2.1}$$

with the weak hypercharge $Y = 1/2$. Here we have assumed that the vacuum of the theory respects the electromagnetic gauge symmetry, which guarantees the vacuum expectation values (vevs) of the two scalar fields ϕ_a to be aligned in the

$SU(2)_L$ space. After performing further a global $SU(2)_L$ transformation to put the non-zero vevs only in the lower (neutral) components of ϕ_a, which guarantees the vacuum to be neutral and not charge-breaking, we can bring the vevs of the two scalar fields to the forms given by $\langle 0|\phi_a^T(x)|0\rangle = (0, v_a e^{i\theta_a}/\sqrt{2})$, where v_1 and v_2 are real and non-negative [115,116]. However, as one global phase can always be rotated away through an appropriate $U(1)_Y$ transformation, we can, without loss of generality, fix $\theta_1 = 0$ and leave the relative phase $\theta = \theta_2 - \theta_1$ [51,115,116].

Performing further a global $SU(2)$ transformation in the scalar space (ϕ_1, ϕ_2), we can rotate the original scalar basis to the so-called Higgs basis [116–119],

$$\begin{pmatrix} \Phi_1 \\ -\Phi_2 \end{pmatrix} \equiv \begin{pmatrix} \cos\beta & \sin\beta \\ \sin\beta & -\cos\beta \end{pmatrix} \begin{pmatrix} \phi_1 \\ e^{-i\theta}\phi_2 \end{pmatrix}, \qquad (2.2)$$

where the rotation angle β is defined by the ratio of the absolute values of the two neutral scalar field vevs, $\tan\beta \equiv \frac{|\langle 0|\phi_2^0|0\rangle|}{|\langle 0|\phi_1^0|0\rangle|} = \frac{v_2}{v_1}$, and, by convention, its value is limited to the first quadrant due to $v_1, v_2 \geq 0$. In fact, both $\tan\beta$ and the relative phase θ are basis-dependent, and we can remove them entirely by transforming from a generic basis (ϕ_1, ϕ_2) to the Higgs basis (Φ_1, Φ_2) [116–119]. The true significance of $\tan\beta$ emerges only in specialized versions of the 2HDM, such as the four conventional 2HDMs with $\mathcal{Z}_2$ symmetries, where $\tan\beta$ is promoted to a physical parameter. In this case, we can remove the relative phase θ by making a phase rotation $\phi_2 \rightarrow e^{-i\theta}\phi_2$, such that the two neutral scalar vevs are real and the CP invariance is not spontaneously broken [116–119]. In the Higgs basis, only the scalar doublet Φ_1 gets a non-zero vev, $\langle 0|\Phi_1^T(x)|0\rangle = (0, v/\sqrt{2})$, with $v = \sqrt{v_1^2 + v_2^2} = 1/\sqrt{\sqrt{2}G_F} \simeq 246.22$ GeV, and plays the role of the SM Higgs doublet. The two scalar doublets in the Higgs basis can now be parametrized, respectively, as [51]

$$\Phi_1 = \begin{bmatrix} G^+ \\ \frac{1}{\sqrt{2}}(v + S_1 + i G^0) \end{bmatrix},$$

$$\Phi_2 = \begin{bmatrix} H^+ \\ \frac{1}{\sqrt{2}}(S_2 + i S_3) \end{bmatrix}, \qquad (2.3)$$

where $G^\pm$ and G^0 denote the electroweak Goldstone fields, and the remaining five physical degrees of freedom are given by the two charged fields $H^\pm(x)$ and the three neutral ones $\varphi_i^0(x) = \{h(x), H(x), A(x)\} = \mathcal{R}_{ij}S_j$, where $\mathcal{R}$ is the orthogonal matrix needed for diagonalizing the mass terms in the scalar potential [92]. Generally, none of these three neutral scalars can have a definite CP quantum number. Here, for simplicity, we shall assume a CP-conserving Higgs sector, as will be detailed in the next two subsections.

2.1 Scalar sector

In the Higgs basis, the most general scalar potential allowed by the electroweak gauge symmetry $SU(2)_L \otimes U(1)_Y$ takes the form [116–118]:

$$\begin{aligned} V = {} & \mu_1 \left(\Phi_1^\dagger\Phi_1\right) + \mu_2 \left(\Phi_2^\dagger\Phi_2\right) + \left[\mu_3 \left(\Phi_1^\dagger\Phi_2\right)\right. \\ & + \mu_3^* \left(\Phi_2^\dagger\Phi_1\right)\right] \\ & + \lambda_1 \left(\Phi_1^\dagger\Phi_1\right)^2 + \lambda_2 \left(\Phi_2^\dagger\Phi_2\right)^2 \\ & + \lambda_3 \left(\Phi_1^\dagger\Phi_1\right)\left(\Phi_2^\dagger\Phi_2\right) + \lambda_4 \left(\Phi_1^\dagger\Phi_2\right)\left(\Phi_2^\dagger\Phi_1\right) \\ & + \left[\left(\lambda_5 \Phi_1^\dagger\Phi_2 + \lambda_6 \Phi_1^\dagger\Phi_1 + \lambda_7 \Phi_2^\dagger\Phi_2\right)\right. \\ & \times \left.\left(\Phi_1^\dagger\Phi_2\right) + \text{h.c.}\right]. \end{aligned} \qquad (2.4)$$

Due to Hermiticity of the scalar potential, the parameters $\mu_{1,2}$ and $\lambda_{1,2,3,4}$ are real, while μ_3 and $\lambda_{5,6,7}$ could be generally complex. The minimization condition of the scalar potential imposes the relations

$$\mu_1 = -\lambda_1 v^2, \quad \mu_3 = -\frac{1}{2}\lambda_6 v^2. \qquad (2.5)$$

Inserting Eq. (2.3) into Eq. (2.4) and imposing the minimization condition given by Eq. (2.5), we can get the charged-Higgs mass

$$m_{H^\pm}^2 = \mu_2 + \frac{1}{2}\lambda_3 v^2, \qquad (2.6)$$

while the masses of the three neutral scalars can be obtained after diagonalizing the mass-squared matrix $\mathcal{M}$ of the three neutral-scalar fields $S_{1,2,3}$ by the orthogonal matrix $\mathcal{R}$, i.e., $\text{diag}\left(m_h^2, m_H^2, m_A^2\right) = \mathcal{R}\mathcal{M}\mathcal{R}^T$ [92]. In the CP-conserving limit of the scalar potential, the parameters $\lambda_{5,6,7}$ are all real and the three neutral scalars h, H, and A are therefore CP eigenstates. In this case, the CP-odd scalar A corresponds to the field S_3, while the two CP-even scalars h and H are the orthogonal combinations of S_1 and S_2:

$$\begin{pmatrix} h \\ H \end{pmatrix} = \begin{pmatrix} \cos\tilde\alpha & \sin\tilde\alpha \\ -\sin\tilde\alpha & \cos\tilde\alpha \end{pmatrix} \begin{pmatrix} S_1 \\ S_2 \end{pmatrix}, \qquad (2.7)$$

where the mixing angle $\tilde\alpha$ is determined by

$$\tan\tilde\alpha = \frac{m_h^2 - 2\lambda_1 v^2}{v^2\lambda_6} = \frac{v^2\lambda_6}{2\lambda_1 v^2 - m_H^2}. \qquad (2.8)$$

Note that one can always restrict $\tilde\alpha$ within the range $0 \leqslant \tilde\alpha < \pi$ by performing a phase redefinition of the two CP-even fields S_1 and S_2. In addition, the masses of h and H satisfy the relation $m_H^2 \sin^2\tilde\alpha + m_h^2 \cos^2\tilde\alpha = 2\lambda_1 v^2$ [93], which, together with our convention $m_h \leq m_H$, implies that

$2\lambda_1 v^2 - m_H^2 \leq 0$ and $m_h^2 - 2\lambda_1 v^2 \leq 0$. Then, from Eq. (2.8), one can see that the sign of $\tan \tilde{\alpha}$ is uniquely determined by that of the parameter λ_6, since the vev $v = \sqrt{v_1^2 + v_2^2}$ is, by definition, always positive. As the Higgs basis of a CP-conserving 2HDM is defined up to a global rephasing of the second scalar doublet $\Phi_2 \rightarrow e^{i\eta}\Phi_2$, we can use this freedom to change the sign of λ_6 [120]. Here, without loss of generality, we shall use the rephasing $\Phi_2 \rightarrow -\Phi_2$ to fix $\lambda_6 \leqslant 0$ so that $\tan \tilde{\alpha} \geq 0$, which, together with $0 \leqslant \tilde{\alpha} < \pi$, results in our final choice $0 \leqslant \tilde{\alpha} \leqslant \pi/2$. The masses of the three neutral scalars are finally given, respectively, by

$$m_h^2 = \frac{1}{2}(\Sigma - \Delta), \quad m_H^2 = \frac{1}{2}(\Sigma + \Delta),$$
$$m_A^2 = m_{H^\pm}^2 + v^2 \left(\frac{\lambda_4}{2} - \lambda_5 \right), \tag{2.9}$$

with

$$\Sigma = m_{H^\pm}^2 + v^2 \left(2\lambda_2 + \frac{\lambda_4}{2} - \lambda_5 \right), \tag{2.10}$$

$$\Delta = \sqrt{\left[m_A^2 + 2v^2 (\lambda_5 - \lambda_1) \right]^2 + 4v^4 \lambda_6^2}. \tag{2.11}$$

Here the convention $m_h \leqslant m_H$ has been chosen, and the SM limit is recovered when $\tilde{\alpha} = 0$.

2.2 Yukawa sector

The Yukawa Lagrangian of a 2HDM in the Higgs basis can be written as [49,51]

$$\mathcal{L}_{Y,\text{weak}} = -\frac{\sqrt{2}}{v} \Big[\bar{Q}'_L (M'_d \Phi_1 + Y'_d \Phi_2) d'_R$$
$$+ \bar{Q}'_L (M'_u \tilde{\Phi}_1 + Y'_u \tilde{\Phi}_2) u'_R$$
$$+ \bar{L}'_L (M'_\ell \Phi_1 + Y'_\ell \Phi_2) \ell'_R \Big] + \text{h.c.} \tag{2.12}$$

Here, Q'_L and L'_L are the left-handed quark and lepton doublets, while u'_R, d'_R, ℓ'_R denote the right-handed fermion singlets, all being given in the weak-interaction basis; $\tilde{\Phi}_a(x) \equiv i\sigma_2 \Phi_a^*(x)$, with σ_2 the Pauli matrix, are the charge-conjugated fields with hypercharge $Y = -1/2$; M'_f ($f = u, d, \ell$) denote the non-diagonal matrices that encode both the fermion masses and the Yukawa couplings of the scalar doublet Φ_1 to fermions, while Y'_f characterize only the Yukawa couplings of the second doublet Φ_2 to fermions.

In general, the two matrices M'_f and Y'_f associated with the same type of right-handed fermion u'_R, d'_R, or ℓ'_R in Eq. (2.12) cannot be simultaneously diagonalized in flavour space. As a consequence, in the fermion mass-eigenstate basis with diagonal mass matrices $M_f = U_L^{f\dagger} M'_f U_R^f$, the corresponding Yukawa matrices $Y_f = U_L^{f\dagger} Y'_f U_R^f$ remain still non-diagonal

Table 1 The one-to-one correspondence between the different choices of the alignment parameters ς_f and the four conventional 2HDMs based on discrete $\mathcal{Z}_2$ symmetries

Model	ς_d	ς_u	ς_ℓ
Type I	$\cot \beta$	$\cot \beta$	$\cot \beta$
Type II	$-\tan \beta$	$\cot \beta$	$-\tan \beta$
Type X	$\cot \beta$	$\cot \beta$	$-\tan \beta$
Type Y	$-\tan \beta$	$\cot \beta$	$\cot \beta$

and hence give rise to non-vanishing tree-level FCNC interactions. These unwanted tree-level FCNC couplings can, however, be eliminated by requiring that the two matrices M'_f and Y'_f are aligned in flavour space [51]. This results in the following alignment relations between the mass and the Yukawa matrices [51]:

$$Y_{d,\ell} = \varsigma_{d,\ell} M_{d,\ell}, \quad Y_u = \varsigma_u^* M_u, \tag{2.13}$$

where ς_f are arbitrary complex parameters and could introduce new sources of CP violation beyond that of the CKM quark-mixing matrix. They are also scalar-basis independent and satisfy universality among the three different generations [51].

In terms of the fermion mass eigenstates, $f_{L,R} = U_{L,R}^{f\dagger} f'_{L,R}$, and making use of the alignment conditions specified by Eq. (2.13), we can finally rewrite the Yukawa Lagrangian of the A2HDM as [51]

$$\mathcal{L}_{Y,\text{mass}} = -i\frac{G^0}{v} \Big\{ \bar{d}_L M_d d_R + \bar{u}_R M_u^\dagger u_L + \bar{\ell}_L M_\ell \ell_R \Big\}$$
$$- \left(1 + \frac{S_1}{v} \right) \Big\{ \bar{u}_L M_u u_R + \bar{d}_L M_d d_R + \bar{\ell}_L M_\ell \ell_R \Big\}$$
$$- \frac{1}{v} (S_2 + i S_3) \Big\{ \bar{d}_L Y_d d_R + \bar{u}_R Y_u^\dagger u_L + \bar{\ell}_L Y_\ell \ell_R \Big\}$$
$$- \frac{\sqrt{2}}{v} G^+ \Big\{ \bar{u}_L V_{\text{CKM}} M_d d_R - \bar{u}_R M_u^\dagger V_{\text{CKM}} d_L + \bar{\nu}_L M_\ell \ell_R \Big\}$$
$$- \frac{\sqrt{2}}{v} H^+ \Big\{ \varsigma_d \, \bar{u}_L V_{\text{CKM}} M_d d_R - \varsigma_u \, \bar{u}_R M_u^\dagger V_{\text{CKM}} d_L$$
$$+ \varsigma_\ell \, \bar{\nu}_L M_\ell \ell_R \Big\} + \text{h.c.}, \tag{2.14}$$

where $V_{\text{CKM}} = U_L^{u\dagger} U_L^d$ is the usual CKM matrix [52,53], and the diagonal fermion mass matrices are now given, respectively, by

$$M_u = \text{diag}(m_u, m_c, m_t), \quad M_d = \text{diag}(m_d, m_s, m_b),$$
$$M_\ell = \text{diag}(m_e, m_\mu, m_\tau). \tag{2.15}$$

For the rare FCNC decays $t \rightarrow cg(g)$ considered here, besides the SM part, only the interactions of the charged scalars $H^\pm$ with the quarks are involved, which means that only the alignment parameters $\varsigma_{u,d}$ and the charged-Higgs mass $m_{H^\pm}$ will be involved throughout this work.

As shown in Table 1, the four conventional 2HDMs [48,49] based on discrete $\mathcal{Z}_2$ symmetries can be easily recovered from the A2HDM by choosing particular values of the alignment parameters ς_f. As the parameter ς_ℓ is not involved in the rare decays $t \to cg(g)$, we are actually left with only two cases, type-I (type-X) 2HDM with $\varsigma_d = \varsigma_u = \cot \beta$, and type-II (type-Y) 2HDM with $\varsigma_d = -1/\varsigma_u = -\tan \beta$. Numerical results of the branching ratios of $t \to cg(g)$ decays in these two specific cases as well as their comparisons with the SM predictions and the results obtained in the A2HDM will also be discussed in Sect. 4.

3 Calculation of the decay rates

3.1 General remarks

The rare top-quark decays $t \to qg(g)$, with $q = u, c$, occur firstly at one-loop level within the SM. As such, the decay rates of these processes are not only suppressed by the loop factor, but also receive a strong CKM and GIM suppression relative to the dominant tree-level decay $t \to bW^+$ [2,27, 39]. Due to the additional charged-Higgs contributions at the loop level, however, these decay rates could be enhanced in the A2HDM as well as in the conventional 2HDMs with $\mathcal{Z}_2$ symmetries [2,3,7]. Here we shall focus on the decays into a charm instead of an up quark, because the decay rates of $t \to ug(g)$ are further suppressed by the ratio $|V_{ub}/V_{cb}|^2 \simeq 0.0087$ compared to that of $t \to cg(g)$, both within the SM as well as in the 2HDMs considered.

Within the SM, due to the hierarchy of the CKM matrix elements, $|V_{tb}| \gg |V_{td}|, |V_{ts}|$, the total width of the top quark is dominated by the tree-level two-body decay $t \to bW^+$, and we can, therefore, take the approximation $\Gamma_{\text{tot}}(t) \simeq \Gamma(t \to bW^+)$. Keeping only the dominant next-to-leading-order (NLO) QCD correction [121–123] while neglecting the W-boson width effect [121], the NLO electroweak [124,125], as well as the next-to-next-to-leading-order QCD correction [126–130], all being only of a few percentages of the Born term [127], we can write the partial decay width of the channel $t \to bW^+$ as [123,125]

$$
\Gamma(t \to bW^+) = \Gamma_0(t \to bW^+) \left\{ 1 + \frac{C_F \alpha_s}{2\pi} \right.
$$
$$
\times \left[2 \frac{(1 - \beta_W^2)(2\beta_W^2 - 1)(\beta_W^2 - 2)}{\beta_W^4 (3 - 2\beta_W^2)} \ln(1 - \beta_W^2) \right.
$$
$$
- \frac{9 - 4\beta_W^2}{3 - 2\beta_W^2} \ln \beta_W^2 + 2\text{Li}_2(\beta_W^2) - 2\text{Li}_2(1 - \beta_W^2)
$$
$$
\left. \left. - \frac{6\beta_W^4 - 3\beta_W^2 - 8}{2\beta_W^2 (3 - 2\beta_W^2)} - \pi^2 \right] \right\}, \tag{3.1}
$$

where $C_F = 4/3$ is the colour factor, and $\alpha_s = g_s^2/(4\pi)$ denotes the strong coupling constant. The parameter $\beta_W = \sqrt{1 - m_W^2/m_t^2}$, with m_W and m_t the W-boson and the top-quark mass respectively, is the velocity of W^+ in the top-quark rest frame, and the dilogarithm function is defined by $\text{Li}_2(x) = -\int_0^x \ln(1-t)/t \, dt$. The leading-order (LO) decay width $\Gamma_0(t \to bW^+)$ in Eq. (3.1) is given by [124]

$$
\Gamma_0(t \to bW^+) = \frac{G_F |V_{tb}|^2 \sqrt{\lambda(m_t, m_b, m_W)}}{8\pi \sqrt{2} \, m_t^3}
$$
$$
\times \left[(m_t^2 - m_b^2)^2 + (m_t^2 + m_b^2)m_W^2 - 2m_W^4 \right], \tag{3.2}
$$

where G_F is the Fermi constant, m_b the bottom-quark mass, and $\lambda(x, y, z) = (x^2 - y^2 - z^2)^2 - 4y^2z^2$ the usual triangle (or Källén) function for a two-body decay.

To a very good approximation, $\Gamma_{\text{tot}}(t) \simeq \Gamma(t \to bW^+)$ holds also in the A2HDM as well as in the four conventional 2HDMs with $\mathcal{Z}_2$ symmetries, except when $m_{H^\pm} < m_t - m_b$; in this regime, the top quark can have an appreciable chance to decay into the final state bH^+, which must be taken into account for the total top width. In this case, we shall have $\Gamma_{\text{tot}}(t) \simeq \Gamma(t \to bW^+) + \Gamma(t \to bH^+)$, with the LO partial width of the decay $t \to bH^+$ in the A2HDM given by [12]

$$
\Gamma(t \to bH^+) = \frac{G_F |V_{tb}|^2 \sqrt{\lambda(m_t, m_b, m_{H^\pm})}}{8\pi \sqrt{2} \, m_t^3}
$$
$$
\times \left[\left(m_t^2 + m_b^2 - m_{H^\pm}^2 \right) \left(m_b^2 |\varsigma_d|^2 + m_t^2 |\varsigma_u|^2 \right) \right.
$$
$$
\left. - 4m_b^2 m_t^2 \, \text{Re}(\varsigma_d \varsigma_u^*) \right]. \tag{3.3}
$$

As we are primarily interested in checking if the "higher-order dominance" phenomenon observed in $t \to cg(g)$ decays within the SM [39] is still valid for the A2HDM and the four conventional 2HDMs with $\mathcal{Z}_2$ symmetries, the charged-Higgs mass $m_{H^\pm}$ will be assumed to be larger than the top-quark mass m_t, and the decay mode $t \to bH^+$ is therefore kinematically forbidden. Thus, the branching ratios of $t \to cg(g)$ decays can be defined as

$$
\mathcal{B}(t \to cg(g)) = \frac{\Gamma(t \to cg(g))}{\Gamma(t \to bW^+)}. \tag{3.4}
$$

In the next two subsections, we shall detail the calculation of the decay rates $\Gamma(t \to cg(g))$ in the A2HDM. To this end, we shall follow the following procedure: Firstly, we implement the A2HDM into the Mathematica-based package FeynRules [131,132] to generate the model file together with a complete set of Feynman rules, which is then fed

into the package FeynArts [133,134] to generate the one-loop Feynman diagrams and the corresponding amplitudes for the $t \to cg(g)$ decays. Then, we resort to the packages FormCalc [135,136] and LoopTools [135] to manipulate the decay amplitudes and evaluate numerically the scalar and tensor one-loop Feynman integrals. Meanwhile, some partial cross-checks have been done by using the package FeynCalc [137–139]. Finally, we can obtain the decay rates from the amplitudes squared by performing the phase space integration. Throughout this work, we carry out the one-loop calculation in $D = 4 - 2\epsilon$ space-time dimensions using the dimensional regularization scheme [140–143] for the ultraviolet divergence in loop integrals, and make the GIM mechanism manifest by dropping the terms independent of the internal down-type quark masses. For the collinear and infrared singularities present in the $t \to cgg$ decay, we take a non-zero charm-quark mass to avoid the collinear divergence generated when one of the gluons in the final state travels parallelly to the charm quark, and introduce phase-space cuts to eliminate the collinear (generated when the two gluons travel parallelly to each other) and infrared (generated when one of the gluons is soft) divergences [39,42].[1]

As the two gluons are both on-shell and hence transversely polarized, care must be taken regarding the gluon polarization sums when squaring the amplitude of $t \to cgg$ decay. One can maintain their transversality either by introducing contributions from the ghost fields while using the simple polarization sums [21,39][2]

$$\sum_{\text{polarizations}} \epsilon_\mu^*(k_3) \epsilon_\nu(k_3)$$
$$= \sum_{\text{polarizations}} \epsilon_\mu^*(k_4) \epsilon_\nu(k_4) = -g_{\mu\nu}, \qquad (3.5)$$

or via the explicit construction [40,42]

$$\sum_{\text{polarizations}} \epsilon_\mu^*(k_3) \epsilon_\nu(k_3)$$
$$= \sum_{\text{polarizations}} \epsilon_\mu^*(k_4) \epsilon_\nu(k_4)$$
$$= -g_{\mu\nu} + \frac{k_{3\mu} k_{4\nu} + k_{4\mu} k_{3\nu}}{k_3 \cdot k_4}, \qquad (3.6)$$

which are now simultaneously transverse with respect to the two gluon momenta k_3 and k_4. Here, $\epsilon_\mu(k_3)$ and $\epsilon_\mu(k_4)$ denote the polarization vectors of the final-state gluons with momenta k_3 and k_4 respectively, while $g_{\mu\nu}$ is the metric tensor in Minkowski space, with the Greek indices running over 0, 1, 2, 3. In this paper, we shall follow the second method. In practice, however, one needs only keep one of the two gluon polarization sums as in Eq. (3.6) while replacing the other one by $-g_{\mu\nu}$ [40]. Conveniently, the package FormCalc provides already a function *PolarizationSum* to achieve such a task.

In our calculation, we shall use the 't Hooft–Feynman gauge and take the external top and charm quarks to be on-shell. However, the gauge independence of our final results has been checked by performing additionally all the calculations in the unitary gauge. Due to the smallness of the down- and strange-quark masses $m_{d,s}$ and the unitarity of the CKM matrix $\sum_{q=d,s,b} V_{tq}^* V_{cq} = 0$, the decay rates turn out to be only sensitive to the bottom-quark mass m_b [27,35]. For these internal quark masses, the most adequate choice is the $\overline{\text{MS}}$ running mass evaluated at a typical scale of $\mathcal{O}(m_t)$ [27,35], and such a prescription will be followed by us. The external top- and charm-quark masses are, on the other hand, taken as the on-shell pole masses. For the sake of simplicity for our presentation, however, we shall set the charm-quark mass m_c to zero and keep only the contributions from the internal bottom quark to these decays, while taking into account all these effects in our numerical analyses presented in Sect. 4.

3.2 Two-body decay $t \to cg$

Let us firstly calculate the decay rate of the two-body decay $t \to cg$ in the A2HDM. The one-loop Feynman diagrams responsible for this decay in the 't Hooft–Feynman gauge are shown in Fig. 1, where the first three ones correspond to the vertex diagrams while the remaining ones to the flavour-changing $(t - c)$ fermion self-energy diagrams. During the calculation of these Feynman diagrams, we have kept all the external and internal quark masses non-vanishing [2,12]. Especially for the flavour-changing fermion self-energy diagrams, we have followed the treatment proposed in Ref. [146]: it is most straightforward to avoid the issue of counterterms [41,42] altogether by simply calculating these diagrams, because the internal top (charm) quark line is off-shell and hence does not contribute to the one-particle pole of the charm (top) quark and needs not be truncated. Furthermore, due to the fact that the flavour-changing fermion self-energies are part of the non-truncated Green's function, one must include their contributions with a factor of 1 rather than a factor of 1/2, as the latter applies only in the standard flavour-conserving case.

---

[1] A more precise approach to obtain a finite result requires both performing a complete NLO QCD calculation of the virtually corrected decay width $\Gamma(t \to cg)$ and achieving a dimensionally regularized version of the decay width $\Gamma(t \to cgg)$ in which both infrared and collinear singularities become manifest [45]. The finiteness of the decay rate is then guaranteed by the Kinoshita–Lee–Nauenberg theorem [144,145].
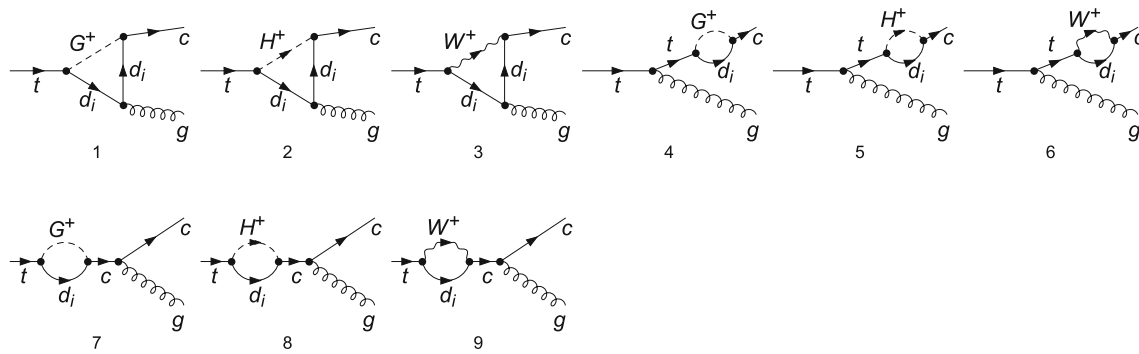
[2] Throughout this work, the colour indices in the gluon polarization vectors will be suppressed.

Fig. 1 One-loop Feynman diagrams contributing to the $t \to cg$ decay in the 't Hooft–Feynman gauge, with $d_i = \{d, s, b\}$, in the A2HDM. The first 1–3 diagrams are the vertex diagrams, and the rest 4–9 are the $t - c$ fermion self-energy diagrams

The resulting transition amplitude for the two-body decay $t \to cg$ can be written as[3]

$$
\mathcal{A}_{t \to cg} = \frac{G_F}{4\sqrt{2}\,\pi^2}\, g_s T_{ij}^a \sum_{q=d,s,b} V_{tq}^* V_{cq}
$$
$$
\times \Big[R_1^{(q)} (\epsilon^*(k_3) \cdot k_1)\, \bar{c}_i(k_2, 0)\, P_R\, t_j(k_1, m_t)
$$
$$
+ R_2^{(q)}\, \bar{c}_i(k_2, 0)\, P_R\, \not{\epsilon}^*(k_3)\, t_j(k_1, m_t) \Big], \qquad (3.7)
$$

where $g_s = \sqrt{4\pi\alpha_s}$ is the strong coupling constant, T_{ij}^a the generators of the $SU(3)$ gauge group with the indexes $a = 1, \ldots, 8$ and $i, j = 1, 2, 3$, and $P_{R,L} = (1 \pm \gamma_5)/2$ the chirality projectors. Here, $\epsilon_\mu^a(k_3)$ is the polarization vector of the gluon, while k_1, k_2, and $k_3 = k_1 - k_2$ are the momenta of the top, the charm, and the gluon, respectively. The two form factors $R_{1,2}^{(q)}$ in Eq. (3.7) are the sums of the contribution from each of the nine diagrams shown in Fig. 1. They can be expressed in terms of the masses of the external and internal quarks and bosons, and contain the D-dimensional loop integrals resulting from dimensional regularization. Specific to the internal bottom-quark contribution, we have explicitly

$$
R_1^{(b)} = 2m_t \Big\{ 2m_W^2 C_{12}(0, m_t^2, 0, m_b^2, m_b^2, m_W^2)
$$
$$
- (m_b^2 - 2m_W^2)\, C_2(0, m_t^2, 0, m_b^2, m_b^2, m_W^2)
$$
$$
- m_b^2 \big[C_0(0, m_t^2, 0, m_b^2, m_b^2, m_W^2)
$$
$$
- C_{12}(0, m_t^2, 0, m_b^2, m_b^2, m_W^2) \big]
$$
$$
+ X_{du} \big(C_0(0, m_t^2, 0, m_b^2, m_b^2, m_{H^\pm}^2)
$$
$$
+ C_2(0, m_t^2, 0, m_b^2, m_b^2, m_{H^\pm}^2) \big)
$$
$$
- X_{dd}\, C_{12}(0, m_t^2, 0, m_b^2, m_b^2, m_{H^\pm}^2) \big] \Big\}, \qquad (3.8)
$$

and

$$
R_2^{(b)} = m_W^2 \Big\{ 2m_t^2 \big[C_1(0, m_t^2, 0, m_b^2, m_b^2, m_W^2)
$$
$$
- m_b^2\, C_0(0, m_t^2, 0, m_b^2, m_b^2, m_W^2)
$$
$$
- C_2(0, m_t^2, 0, m_b^2, m_b^2, m_W^2) \big] + 2B_1(m_t^2, m_b^2, m_W^2)
$$
$$
- 4C_{00}(0, m_t^2, 0, m_b^2, m_b^2, m_W^2) \Big\}
$$
$$
+ m_b^2\, X_{dd} \Big[(m_{H^\pm}^2 - m_b^2) C_0(0, m_t^2, 0, m_b^2, m_b^2, m_{H^\pm}^2)
$$
$$
- 2C_{00}(0, m_t^2, 0, m_b^2, m_b^2, m_{H^\pm}^2)
$$
$$
+ B_1(m_t^2, m_b^2, m_{H^\pm}^2) \Big]
$$
$$
- \big(m_b^4 - m_t^2 m_b^2 - 2m_W^4 \big) C_0(0, m_t^2, 0, m_b^2, m_b^2, m_W^2)
$$
$$
+ m_b^2 \Big\{ m_t^2 \big[C_1(0, m_t^2, 0, m_b^2, m_b^2, m_W^2)
$$
$$
+ X_{dd}\, C_1(0, m_t^2, 0, m_b^2, m_b^2, m_{H^\pm}^2)
$$
$$
+ X_{du}\, C_0(0, m_t^2, 0, m_b^2, m_b^2, m_{H^\pm}^2) \big]
$$
$$
- X_{du} \big[B_0(0, m_b^2, m_{H^\pm}^2) + B_0(m_t^2, m_b^2, m_{H^\pm}^2) \big]
$$
$$
- B_0(0, m_b^2, m_W^2) + B_0(m_t^2, m_b^2, m_W^2)
$$
$$
+ B_1(m_t^2, m_b^2, m_W^2)
$$
$$
- 2C_{00}(0, m_t^2, 0, m_b^2, m_b^2, m_W^2) \Big\}
$$
$$
+ \big[(X_{dd} + 1)m_b^2 + 2m_W^2 \big] B_0(0, m_b^2, m_b^2). \qquad (3.9)
$$

Here, following the standard procedure and notation of Refs. [147–150], we have reduced the vector and tensor integrals via the Passarino–Veltman method [150] to the scalar one-loop integrals B_l and $C_{l,lm}$, which can be further decomposed into the basic scalar functions A_0, B_0, and C_0. However, as the package `FormCalc` does not require such a further reduction, we have expressed our results in terms of B_l and $C_{l,lm}$ instead of the more basic ones to save CPU time. This is especially preferable for the three-body decay $t \to cgg$, in which the more complicated four-point one-loop integrals $D_{l,lm,lmn}$ will be involved. In addition, we have introduced

---

[3] When the charm-quark mass is kept, there are two more form factors in Eq. (3.7), with the associated Dirac strings obtained by replacing P_R with P_L. Applying the on-shell conditions and the Gordon identities, we can also recast Eq. (3.7) into the standard dipole structure form [3], as will be discussed in Sect. 4.

the symbols $X_{qq'} = \varsigma_q \varsigma_{q'}^*$, with $q, q' = d, u$, to represent the possible combinations of the alignment parameters in the A2HDM, and the SM result [2,27] is reproduced by setting $X_{qq'} = 0$. It should be noted that, although the individual contribution from each internal quark $d_i \in \{d, s, b\}$ is separately divergent, the total amplitude is of course ultraviolet finite after summing over all the three internal quark flavours and taking into account the unitarity of the CKM matrix, $\sum_{q=d,s,b} V_{tq}^* V_{cq} = 0$.

With the transition amplitude at hand, it is straightforward to calculate the decay rate $\Gamma(t \to cg)$, with the result given in the top-quark rest frame and in the limit $m_c = 0$ by

$$\Gamma(t \to cg) = \frac{\sqrt{\lambda(m_t, m_c, 0)}}{16\pi m_t^3}$$
$$\times \sum_{\text{polarizations}} \frac{1}{3} \sum_{\text{colours}} \frac{1}{2} \sum_{\text{spins}} |\mathcal{A}_{t \to cg}|^2 . \quad (3.10)$$

For our later numerical analyses, however, we always take into account the finite charm-quark mass effect.

3.3 Three-body decay $t \to cgg$

In the A2HDM, the three-body decay $t \to cgg$ receives contributions from the one-loop Feynman diagrams shown in Fig. 2, where $d_i = \{d, s, b\}$ and the 't Hooft–Feynman gauge is adopted. The transition amplitude of the decay can be written as

$$\mathcal{A}_{t \to cgg} = \sum_{q=d,s,b} \left[\mathcal{A}_{(q)}^{\text{vertex}} + \mathcal{A}_{(q)}^{\text{box}} + \mathcal{A}_{(q)}^{\text{self}} \right], \quad (3.11)$$

where $\mathcal{A}_{(q)}^{\text{vertex}}$, $\mathcal{A}_{(q)}^{\text{box}}$, and $\mathcal{A}_{(q)}^{\text{self}}$ represent the contributions from the vertex, the box, and the self-energy diagrams, respectively. Specific again to the internal bottom-quark contribution and in the limit $m_c = 0$, these separate terms can be written in a compact form as

$$\mathcal{A}_{(b)}^{\text{vertex}} = \frac{G_F \alpha_s V_{tb}^* V_{cb}}{\sqrt{2}\,\pi\, t_{12}\, s_{23}\, t\, R_1 R_2} \Big[T_d\, t_{12}\, t\, R_2 \big(R_1 R_1^{\text{vertex}}$$
$$+ s_{23} R_2^{\text{vertex}} \big) + T_e\, t_{12}\, s_{23}\, R_1 \big(R_2 R_3^{\text{vertex}} + t R_4^{\text{vertex}} \big)$$
$$+ (T_d - T_e) s_{23}\, t\, R_1 R_2 R_5^{\text{vertex}} \Big], \quad (3.12)$$

$$\mathcal{A}_{(b)}^{\text{box}} = \frac{G_F \alpha_s V_{tb}^* V_{cb}}{\sqrt{2}\,\pi\, t_{12}\, s_{23}\, t\, R_1 R_2} \Big[m_t \big(F_1 R_1^{\text{box}} + F_{12} R_5^{\text{box}}$$
$$+ 2 F_{13} R_6^{\text{box}} + 2 F_{14} R_7^{\text{box}} \big)$$
$$- \big(F_3 R_2^{\text{box}} + F_4 R_3^{\text{box}} + F_5 R_4^{\text{box}} - F_{16} R_8^{\text{box}} \big) \Big], \quad (3.13)$$

$$\mathcal{A}_{(b)}^{\text{self}} = \frac{G_F \alpha_s V_{tb}^* V_{cb}}{\sqrt{2}\,\pi\, t_{12}\, s_{23}\, t\, R_1 R_2} \Big[T_d\, t_{12}\, t\, R_2 \big(R_1 R_1^{\text{self}}$$
$$+ s_{23}\, m_b^2 R_2^{\text{self}} + R_6^{\text{self}} \big)$$

$$+ T_e\, t_{12}\, s_{23}\, R_1 \big(R_2 R_3^{\text{self}} + t\, m_b^2 R_4^{\text{self}} + R_7^{\text{self}} \big)$$
$$+ (T_d - T_e) s_{23}\, t\, R_1 R_2 R_5^{\text{self}} \Big]. \quad (3.14)$$

Here the kinematics of the process is specified in the parentheses of the initial- and final-state particles as $t(k_1) \to c(k_2) + g(k_3) + g(k_4)$. For convenience, we have also introduced in Eqs. (3.12)–(3.14) two products of the colour generators, $T_d = (T^a T^b)_{ij}$ and $T_e = (T^b T^a)_{ij}$, as well as the (generalized) Mandelstam variables $t = (k_1 - k_3)^2$, $t_{12} = (k_1 - k_2)^2$, and $s_{23} = (k_2 + k_3)^2$.[4] In addition, the independent fermion chains involved are defined, respectively, by

$$F_1 = \bar{c}_i(k_2, 0)\, P_R\, t_j(k_1, m_t),$$
$$F_2 = \bar{c}_i(k_2, 0)\, P_L\, t_j(k_1, m_t),$$
$$F_3 = \bar{c}_i(k_2, 0)\, P_R\, \not{\epsilon}^*(k_3)\, t_j(k_1, m_t),$$
$$F_4 = \bar{c}_i(k_2, 0)\, P_R\, \not{\epsilon}^*(k_4)\, t_j(k_1, m_t),$$
$$F_5 = \bar{c}_i(k_2, 0)\, P_R\, \not{k}_3\, t_j(k_1, m_t),$$
$$F_6 = \bar{c}_i(k_2, 0)\, P_L\, \not{\epsilon}^*(k_3)\, t_j(k_1, m_t),$$
$$F_7 = \bar{c}_i(k_2, 0)\, P_L\, \not{\epsilon}^*(k_4)\, t_j(k_1, m_t),$$
$$F_8 = \bar{c}_i(k_2, 0)\, P_L\, \not{k}_3\, t_j(k_1, m_t),$$
$$F_9 = \bar{c}_i(k_2, 0)\, P_L\, \not{\epsilon}^*(k_3)\, \not{\epsilon}^*(k_4)\, t_j(k_1, m_t),$$
$$F_{10} = \bar{c}_i(k_2, 0)\, P_L\, \not{\epsilon}^*(k_3)\, \not{k}_3\, t_j(k_1, m_t),$$
$$F_{11} = \bar{c}_i(k_2, 0)\, P_L\, \not{\epsilon}^*(k_4)\, \not{k}_3\, t_j(k_1, m_t),$$
$$F_{12} = \bar{c}_i(k_2, 0)\, P_R\, \not{\epsilon}^*(k_3)\, \not{\epsilon}^*(k_4)\, t_j(k_1, m_t),$$
$$F_{13} = \bar{c}_i(k_2, 0)\, P_R\, \not{\epsilon}^*(k_3)\, \not{k}_3\, t_j(k_1, m_t),$$
$$F_{14} = \bar{c}_i(k_2, 0)\, P_R\, \not{\epsilon}^*(k_4)\, \not{k}_3\, t_j(k_1, m_t),$$
$$F_{15} = \bar{c}_i(k_2, 0)\, P_L\, \not{\epsilon}^*(k_3)\, \not{\epsilon}^*(k_4)\, \not{k}_3\, t_j(k_1, m_t),$$
$$F_{16} = \bar{c}_i(k_2, 0)\, P_R\, \not{\epsilon}^*(k_3)\, \not{\epsilon}^*(k_4)\, \not{k}_3\, t_j(k_1, m_t). \quad (3.15)$$

For the R functions present in Eqs. (3.12)–(3.14), we have $R_1 = s_{23} - m_t^2$ and $R_2 = t - m_t^2$, while the explicit expressions of all the remaining ones are collected in Appendix A.

In the top-quark rest frame, the differential decay rate of $t \to cgg$ can be written as

$$d\Gamma(t \to cgg) = \frac{1}{2m_t} \left(\prod_{i=2}^4 \int \frac{d^3 k_i}{(2\pi)^3} \frac{1}{2E_i} \right) (2\pi)^4 \delta^{(4)}$$
$$\times (k_1 - k_2 - k_3 - k_4)$$
$$\times \sum_{\text{polarizations}} \frac{1}{3} \sum_{\text{colours}} \frac{1}{2} \sum_{\text{spins}} \frac{1}{2} |\mathcal{A}_{t \to cgg}|^2 , \quad (3.16)$$

---

[4] It should be noted that we can also organize Eqs. (3.12)–(3.14) according to whether the two on-shell final-state gluons are in a colour-symmetric ($\{T^a, T^b\}$) or in a colour-antisymmetric ($[T^a, T^b]$) configuration [42,45]. Although taking the same symbol, the Mandelstam variable t can be clearly distinguished from the top-quark spinor through the context.
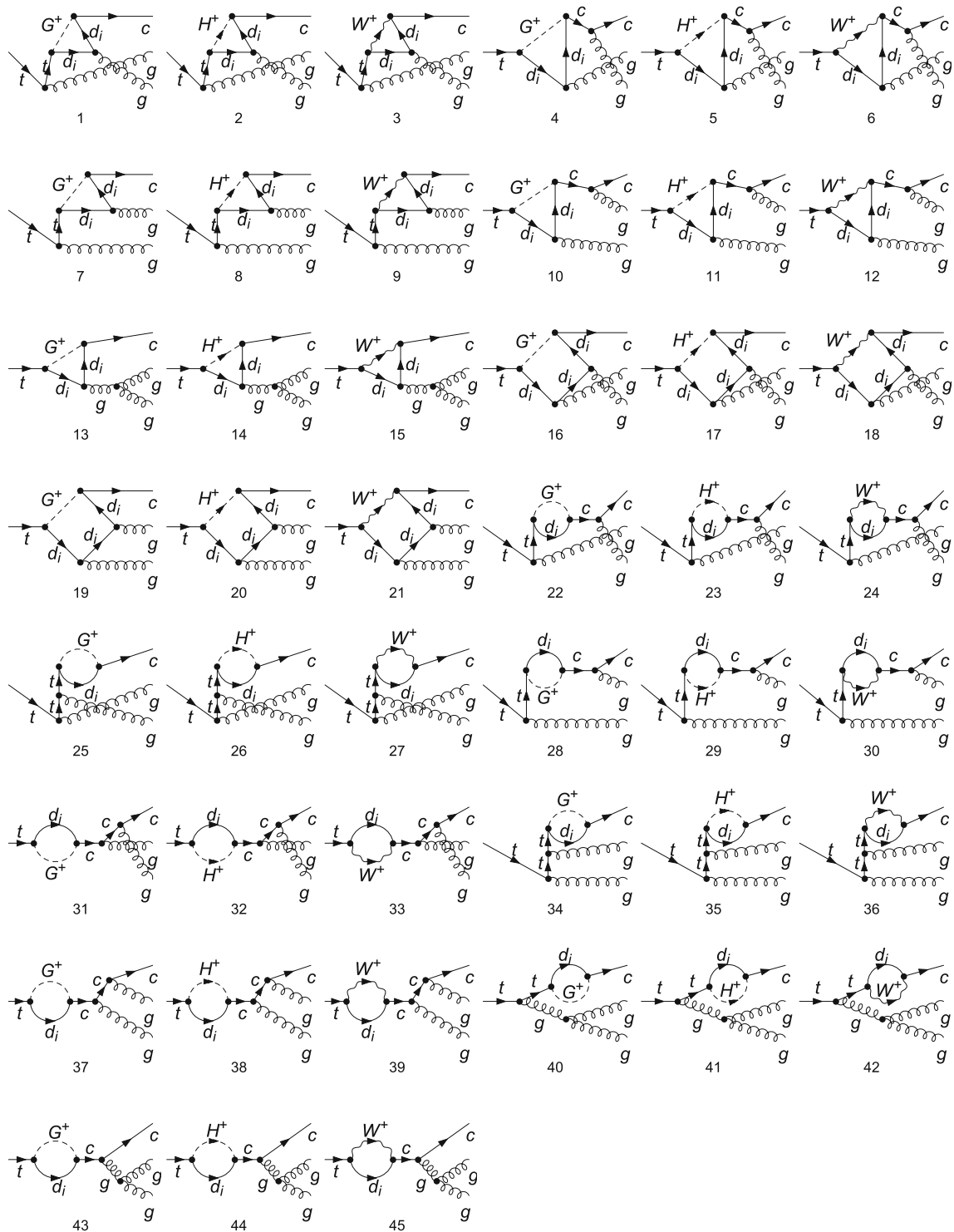
Fig. 2 One-loop Feynman diagrams contributing to the $t \to cgg$ decay in the 't Hooft–Feynman gauge, with $d_i = \{d, s, b\}$, in the A2HDM. The first 1–15 diagrams are the vertex diagrams, the diagrams 16–21 are the box diagrams, and the rest 22–45 are the $t - c$ fermion self-energy diagrams

where $E_i = k_i^0$ represents the energy of the $(i$-1)-th final-state particle in the top-quark rest frame, and the last factor $1/2$ accounts for the statistical factor due to the two gluons in the final state. In this frame, we have $\vec{k}_2 + \vec{k}_3 + \vec{k}_4 = 0$, and thus the three final-state momentum vectors lie in a plane. Then, the three-body phase space in Eq. (3.16) can be integrated over the orientation of this plane by using the momentum delta functions and the azimuthal symmetry. In this way, we are left with only two non-trivial integration variables, which can be chosen as the energy of the charm quark (k_2^0) and the energy of one of the gluons (say k_3^0), and the decay width of $t \to cgg$ can be finally written as

$$\Gamma(t \to cgg) = \frac{1}{64\,\pi^3\,m_t} \sum_{\text{polarizations}}$$
$$\times \frac{1}{3}\sum_{\text{colours}} \frac{1}{2}\sum_{\text{spins}} \int dk_3^0 \int dk_2^0 \times \frac{1}{2}\left|\mathcal{A}_{t \to cgg}\right|^2. \quad (3.17)$$

Because of the infrared and collinear divergences mentioned in Sect. 3.1, which are also evident from Eqs. (3.12)–(3.14) and appear at the vertices and along the boundary lines of the Dalitz plot in the (k_2^0, k_3^0) space respectively, we have to impose proper cuts on both k_2^0 and k_3^0 when performing the integration of Eq. (3.17) over these two variables. Following the treatment of Refs. [39,42], we shall use the kinematic constraints

$$\begin{aligned}
t &= (k_1 - k_3)^2 = m_t^2 - 2m_t k_3^0 \geqslant C \cdot 2m_t^2, \\
t_{12} &= (k_1 - k_2)^2 = m_t^2 - 2m_t k_2^0 \geqslant C \cdot 2m_t^2, \\
s_{23} &= (k_2 + k_3)^2 = (k_1 - k_4)^2 \\
&= -m_t^2 + 2m_t(k_2^0 + k_3^0) \geqslant C \cdot 2m_t^2,
\end{aligned} \quad (3.18)$$

along with the fact that $k_{2,\text{max}}^0 \geqslant k_{2,\text{min}}^0$, to get the integration ranges of the two variables:[5]

$$\begin{aligned}
k_2^0 &\in \left[\frac{m_t}{2} - k_3^0 + Cm_t, \frac{m_t}{2}(1-2C)\right], \\
k_3^0 &\in \left[2Cm_t, \frac{m_t}{2}(1-2C)\right],
\end{aligned} \quad (3.19)$$

where C is the cutoff parameter, and its value must be taken within the range of jet energy resolution of a detector. Note that, when a non-zero charm-quark mass is considered, Eq. (3.19) must be modified as

$$\begin{aligned}
k_2^0 &\in \left[\frac{m_t}{2} - k_3^0 + Cm_t + \frac{m_c^2}{2m_t}, \frac{m_t}{2}(1-2C) + \frac{m_c^2}{2m_t}\right], \\
k_3^0 &\in \left[2Cm_t, \frac{m_t}{2}(1-2C) - \frac{m_c^2}{2m_t}\right].
\end{aligned} \quad (3.20)$$

Here, for simplicity, we shall take $C \simeq 0.01$ as the default value (i.e., requiring the energy of each decay product to be larger than 2.0 GeV in the top-quark rest frame), while varying C within the range [0.001, 0.05] to study its numerical impacts on the branching ratio of $t \to cgg$ decay. Note that the choice $C = 0.01$ is already large enough to reach the jet energy resolution sensitivity of the HL-LHC [108] and FCC [109–112] facilities.

4 Numerical results and discussions

4.1 Input parameters

The relevant input parameters needed for evaluating the branching ratios of $t \to cg(g)$ decays are listed in Table 2. For the QCD and electroweak parameters as well as the quark masses, their values are taken from the PARTICLE DATA GROUP [151]. Here, for the external on-shell quarks, we take their pole masses as input, and evolve the internal quark masses from their respective initial scales to the scale $\mu_t = m_t^{\text{pole}}$ characteristic for the top-quark decay, using the two-loop renormalization group equations for the $\overline{\text{MS}}$ running quark masses.[6] The $\overline{\text{MS}}$ coupling constant α_s is given at the Z-boson mass scale with the top quark decoupled (i.e., with $n_f = 5$ active quark flavours). To obtain its values at the scale μ_t and also at other scales when evolving the $\overline{\text{MS}}$ running quark masses, we use the two-loop running of α_s by taking into account the decoupling effect when crossing a flavour threshold [154,155]. For convenience, we compile also in Table 2 the derived values of the $\overline{\text{MS}}$ running parameters evaluated at the scale $\mu_t = m_t^{\text{pole}}$ following the above prescription.

Concerning the needed entries of the CKM matrix, we adopt the Wolfenstein parametrization [152], generalized to include the higher-order terms of $\lambda = |V_{us}|$ [153]. To be consistent with the study of NP, the four Wolfenstein parameters λ, A, $\bar\rho = \rho(1 - \lambda^2/2)$, and $\bar\eta = \eta(1 - \lambda^2/2)$ should be fitted to the tree-level observables as well as the ratio of the mass differences between the neutral B-meson eigenstates, $\Delta M_d/\Delta M_s$, which are all expected to have only a minimal sensitivity to the charged-Higgs contributions [60]. To this end, we shall use as input the central values of the fitting results obtained in Ref. [75]. For any further details, the readers are referred to Ref. [75].

As pointed out already in Sect. 2, only the parameters ς_u, ς_d, and $m_{H^\pm}$ are involved for the rare decays $t \to cg(g)$ in the A2HDM. Let us now fix the allowed ranges of these

---

[5] To ensure that the divergent point at $k_2^0 + k_3^0 = m_t/2$ resulting from $s_{23} = 0$ in Eqs. (3.12)–(3.14) is also excluded, our choice is slightly different from that of Ref. [39]. Recall that $m_c = 0$ is assumed here.

[6] Note that the down- and strange-quark running masses $\bar{m}_{d,s}$ are quoted in the $\overline{\text{MS}}$ scheme at a scale $\mu = 2\,\text{GeV}$, while the bottom-quark running mass $\bar{m}_b$ is evaluated at a scale equal to its mass, i.e., $\bar{m}_b(\bar{m}_b)$.

Table 2 Summary of the input parameters used throughout this work. For convenience, the derived values of the $\overline{\text{MS}}$ running parameters evaluated at the scale $\mu_t = m_t^{\text{pole}}$ are also given. In the Wolfenstein parametrization [152] of the CKM matrix, the four independent Wolfenstein parameters can be chosen as λ, A, $\bar{\rho} = \rho(1 - \lambda^2/2)$, and $\bar{\eta} = \eta(1 - \lambda^2/2)$ [153]

QCD and electroweak parameters [151]			
$G_F [10^{-5}\,\text{GeV}^{-2}]$	$m_W [\text{GeV}]$	$m_Z [\text{GeV}]$	$\alpha_s^{(5)}(m_Z)$
1.1663787	80.379	91.1876	0.1179
			$\alpha_s^{(6)}(m_t^{\text{pole}})$
			0.1076

Quark masses [GeV] [151]					
m_t^{pole}	m_b^{pole}	m_c^{pole}	$\bar{m}_b(\bar{m}_b)$	$\bar{m}_s(2\,\text{GeV})$	$\bar{m}_d(2\,\text{GeV})$
172.5	4.78	1.67	4.18	0.093	0.00467
			$\bar{m}_b(m_t^{\text{pole}})$	$\bar{m}_s(m_t^{\text{pole}})$	$\bar{m}_d(m_t^{\text{pole}})$
			2.60	0.048	0.00241

CKM parameters [75]			
λ	A	$\bar{\rho}$	$\bar{\eta}$
0.2256	0.829	0.182	0.360

model parameters. For simplicity, we shall entertain ourselves with the CP-conserving limit and assume that the observed 125 GeV Higgs is the lightest CP-even scalar of the model, which corresponds exactly to the *light scenario* considered in Ref. [75]. For the two alignment parameters $\varsigma_{u,d}$, we choose the ranges

$$|\varsigma_u| \in [0, 1.5], \quad |\varsigma_d| \in [0, 50], \tag{4.1}$$

as constrained mostly by the precision flavour physics, such as $Z \to b\bar{b}$, $\bar{B} \to X_s\gamma$, as well as $B_{s,d}^0 - \bar{B}_{s,d}^0$ and $K^0 - \bar{K}^0$ mixings [60–64]. It is especially interesting to note that, for large values of $|\varsigma_u\varsigma_d|$, important correlated constraints on ς_u and ς_d can be derived from the weak radiative decay $\bar{B} \to X_s\gamma$, with the region $\varsigma_d\varsigma_u < 0$ almost excluded by the current data on the branching ratio of $\bar{B} \to X_s\gamma$ [60]. The ranges in Eq. (4.1) are also roughly consistent with the perturbativity requirement, $|\sqrt{2}\varsigma_{u,d}m_{u,d}/v| \lesssim 1$. For the charged-Higgs mass, we focus only on the case with $m_{H^\pm}$ varied within the ranges $m_{H^\pm} \in [200, 600]\,\text{GeV}$ for the $t \to cg$ and $m_{H^\pm} \in [200, 400]\,\text{GeV}$ for the $t \to cgg$ decay. Here the lower limit is chosen to be larger than the top-quark mass such that the decay mode $t \to bH^+$ is kinematically forbidden, while the upper limit is motivated by the observation that the maximum branching ratio of $t \to cg(g)$ for $m_{H^\pm} \gtrsim 600\,(400)\,\text{GeV}$ approaches already the corresponding SM prediction, as will be demonstrated in the next subsection.[7] Recently, a detailed global fit has been performed to

the A2HDM by considering a CP-conserving scalar potential and real alignment parameters, and including the most constraining flavour observables, electroweak precision measurements, and the available data on Higgs signal strengths and collider searches for heavy scalars, together with the theoretical requirements of perturbativity and positivity of the scalar potential [75]. We shall use the relevant constraints on the alignment parameters $\varsigma_{u,d}$ resulting from such a global fit obtained at the 95.5% CL (cf. the brown region in the left plot of Fig. 9) in Ref. [75]; for further details, the readers are also referred to Ref. [75].

4.2 $\mathcal{B}(t \to cg(g))$ in the A2HDM

Firstly, with the input parameters collected in Table 2, we give for reference the partial width of the dominant tree-level $t \to bW^+$ decay,

$$\Gamma(t \to bW^+) = 1.35\,(1.47)\,\text{GeV}, \tag{4.2}$$

at the NLO (LO) in QCD, which is found to be well consistent with the current data on the top-quark total width, $\Gamma_{\text{tot}}^{\text{exp}}(t) = 1.42^{+0.19}_{-0.15}\,\text{GeV}$ [151]. This in turn implies that the extra contribution from the partial width $\Gamma(t \to bH^+)$ in the $m_{H^\pm} < m_t - m_b$ case should be small, supporting therefore our choice of the lower limit of the charged-Higgs mass,

---

[7] Direct constraints on the charged-Higgs mass can also be obtained from collider searches for the production and decay of on-shell charged-

Footnote 7 continued
Higgs bosons [156–160]; see, e.g., Refs. [161,162] for recent reviews. Our choices of the model parameters comply with these direct constraints.

$m_{H^\pm} \geq 200\,\text{GeV}$, as required to forbid the decay $t \to bH^+$ kinematically. Otherwise, for $m_{H^\pm} < 150\,\text{GeV}$, the alignment parameter ς_d is constrained to be small by the direct charged-Higgs searches at the LHC via the decay $t \to bH^+$ [157,159], implying a very strong suppression on the decay rates of $t \to cV$ ($V = \gamma, Z$) and $t \to ch$ processes [12].

To display the dependence of the branching ratios of $t \to cg$ and $t \to cgg$ decays on the alignment parameters $\varsigma_{u,d}$, we fix the charged-Higgs mass to three benchmark values, $m_{H^\pm} = 200, 300,$ and $500\,(400)\,\text{GeV}$. In this way, we obtain numerically

$$\mathcal{B}^{\text{A2HDM}}(t \to cg) = 4.50 \times 10^{-12}$$

$$\times \begin{cases} \begin{aligned} &\big[1 + 2.46 \times 10^{-5}\,\varsigma_u^4 + 7.19 \times 10^{-5}\,\varsigma_d\varsigma_u^3 + 0.261\,\varsigma_d^2\varsigma_u^2 \\ &\quad - 1.30 \times 10^{-2}\,\varsigma_d^3\varsigma_u + 1.63 \times 10^{-4}\,\varsigma_d^4 + 4.91 \times 10^{-6}\,\varsigma_u^2 \\ &\quad + 0.848\,\varsigma_d\varsigma_u - 2.12 \times 10^{-2}\,\varsigma_d^2\big], \quad \text{for } m_{H^\pm} = 200\,\text{GeV}, \end{aligned} \\ \begin{aligned} &\big[1 + 1.96 \times 10^{-7}\,\varsigma_u^4 + 2.88 \times 10^{-6}\,\varsigma_d\varsigma_u^3 + 3.48 \times 10^{-2}\,\varsigma_d^2\varsigma_u^2 \\ &\quad - 1.49 \times 10^{-3}\,\varsigma_d^3\varsigma_u + 1.60 \times 10^{-5}\,\varsigma_d^4 + 2.92 \times 10^{-6}\,\varsigma_u^2 \\ &\quad + 0.310\,\varsigma_d\varsigma_u - 6.63 \times 10^{-3}\,\varsigma_d^2\big], \quad \text{for } m_{H^\pm} = 300\,\text{GeV}, \end{aligned} \\ \begin{aligned} &\big[1 + 3.42 \times 10^{-9}\,\varsigma_u^4 + 1.49 \times 10^{-7}\,\varsigma_d\varsigma_u^3 + 4.64 \times 10^{-3}\,\varsigma_d^2\varsigma_u^2 \\ &\quad - 1.73 \times 10^{-4}\,\varsigma_d^3\varsigma_u + 1.61 \times 10^{-6}\,\varsigma_d^4 + 5.41 \times 10^{-7}\,\varsigma_u^2 \\ &\quad + 0.113\,\varsigma_d\varsigma_u - 2.11 \times 10^{-3}\,\varsigma_d^2\big], \quad \text{for } m_{H^\pm} = 500\,\text{GeV}, \end{aligned} \end{cases}$$

$$(4.3)$$

for the two-body decay $t \to cg$, and

$$\mathcal{B}^{\text{A2HDM}}(t \to cgg) = 8.31 \times 10^{-10}$$

$$\times \begin{cases} \begin{aligned} &\big[1 + 6.31 \times 10^{-7}\,\varsigma_u^4 + 2.47 \times 10^{-7}\,\varsigma_d\varsigma_u^3 + 1.06 \times 10^{-3}\,\varsigma_d^2\varsigma_u^2 \\ &\quad - 4.67 \times 10^{-5}\,\varsigma_d^3\varsigma_u + 5.67 \times 10^{-7}\,\varsigma_d^4 - 1.19 \times 10^{-6}\,\varsigma_u^2 \\ &\quad + 2.72 \times 10^{-3}\,\varsigma_d\varsigma_u - 9.63 \times 10^{-5}\,\varsigma_d^2\big], \quad \text{for } m_{H^\pm} = 200\,\text{GeV}, \end{aligned} \\ \begin{aligned} &\big[1 + 4.99 \times 10^{-8}\,\varsigma_u^4 + 1.40 \times 10^{-8}\,\varsigma_d\varsigma_u^3 + 1.35 \times 10^{-4}\,\varsigma_d^2\varsigma_u^2 \\ &\quad - 5.20 \times 10^{-6}\,\varsigma_d^3\varsigma_u + 5.47 \times 10^{-8}\,\varsigma_d^4 - 3.11 \times 10^{-7}\,\varsigma_u^2 \\ &\quad + 1.02 \times 10^{-3}\,\varsigma_d\varsigma_u - 3.00 \times 10^{-5}\,\varsigma_d^2\big], \quad \text{for } m_{H^\pm} = 300\,\text{GeV}, \end{aligned} \\ \begin{aligned} &\big[1 + 1.32 \times 10^{-8}\,\varsigma_u^4 + 3.17 \times 10^{-9}\,\varsigma_d\varsigma_u^3 + 4.12 \times 10^{-5}\,\varsigma_d^2\varsigma_u^2 \\ &\quad - 1.49 \times 10^{-6}\,\varsigma_d^3\varsigma_u + 1.45 \times 10^{-8}\,\varsigma_d^4 - 1.52 \times 10^{-7}\,\varsigma_u^2 \\ &\quad + 5.78 \times 10^{-4}\,\varsigma_d\varsigma_u - 1.54 \times 10^{-5}\,\varsigma_d^2\big], \quad \text{for } m_{H^\pm} = 400\,\text{GeV}, \end{aligned} \end{cases}$$

$$(4.4)$$

for the three-body decay $t \to cgg$. Here, the SM results are obtained by taking the limits $\varsigma_{u,d} \to 0$ and read

$$\mathcal{B}^{\text{SM}}(t \to cg) = 4.50 \times 10^{-12}, \tag{4.5}$$

$$\mathcal{B}^{\text{SM}}(t \to cgg) = 8.31 \times 10^{-10}. \tag{4.6}$$

It is found that our SM predictions are generally consistent with that made in Refs. [14,27] for the two-body decay $t \to cg$, as well as in Ref. [39] for the three-body decay $t \to cgg$. Especially, the branching ratio of the three-body decay $t \to cgg$ is predicted to be about two orders of magnitude larger than that of the two-body decay $t \to cg$, which is

a clear demonstration of the "higher-order dominance" phenomenon observed already in Ref. [39]. It should be noted that the branching ratio of $t \to cgg$ depends on the cutoff parameter C, and the results given by Eqs. (4.4) and (4.6) are obtained with the default value $C = 0.01$. The cutoff dependence of this branching ratio within the SM is shown in Table 3 for six different values of C, together with the comparison with that obtained in Ref. [39]. It can be seen that, although being increased by about 7% compared to that obtained in Ref. [39] for the same choice of C,[8] our updated results depend only slightly on the cutoff parameter C, with the variation being only about two times when C varies within the range $[0.001, 0.05]$. From Eqs. (4.3) and (4.4), one can also see that the branching ratios of $t \to cg(g)$ decays display a different dependence on the alignment parameters $\varsigma_{u,d}$: Firstly, due to the much smaller coefficients, together with the allowed ranges of ς_u and ς_d specified by Eq. (4.1), the terms proportional to ς_u^4, $\varsigma_d\varsigma_u^3$, and ς_u^2 can be safely neglected. Secondly, for moderate values of $|\varsigma_d|$ and large values of $|\varsigma_u|$, the branching ratios will be dominated by the product $\varsigma_d\varsigma_u$ and, to a less extent, also by $\varsigma_d^2\varsigma_u^2$. Finally, the significance of ς_d occurs only when $|\varsigma_d|$ and $|\varsigma_u|$ take much larger and smaller values, respectively.

Picking up randomly the values of the alignment parameters $\varsigma_{u,d}$ within the brown region (corresponding to the global fit obtained at the 95.5% CL) shown by the left plot of Figure 9 in Ref. [75], we show in Figs. 3 and 4 the branching ratios $\mathcal{B}(t \to cg)$ and $\mathcal{B}(t \to cgg)$ as a function of ς_u (left) and ς_d (right), for three benchmark values of the charged-Higgs mass, $m_{H^\pm} = 200, 300,$ and $500\,(400)\,\text{GeV}$, represented by the orange (top), brown (middle), and dark green (purple) (bottom) scatter plots, respectively. It can be seen that the maximum branching ratios of both $t \to cg$ and $t \to cgg$ decays are reached in the limits $|\varsigma_u| \to 0$ and $|\varsigma_d| \to 48$, which correspond to the minimum $|\varsigma_u|$ and maximum $|\varsigma_d|$ allowed by the combined constraints from the most constraining observables and the theoretical requirements [75]. Furthermore, almost irrespective of the values of the charged-Higgs mass, the maxima of the branching ratios are always reached with the same set of alignment parameters, $(\varsigma_u, \varsigma_d) \simeq (-0.047, -48)$, when $m_{H^\pm}$ varies within the ranges $[200, 600]\,\text{GeV}$ for the $t \to cg$ and $[200, 400]\,\text{GeV}$ for the $t \to cgg$ decay. Numerically, we obtain

$$\mathcal{B}^{\text{A2HDM}}_{\text{max}}(t \to cg) = \begin{cases} 3.36 \times 10^{-9}, & \text{for } m_{H^\pm} = 200\,\text{GeV}, \\ 2.84 \times 10^{-10}, & \text{for } m_{H^\pm} = 300\,\text{GeV}, \\ 1.82 \times 10^{-11}, & \text{for } m_{H^\pm} = 500\,\text{GeV}, \end{cases}$$

$$(4.7)$$

---

[8] Note that the $\overline{\text{MS}}$ running masses of both the top and charm quarks as well as the α scheme for the electroweak parameters were used in Ref. [39], while we take the pole masses for the external on-shell quarks as input and adopt the G_F scheme for the electroweak parameters [125].

Table 3 The cutoff dependence of the branching ratio of $t \to cgg$ decay within the SM, as well as the comparison with that obtained in Ref. [39]. Note that the $\overline{\text{MS}}$ running masses of both the top and charm quarks as well as the α scheme for the electroweak parameters were used in Ref. [39]

| C	0.001	0.003	0.005	0.01	0.03	0.05	
$\mathcal{B}^{\text{SM}}(t \to cgg)\,[10^{-10}]$	10.7	9.80	9.33	8.31	6.06	4.68	This work
$\mathcal{B}^{\text{SM}}(t \to cgg)\,[10^{-10}]$	10.2	9.04	8.76	7.78	–	–	Reference [39]
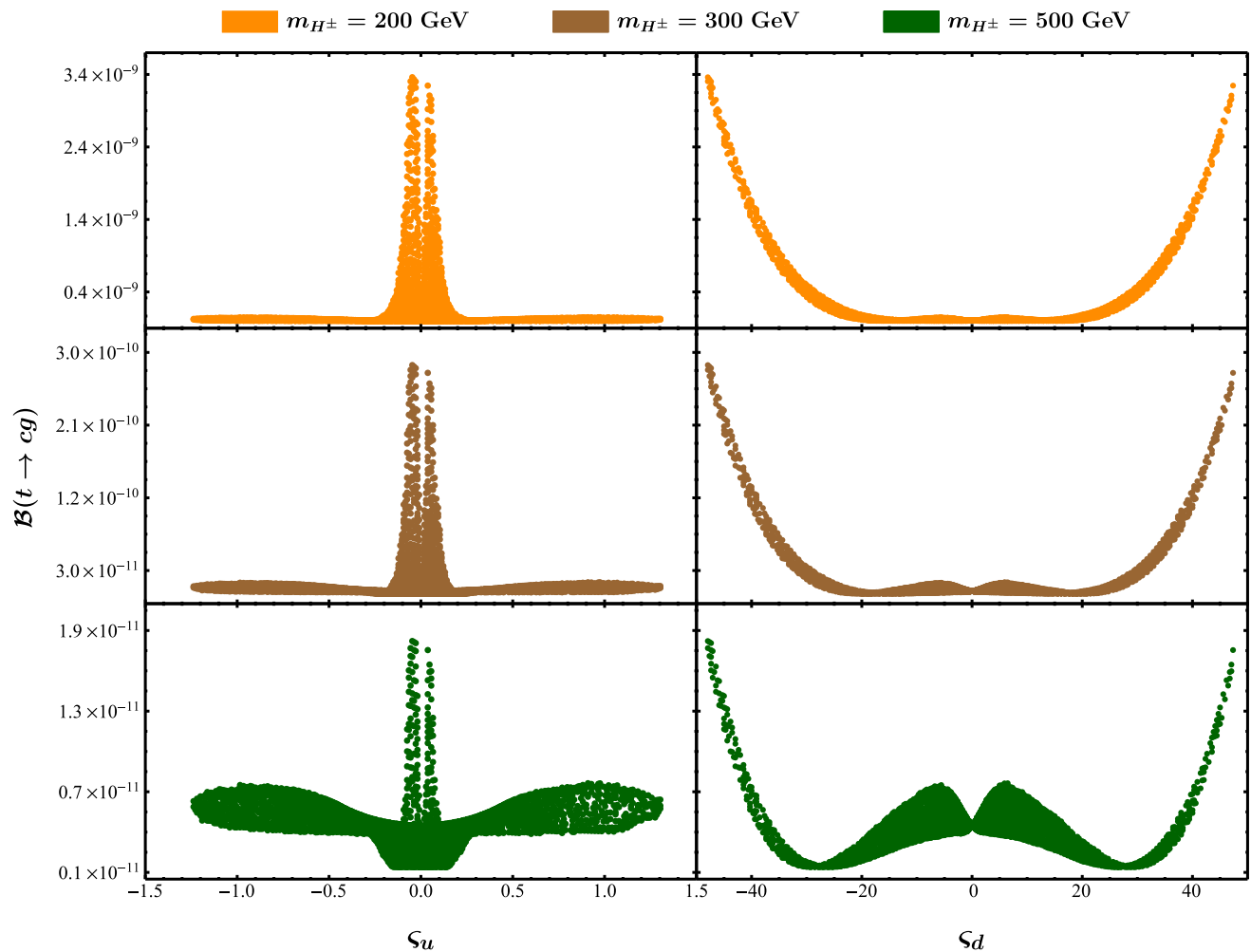
Fig. 3 The branching ratio $\mathcal{B}(t \to cg)$ as a function of the alignment parameters ς_u (left) and ς_d (right), for three benchmark values of the charged-Higgs mass, $m_{H^\pm} = 200$, 300, and 500 GeV, represented by the orange (top), brown (middle), and dark green (bottom) scatter plots, respectively. Here we have used the relevant constraints on the align-ment parameters $\varsigma_{u,d}$ from a global fit obtained at the 95.5% CL in Ref. [75]. The thickness of the shaded regions reflects the corresponding allowed range for $\varsigma_{d(u)}$ for a given value of $\varsigma_{u(d)}$, as can be read from the brown region of the left plot of Figure 9 in Ref. [75]

and

$$\mathcal{B}_{\text{max}}^{\text{A2HDM}}(t \to cgg) = \begin{cases} 2.95 \times 10^{-9}, & \text{for } m_{H^\pm} = 200\,\text{GeV}, \\ 9.94 \times 10^{-10}, & \text{for } m_{H^\pm} = 300\,\text{GeV}, \\ 8.60 \times 10^{-10}, & \text{for } m_{H^\pm} = 400\,\text{GeV}. \end{cases}$$

$$(4.8)$$

It can be seen that, with the 95.5%-CL constraints on the alignment parameters from the global fit taken into account

[75], the maximum branching ratios of $t \to cg$ and $t \to cgg$ decays are both reached at $m_{H^\pm} = 200$ GeV and given by 3.36×10^{-9} and 2.95×10^{-9} respectively, being therefore of the same order, in the A2HDM. This is obviously differ-ent from the SM case, where the predicted branching ratio of $t \to cgg$ is about two orders of magnitude larger than that of $t \to cg$ (cf. Eqs. (4.5) and (4.6)) [39]. For conve-
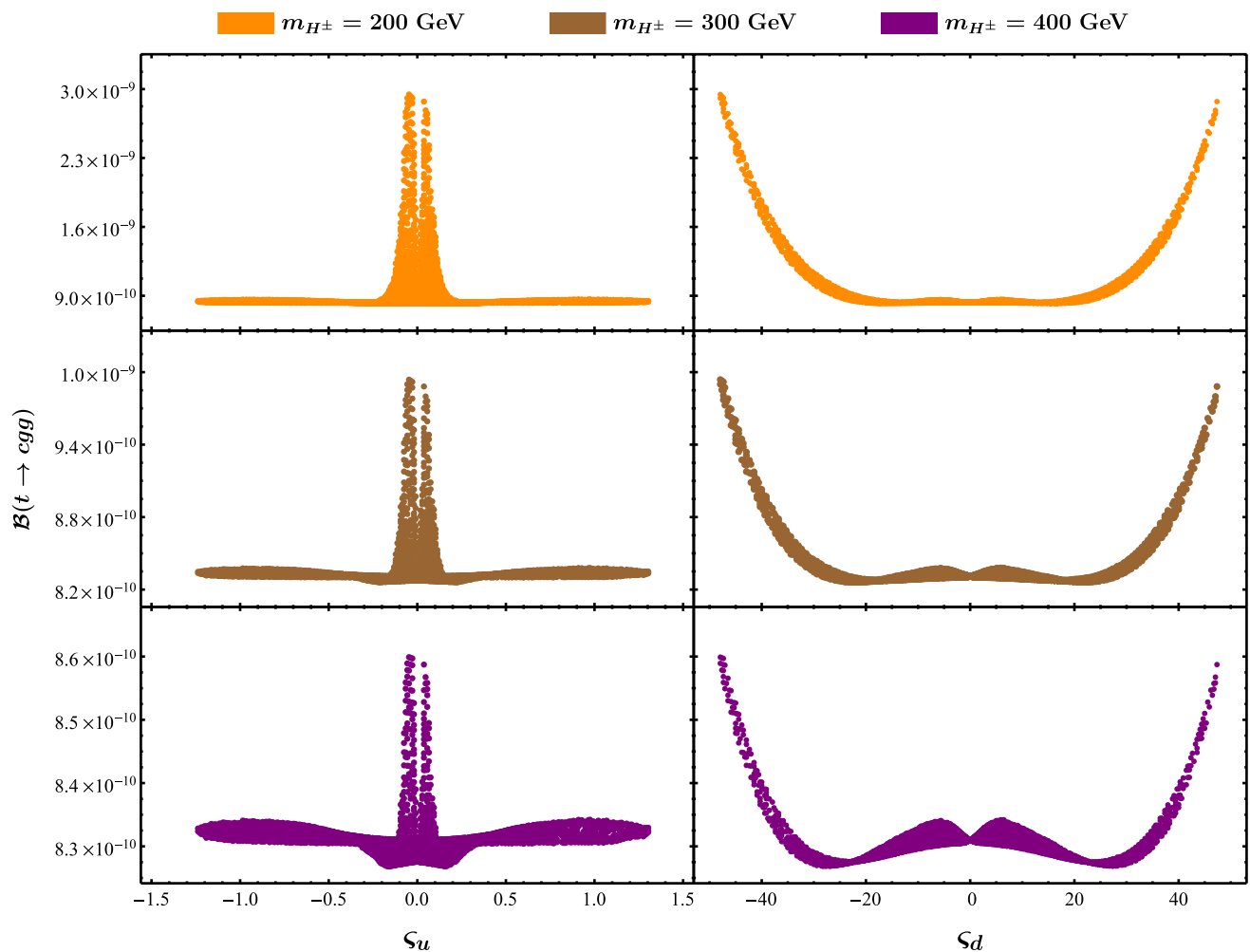
Fig. 4 The branching ratio $\mathcal{B}(t \to cgg)$ as a function of the alignment parameters ς_u (left) and ς_d (right), for three benchmark values of the charged-Higgs mass, 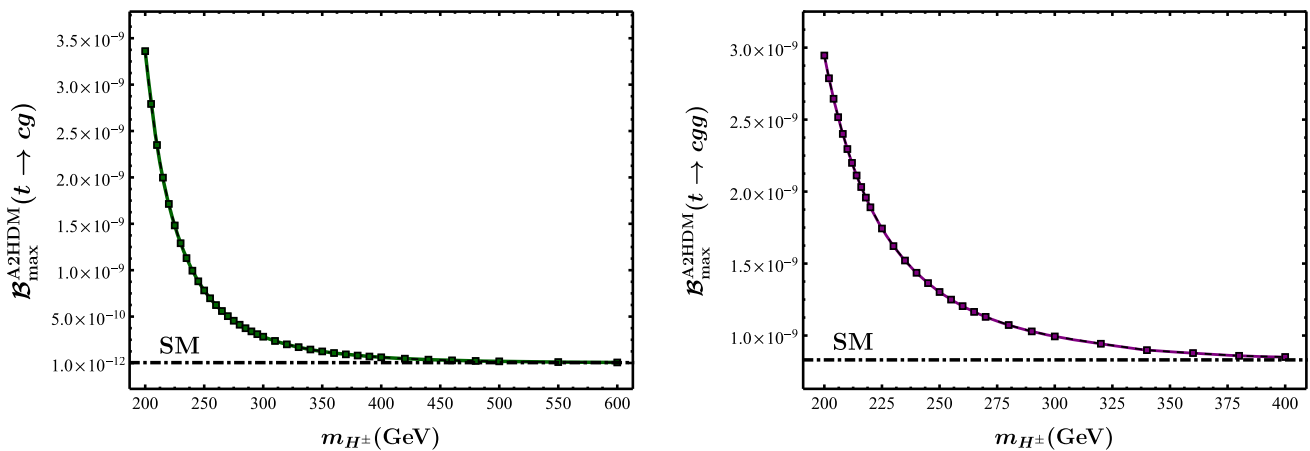$m_{H^\pm} = 200, 300$, and 400 GeV, represented by the orange (top), brown (middle), and purple (bottom) scatter plots, respectively. The other captions are the same as in Fig. 3

nience, we show in Fig. 5 the dependence of the maximum branching ratios of $t \to cg$ (left) and $t \to cgg$ (right) on the charged-Higgs mass $m_{H^\pm}$, with the alignment parameters fixed at $(\varsigma_u, \varsigma_d) \simeq (-0.047, -48)$.[9] One can see that the maximum branching ratios of $t \to cg$ and $t \to cgg$ decays decrease sharply as the charged-Higgs mass $m_{H^\pm}$ increases, and approach the corresponding SM predictions for $m_{H^\pm} \gtrsim 600$ GeV and $m_{H^\pm} \gtrsim 400$ GeV, respectively.[10] In addition,

the maximum branching ratio $\mathcal{B}_{\max}^{\text{A2HDM}}(t \to cg(g))$ will change only slightly when $m_{H^\pm} \gtrsim 600 \ (400)$ GeV. These observations motivate our choice of the upper limits for the charged-Higgs mass mentioned before. On the other hand, although being enhanced by about three orders of magnitude relative to the SM prediction, the maximum branching ratio of $t \to cg$ decay that can be reached in the A2HDM, $\mathcal{B}_{\max}^{\text{A2HDM}}(t \to cg) = 3.36 \times 10^{-9}$, is still at least one order of magnitude lower than the projected 95%-CL limits at the future colliders, which are estimated to be 3.21×10^{-5} at the HL-LHC with 3-ab^{-1} luminosity data [107,108], and of $\mathcal{O}(10^{-7}-10^{-8})$ at the 100-TeV FCC-hh with an integrated luminosity of 10 ab^{-1} [113,114], respectively. As a consequence, the predicted branching ratios of $t \to cg$ and $t \to cgg$ decays in the A2HDM are still out of the expected sensitivities of the future HL-LHC and FCC-hh.

---

[9] Here the plots are obtained by firstly calculating the maximum branching ratios of $t \to cg$ and $t \to cgg$ decays with different values of $m_{H^\pm}$ and the same set of alignment parameters $(\varsigma_u, \varsigma_d) \simeq (-0.047, -48)$, and then constructing an interpolation of the maximum branching ratios as a function of $m_{H^\pm}$.

[10] Numerically, we find that the maximum branching ratios of $t \to cg$ and $t \to cgg$ decays in the A2HDM are given by 6.63×10^{-12} for $m_{H^\pm} = 600$ GeV and 8.60×10^{-10} for $m_{H^\pm} = 400$ GeV respectively, which indeed approach the corresponding SM predictions given by Eqs. (4.5) and (4.6).

Fig. 5 The dependence of the maximum branching ratios of $t \rightarrow cg$ (left) and $t \rightarrow cgg$ (right) on the charged-Higgs mass $m_{H^\pm}$, with the alignment parameters fixed at $(\varsigma_u, \varsigma_d) \simeq (-0.047, -48)$. The horizontal dash-dotted lines represent the SM predictions given by Eqs. (4.5) and (4.6), respectively
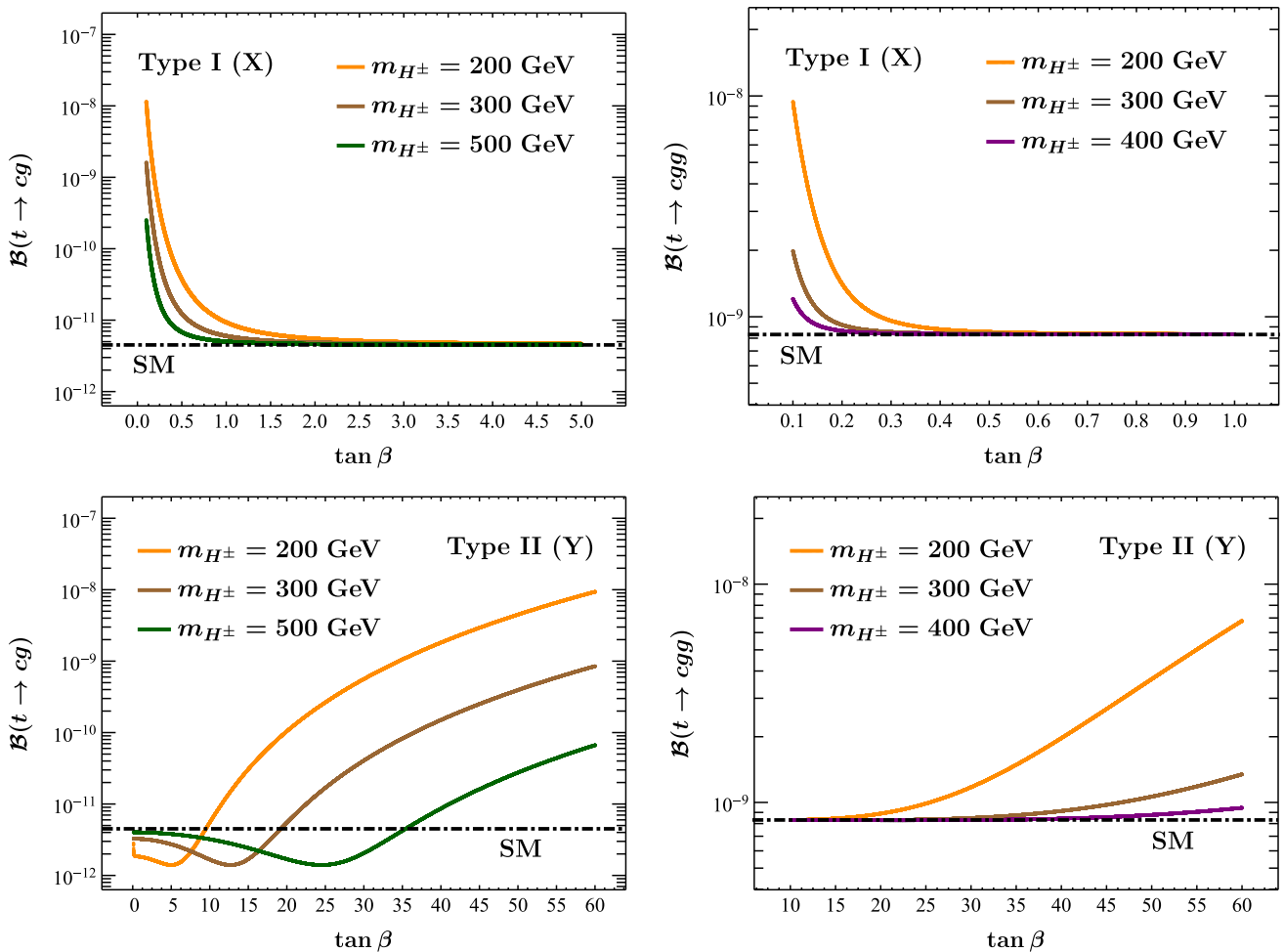
4.3 $\mathcal{B}(t \rightarrow cg(g))$ in the conventional 2HDMs with $\mathcal{Z}_2$ symmetries

Let us now discuss the branching ratios of $t \rightarrow cg$ and $t \rightarrow cgg$ decays in the four conventional 2HDMs with $\mathcal{Z}_2$ symmetries, the Yukawa types of which have been given explicitly in Table 1. As only the charged-Higgs interactions with the quark sector are involved, we are actually left with only two different cases, type-I (type-X) 2HDM with $\varsigma_d = \varsigma_u = 1/\tan \beta$, and type-II (type-Y) 2HDM with $\varsigma_d = -1/\varsigma_u = -\tan \beta$. Here, to predict the branching ratios of $t \rightarrow cg$ and $t \rightarrow cgg$ decays, we need only the knowledge of the charged-Higgs mass $m_{H^\pm}$ and the parameter $\tan \beta$, both of which receive severe constraints from many flavour processes and theoretical considerations [161–164]. For convenience, we show in Fig. 6 the dependence of the two branching ratios $\mathcal{B}(t \rightarrow cg)$ (left) and $\mathcal{B}(t \rightarrow cgg)$ (right) on $\tan \beta$, for three different choices of $m_{H^\pm}$, in the four conventional 2HDMs with $\mathcal{Z}_2$ symmetries. It should be noted that the branching ratios of $t \rightarrow cg$ and $t \rightarrow cgg$ decays are calculated in these four models by varying $\tan \beta = [0.1, 60]$, while the ranges where the resulting branching ratios are not significantly enhanced compared with the corresponding SM predictions are not shown in Fig. 6. It can be seen that the sensitivity of the two branching ratios to $m_{H^\pm}$ occurs at low and high $\tan \beta$ for the type-I (type-X) and the type-II (type-Y) 2HDM respectively, and such a sensitivity becomes, however, less significant for larger $m_{H^\pm}$.

For the type-II 2HDM, the branching ratio of the weak radiative decay $\bar{B} \rightarrow X_s \gamma$ plays a significant role in setting a lower bound on the charged-Higgs mass $m_{H^\pm}$, with the latest updated results given by $m_{H^\pm} \gtrsim 800$ GeV at 95% CL [165] and $m_{H^\pm} \gtrsim 790\,(1510)$ GeV at $2\sigma\,(1\sigma)$ [166]. These bounds are nearly $\tan \beta$-independent for $\tan \beta > 2$

and show a strong dependence on $\tan \beta$ only for $\tan \beta < 2$ [167]. Quite recently, a comprehensive study of the allowed parameter space of the type-II 2HDM has been performed by combining the most recent flavour, collider, and electroweak precision observables with theoretical constraints, with the best fit point lying around $m_{H^\pm} \simeq 2$ TeV and $\tan \beta \simeq 4$ [166]. The experimental lower bound on $m_{H^\pm}$ from direct collider searches is, however, only $m_{H^\pm} \gtrsim 160$ GeV [157], and hence well below the indirect constraints from flavour physics. With these bounds taken into account, it is then found that the branching ratios of both $t \rightarrow cg$ and $t \rightarrow cgg$ decays remain almost identical with the corresponding SM predictions, as given by Eqs. (4.5) and (4.6) respectively. The same conclusion can also be applied to the type-Y 2HDM, because its Yukawa type shares the same coupling pattern for the quarks as of the type-II 2HDM [162]. In fact, for these two types of 2HDMs, we have $\varsigma_d = -1/\varsigma_u = -\tan \beta$ and hence $\varsigma_d \varsigma_u = -1$, while the region $\varsigma_d \varsigma_u < 0$ is almost excluded by the current data on the branching ratio of the weak radiative decay $\bar{B} \rightarrow X_s \gamma$ [60]. This also implies that significant enhancements of the branching ratios of $t \rightarrow cg$ and $t \rightarrow cgg$ decays relative to the SM predictions are impossible in these two types of 2HDMs.

For the type-I (type-X) 2HDM, on the other hand, a 95%-CL lower limit on $m_{H^\pm}$ from the branching ratio of $\bar{B} \rightarrow X_s \gamma$ can be derived for low $\tan \beta$ only [167]. As an illustration, a bound $\tan \beta \lesssim 2.5$ can be set when the robust lower charged-Higgs mass limit $m_{H^\pm} \gtrsim 80$ GeV from the combined charged-Higgs searches at LEP [156] is considered. A detailed analysis of the phenomenological status of the charged-Higgs sector in the conventional 2HDMs with $\mathcal{Z}_2$ symmetries has been performed by combing all the constraints from direct collider searches for charged and neutral Higgs bosons, as well as the most relevant constraints from

Fig. 6 The branching ratios of $t \to cg$ (left) and $t \to cgg$ (right) as a function of the parameter $\tan \beta = [0.1, 60]$, for three different choices of the charged-Higgs mass $m_{H^\pm}$, in the four conventional 2HDMs with $\mathcal{Z}_2$ symmetries. The horizontal dash-dotted lines represent the SM predictions. We show only the ranges of $\tan \beta$ where the resulting branching ratios display significant enhancements compared with the corresponding SM predictions. Note that the charged-Higgs mass $m_{H^\pm}$ in type-II (type-Y) 2HDM is already bounded to be larger than 600 GeV [165–167], while the parameter $\tan \beta$ in type-I (type-X) 2HDM is constrained to be larger than one [162], both of which imply that no significant enhancements of the branching ratios are possible in these conventional 2HDMs

flavour physics [162]. Using the combined flavour constraints at 95% CL obtained there, we extract the values $\tan \beta \simeq 1.8$ for $m_{H^\pm} = 200 \, \text{GeV}$, $\tan \beta \simeq 1.5$ for $m_{H^\pm} = 300 \, \text{GeV}$, and $\tan \beta \simeq 1.2$ for $m_{H^\pm} = 500 \, \text{GeV}$ [162]. With these typical values taken as inputs, the corresponding branching ratios of $t \to cg$ and $t \to cgg$ decays are given in Table 4. It can be seen that, in these two types of 2HDMs, the branching ratio of $t \to cg$ decay is predicted to be of the same order as in the SM (cf. Eq. (4.5)), while the branching ratio of $t \to cgg$ decay remains almost identical with the SM expectation (cf. Eq. (4.6)).

In fact, at low $\tan \beta$, the flavour constraints are similar among all the four conventional 2HDMs with $\mathcal{Z}_2$ symmetries, because the contributions in this case are now dominated by the universal charged-Higgs couplings to the up-type quarks

(cf. Table 1). Then, it is found that values of $\tan \beta < 1$ are ruled out for all values of $m_{H^\pm} < 650 \, \text{GeV}$, irrespective of the Yukawa types considered [162]. As a summary, we can therefore conclude that, compared with the SM predictions, no significant enhancements are observed in the four conventional 2HDMs with $\mathcal{Z}_2$ symmetries for the branching ratios of both $t \to cg$ and $t \to cgg$ decays, once the flavour constraints on the model parameters are taken into account.

4.4 Further discussions and comments

Let us now explain why the "higher-order dominance" phenomenon is more obvious within the SM than in the A2HDM as well as the four conventional 2HDMs with $\mathcal{Z}_2$ symmetries. Naively, one would expect that the rate of the two-body decay

Table 4 The branching ratios of $t \to cg$ and $t \to cgg$ decays in the type-I (type-X) 2HDM, with three sets of input parameters of $(m_{H^\pm}, \tan \beta)$ extracted from Ref. [162]

$(m_{H^\pm} \text{ [GeV]}, \tan \beta)$	(200, 1.8)	(300, 1.5)	(500, 1.2)
$\mathcal{B}^{\text{Type I}(X)}(t \to cg)$	5.75×10^{-12}	5.13×10^{-12}	4.85×10^{-12}
$\mathcal{B}^{\text{Type I}(X)}(t \to cgg)$	8.32×10^{-10}	8.31×10^{-10}	8.31×10^{-10}

$t \to cg$ is larger than that of the three-body decay $t \to cgg$, due to the coupling-constant and phase-space suppression of the latter. This is, however, not true within the SM; instead, we find that the predicted branching ratio of $t \to cgg$ is about two orders of magnitude larger than that of $t \to cg$ (cf. Eqs. (4.5) and (4.6)) [39]. To understand such a "higher-order dominance" phenomenon, one should firstly note that both the $t \to cg$ and $t \to cgg$ decays are dominated by the one-loop effective vertex $V_{tcg^*}^{\mu}$, which can be generically written as [3]

$$V_{tcg^*}^{\mu} = \left(k^2 \gamma^{\mu} - k^{\mu} \slashed{k}\right) \left(F_1^L P_L + F_1^R P_R\right) + i \sigma^{\mu\nu} k_{\nu} \left(F_2^L m_c P_L + F_2^R m_t P_R\right), \tag{4.9}$$

as required by Lorentz and gauge invariance. Here we have suppressed both the colour labels and a sum over the internal quark flavours together with the CKM matrix elements. The form factors $F_1^{L,R}$ and $F_2^{L,R}$ are a function of the gluon virtuality k^2, and are called the monopolar (or charge radius) and the dipolar (or dipole moment) form factors, respectively. Note that when $k^2 \to 0$, i.e., when the gluon goes on-shell, the $F_1^{L,R}$ contributions vanish. Therefore, the two-body decay $t \to cg$ is entirely determined by the dipole structure, while both the dipole and the monopole structure contribute to the three-body decay $t \to cgg$. It also turns out that the contribution from the monopolar form factors can be considerably larger than from the dipolar ones within the SM [39–42]. This explains the "higher-order dominance" phenomenon observed within the SM. For the A2HDM, however, the charged-Higgs enhancements are mostly through the dipolar form factors, and hence show up only through a greatly enhanced branching ratio of the two-body decay $t \to cg$. This helps us to understand why the branching ratios of $t \to cg$ and $t \to cgg$ decays are predicted to be of the same order in the A2HDM. For the four conventional 2HDMs with $\mathcal{Z}_2$ symmetries, on the other hand, after taking into account the relevant flavour constraints on the model parameters, significant enhancements are no longer allowed for the branching ratios of both $t \to cg$ and $t \to cgg$ decays.

Finally, we would like to make a brief comment on the observability of $t \to cgg$ decay. Note that this process can generally be treated in twofold way: One can either treat it inclusively with $t \to cg$ or consider it as a separate channel [21]. The former means that the process $t \to cgg$ can be

considered as a QCD correction to the $t \to cg$ decay by assuring that two of the three final-state jets are collinear so that only two can be resolved by the detector. The latter is especially promising if the branching ratio of $t \to cgg$ is considerably larger than that of $t \to cg$, as observed within the SM [39]. However, to detect $t \to cgg$ before $t \to cg$, one must avoid collinearity by applying certain cuts. To this end, the cutoff parameter C introduced in the phase space plays an essential role in distinguishing the $t \to cgg$ from the $t \to cg$ decay. Here, C must be taken in the range of jet-energy resolution of the detector, and a better jet resolution will be definitely welcome.

5 Conclusion

In this paper, we have firstly updated the SM predictions for the branching ratios of both $t \to cg$ and $t \to cgg$ decays, with the results given respectively by $\mathcal{B}^{\text{SM}}(t \to cg) = 4.50 \times 10^{-12}$ and $\mathcal{B}^{\text{SM}}(t \to cgg) = 8.31 \times 10^{-10}$, finding that the latter is about two orders of magnitude larger than the former, which is a clear demonstration of the "higher-order dominance" phenomenon observed in Ref. [39]. This is due to the fact that the contribution from the monopolar form factors can be considerably larger than from the dipolar ones within the SM [39–42]. Note that the branching ratio of the three-body decay $t \to cgg$ is obtained with the cutoff parameter $C = 0.01$.

To check if such a "higher-order dominance" phenomenon is also applied in the A2HDM as well as in the four conventional 2HDMs with $\mathcal{Z}_2$ symmetries, we have also evaluated the maximum branching ratios of $t \to cg$ and $t \to cgg$ decays that can be reached in these different models. After taking into account the relevant constraints on the model parameters resulting from a global fit obtained at the 95.5% CL [75], we find that the branching ratios of $t \to cg$ and $t \to cgg$ decays can reach up to 3.36×10^{-9} and 2.95×10^{-9} respectively, being therefore of the same order, in the A2HDM. This is obviously different from the SM case, and can be understood by the fact that the charged-Higgs enhancements are mostly through the dipolar form factors, and hence show up only through a greatly enhanced branching ratio of the two-body decay $t \to cg$. On the other hand, compared with the SM predictions, significant enhancements are no longer possible in the four conventional

2HDMs with $\mathcal{Z}_2$ symmetries for the branching ratios of these two decays, once the flavour constraints on the model parameters [162,166] are properly taken into account.

Nevertheless, the predicted branching ratios of $t \to cg$ and $t \to cgg$ decays in the A2HDM are still out of the expected sensitivities of the future HL-LHC and FCC-hh. To have an opportunity to detect $t \to cgg$ before $t \to cg$, we have to improve the jet resolution of the future detector. Note that, due to the imaginary components of the loop functions, the CKM matrix elements, as well as the complex alignment parameters $\varsigma_{u,d}$ in the A2HDM, it would also be interesting to investigate the CP asymmetries in these rare top-quark decays [14,27].

Data Availability Statement This manuscript has no associated data or the data will not be deposited. [Authors' comment: Since this work is of theoretical nature, there is no data to deposit.]

Appendix A: The *R* functions relevant for $t \to cgg$ decay

In this appendix, we give the explicit expressions of the remaining *R* functions present in Eqs. (3.12)–(3.14). For convenience, the scalar products involved are defined in the same way as in Ref. [39], with

$$SP1 = \epsilon^*(k_3) \cdot \epsilon^*(k_4), \quad SP2 = \epsilon^*(k_3) \cdot k_1, \quad SP3 = \epsilon^*(k_3) \cdot k_2,$$
$$SP4 = \epsilon^*(k_4) \cdot k_1, \qquad SP5 = \epsilon^*(k_4) \cdot k_2. \qquad (A.1)$$

For the vertex part (cf. Eq. (3.12)), we have

$$
\begin{aligned}
R_1^{\text{vertex}} = & -(SP1\, F_5 - F_{16})(m_W^2(1 - 2(B_0^{(3)}(m_W^2) \\
& - 2C_{00}^{(3)}(m_W^2) - s_{23}C_2^{(3)}(m_W^2))) \\
& - m_b^2(m_t^2(C_0^{(3)}(m_W^2) + C_2^{(3)}(m_W^2) + X_{dd}C_2^{(3)}(m_{H^\pm}^2)
\end{aligned}
$$

$$
\begin{aligned}
& + X_{du}C_0^{(3)}(m_{H^\pm}^2)) + B_0^{(3)}(m_W^2) \\
& + X_{dd}B_0^{(3)}(m_{H^\pm}^2) - 2(C_{00}^{(3)}(m_W^2) + X_{dd}C_{00}^{(3)}(m_{H^\pm}^2)))) \\
& + m_t(s_{23}(SP1\, F_1 - F_{12}) \\
& \times (2m_W^2 C_2^{(3)}(m_W^2) - m_b^2(C_0^{(3)}(m_W^2) + C_2^{(3)}(m_W^2) \\
& + X_{dd}C_2^{(3)}(m_{H^\pm}^2) + X_{du}C_0^{(3)}(m_{H^\pm}^2))) \\
& + 2SP4(2SP3\, F_1 - F_{13})(m_b^2(C_0^{(3)}(m_W^2) + 2C_2^{(3)}(m_W^2) \\
& + C_{22}^{(3)}(m_W^2) + X_{dd}(C_{12}^{(3)}(m_{H^\pm}^2) + C_2^{(3)}(m_{H^\pm}^2) \\
& + C_{22}^{(3)}(m_{H^\pm}^2)) + X_{du}(C_0^{(3)}(m_{H^\pm}^2) \\
& + C_2^{(3)}(m_{H^\pm}^2))) + 2m_W^2 C_{22}^{(3)}(m_W^2) \\
& + (m_b^2 + 2m_W^2)C_{12}^{(3)}(m_W^2))) \\
& + F_3(-(m_t^2(SP4C_2^{(3)}(m_W^2) - SP5\, X_{dd}C_2^{(3)}(m_{H^\pm}^2)) \\
& + SP4(B_0^{(3)}(m_W^2) - 2C_{00}^{(3)}(m_W^2)) \\
& + (SP4 - SP5)(m_t^2(C_0^{(3)}(m_W^2) + X_{du}C_0^{(3)}(m_{H^\pm}^2)) \\
& + (B_0^{(3)}(m_{H^\pm}^2) - 2C_{00}^{(3)}(m_{H^\pm}^2))X_{dd})m_b^2 + (SP4 \\
& - SP5)m_W^2 + (B_0^{(3)}(m_W^2) - 2C_{00}^{(3)}(m_W^2))(SP5m_b^2 \\
& - 2(SP4 - SP5)m_W^2) + C_2^{(3)}(m_W^2) \\
& \times (SP5m_b^2 m_t^2 - 2s_{23}(SP4 + SP5)m_W^2) \\
& - SP4((2s_{23}C_{12}^{(3)}(m_{H^\pm}^2) \\
& + m_t^2 C_2^{(3)}(m_{H^\pm}^2))X_{dd}m_b^2 + 2s_{23}C_{12}^{(3)}(m_W^2)(m_b^2 + 2m_W^2))) \\
& + SP3\, F_4((4(C_{00}^{(3)}(m_W^2) \\
& + C_{00}^{(3)}(m_{H^\pm}^2)X_{dd}) - 2((C_0^{(3)}(m_W^2) + C_2^{(3)}(m_W^2) \\
& + C_2^{(3)}(m_{H^\pm}^2)X_{dd} + C_0^{(3)}(m_{H^\pm}^2)X_{du})m_t^2 + B_0^{(3)}(m_W^2) \\
& + B_0^{(3)}(m_{H^\pm}^2)X_{dd}))m_b^2 \\
& + (-4B_0^{(3)}(m_W^2) + 8C_{00}^{(3)}(m_W^2) + 4s_{23}C_2^{(3)}(m_W^2) + 2)m_W^2), \\
& \hspace{8cm} (A.2)
\end{aligned}
$$

$$
\begin{aligned}
R_2^{\text{vertex}} = & (2(s_{23}(SP4 - SP5)C_2^{(2)}(m_W^2)F_3 + SP3\, F_4)m_W^2 \\
& - (SP1\, F_5 - F_{16})((-2B_0^{(3)}(m_W^2) \\
& + 4C_{00}^{(2)}(m_W^2) + 2s_{23}C_2^{(2)}(m_W^2) + 1)m_W^2 - m_b^2((C_0^{(2)}(m_W^2) \\
& + C_0^{(2)}(m_{H^\pm}^2)X_{du})m_t^2 + B_0^{(3)}(m_W^2) \\
& + B_0^{(3)}(m_{H^\pm}^2)X_{dd} - 2(C_{00}^{(2)}(m_W^2) \\
& + C_{00}^{(2)}(m_{H^\pm}^2)X_{dd}))) + (SP4 - SP5)F_3 \\
& \times (-B_0^{(3)}(m_{H^\pm}^2)X_{dd}m_b^2 + (2(C_{00}^{(2)}(m_W^2) \\
& + C_{00}^{(2)}(m_W^2)X_{dd}) - m_t^2(C_0^{(2)}(m_W^2) + C_0^{(2)}(m_{H^\pm}^2)X_{du}))m_b^2 \\
& + (4C_{00}^{(2)}(m_W^2) + 1)m_W^2 - B_0^{(3)}(m_W^2)(m_b^2 + 2m_W^2)) \\
& - SP3\, F_4(4(B_0^{(3)}(m_W^2) - 2C_{00}^{(2)}(m_W^2))m_W^2 \\
& + 2((-(C_2^{(2)}(m_W^2) + C_2^{(2)}(m_{H^\pm}^2)X_{du})m_t^2 \\
& + B_0^{(3)}(m_W^2) + B_0^{(3)}(m_{H^\pm}^2)X_{dd} - 2(C_{00}^{(2)}(m_W^2) \\
& + C_{00}^{(2)}(m_{H^\pm}^2)X_{dd}))m_b^2 \\
& + s_{23}(C_{12}^{(2)}(m_{H^\pm}^2)X_{dd}m_b^2 + C_{12}^{(2)}(m_W^2)(m_b^2 + 2m_W^2)))) \\
& + m_t(-F_{12}((1 - 2(B_0^{(3)}(m_W^2) \\
& - 2C_{00}^{(2)}(m_W^2) - s_{23}C_2^{(2)}(m_W^2)))m_W^2 - m_b^2(B_0^{(3)}(m_W^2) \\
& + B_0^{(3)}(m_{H^\pm}^2)X_{dd} - 2(C_{00}^{(2)}(m_W^2) + C_{00}^{(2)}(m_{H^\pm}^2)X_{dd}) \\
& + s_{23}(C_0^{(2)}(m_W^2) + C_0^{(2)}(m_{H^\pm}^2)X_{du})))
\end{aligned}
$$

$-\text{SP3}\,F_{14}((2(C_{12}^{(2)}(m_W^2)+C_{12}^{(2)}(m_{H^\pm}^2)X_{dd})$

$-2(C_0^{(2)}(m_W^2)+C_2^{(2)}(m_W^2)$

$+(C_0^{(2)}(m_{H^\pm}^2)+C_2^{(2)}(m_{H^\pm}^2))X_{du})m_b^2+4(C_{12}^{(2)}(m_W^2)$

$+C_2^{(2)}(m_W^2))m_W^2)$

$+F_1(-((s_{23}\text{SP1}-2\text{SP3}(\text{SP4}-\text{SP5}))C_0^{(2)}(m_W^2)$

$-2(\text{SP1}(C_{00}^{(2)}(m_W^2)+C_{00}^{(2)}(m_{H^\pm}^2)X_{dd})$

$+\text{SP3}(\text{SP4}-\text{SP5})C_0^{(2)}(m_{H^\pm}^2)X_{du})m_b^2$

$+2C_2^{(2)}(m_W^2)(s_{23}\text{SP1}m_W^2$

$+\text{SP3}(\text{SP4}-\text{SP5})(m_b^2-2m_W^2))$

$+\text{SP1}(-(B_0^{(3)}(m_{H^\pm}^2)X_{dd}+s_{23}C_0^{(2)}(m_{H^\pm}^2)X_{du})m_b^2$

$+(4C_{00}^{(2)}(m_W^2)+1)m_W^2-B_0^{(3)}(m_W^2)(m_b^2+2m_W^2))$

$-2\text{SP3}(\text{SP4}-\text{SP5})((C_{12}^{(2)}(m_{H^\pm}^2)X_{dd}$

$-C_2^{(2)}(m_{H^\pm}^2)X_{du})m_b^2+C_{12}^{(2)}(m_W^2)(m_b^2+2m_W^2)))), \quad (A.3)$

$R_3^{\text{vertex}}=-((2(\text{SP4}-\text{SP5})tC_2^{(5)}(m_W^2)F_3-2\text{SP2}\,F_4)m_W^2$

$-\text{SP1}\,F_5((-2B_0^{(4)}(m_W^2)$

$+4C_{00}^{(5)}(m_W^2)+2tC_2^{(5)}(m_W^2)+1)m_W^2$

$-m_b^2(m_t^2(C_0^{(5)}(m_W^2)+C_2^{(5)}(m_W^2)$

$+C_2^{(5)}(m_{H^\pm}^2)X_{dd}+C_0^{(5)}(m_{H^\pm}^2)X_{du}$

$+B_0^{(4)}(m_W^2)+B_0^{(4)}(m_{H^\pm}^2)X_{dd}-2(C_{00}^{(5)}(m_W^2)$

$+C_{00}^{(5)}(m_{H^\pm}^2)X_{dd})))-F_{16}((1-2(B_0^{(4)}(m_W^2)$

$-2C_{00}^{(5)}(m_W^2)-tC_2^{(5)}(m_W^2)))m_W^2$

$-m_b^2(m_t^2(C_0^{(5)}(m_W^2)+C_2^{(5)}(m_W^2)$

$+C_2^{(5)}(m_{H^\pm}^2)X_{dd}+C_0^{(5)}(m_{H^\pm}^2)X_{du}$

$+B_0^{(4)}(m_W^2)+B_0^{(4)}(m_{H^\pm}^2)X_{dd}-2(C_{00}^{(5)}(m_W^2)$

$+C_{00}^{(5)}(m_{H^\pm}^2)X_{dd}))$

$+(\text{SP4}-\text{SP5})F_3(-B_0^{(4)}(m_{H^\pm}^2)X_{dd}m_b^2$

$+m_b^2(2(C_{00}^{(5)}(m_W^2)+C_{00}^{(5)}(m_{H^\pm}^2)X_{dd})$

$-m_t^2(C_0^{(5)}(m_W^2)+C_2^{(5)}(m_W^2)+C_2^{(5)}(m_{H^\pm}^2)X_{dd}$

$+C_0^{(5)}(m_{H^\pm}^2)X_{du})$

$+(4C_{00}^{(5)}(m_W^2)+1)m_W^2-B_0^{(4)}(m_W^2)(m_b^2+2m_W^2))$

$+\text{SP2}\,F_4(-(2m_b^2(C_2^{(5)}(m_W^2)$

$+C_{22}^{(5)}(m_W^2)+C_{22}^{(5)}(m_{H^\pm}^2)X_{dd}$

$+C_2^{(5)}(m_{H^\pm}^2)X_{du}$

$+4C_{22}^{(5)}(m_W^2)m_W^2)m_t^2$

$+4m_W^2(B_0^{(4)}(m_W^2)-2C_{00}^{(5)}(m_W^2))$

$+2((-C_{12}^{(5)}(m_W^2)m_t^2+B_0^{(4)}(m_W^2)+(B_0^{(4)}(m_{H^\pm}^2)$

$-(s_{23}+t_{12})C_{12}^{(5)}(m_{H^\pm}^2))X_{dd}-2(C_{00}^{(5)}(m_W^2)$

$+C_{00}^{(5)}(m_{H^\pm}^2)X_{dd})m_b^2+C_{12}^{(5)}(m_W^2)(tm_b^2$

$-2(s_{23}+t_{12})m_W^2)))+m_t(-\text{SP2}\,F_{14}(2m_b^2(C_0^{(5)}(m_W^2)$

$+C_{12}^{(5)}(m_W^2)+C_{22}^{(5)}(m_W^2)$

$+(C_{12}^{(5)}(m_{H^\pm}^2)+C_{22}^{(5)}(m_{H^\pm}^2))X_{dd}$

$+C_0^{(5)}(m_{H^\pm}^2)X_{du}$

$+C_2^{(5)}(m_{H^\pm}^2)(X_{dd}+X_{du}))$

$+4(C_2^{(5)}(m_W^2)m_b^2+(C_{12}^{(5)}(m_W^2)$

$+C_{22}^{(5)}(m_W^2))m_W^2))+F_{12}(m_W^2(-2B_0^{(4)}(m_W^2)$

$+4C_{00}^{(5)}(m_W^2)+1)-m_b^2(B_0^{(4)}(m_W^2)$

$+B_0^{(4)}(m_{H^\pm}^2)X_{dd}-2(C_{00}^{(5)}(m_W^2)$

$+C_{00}^{(5)}(m_{H^\pm}^2)X_{dd})+(s_{23}+t_{12})(C_0^{(5)}(m_W^2)$

$+C_2^{(5)}(m_W^2)$

$+C_2^{(5)}(m_{H^\pm}^2)X_{dd}$

$+C_0^{(5)}(m_{H^\pm}^2)X_{du}))-F_1(m_b^2((s_{23}\text{SP1}+t_{12}\text{SP1}$

$+\text{SP2}(2\text{SP5}-2\text{SP4}))C_0^{(5)}(m_W^2)$

$-(4\text{SP2}(\text{SP4}-\text{SP5})+\text{SP1}t)C_2^{(5)}(m_W^2)$

$-\text{SP1}(-C_2^{(5)}(m_W^2)m_t^2+2C_{00}^{(5)}(m_W^2)$

$+(2C_{00}^{(5)}(m_{H^\pm}^2)+tC_2^{(5)}(m_{H^\pm}^2))X_{dd}$

$-2\text{SP2}(\text{SP4}C_{22}^{(5)}(m_W^2)$

$+(\text{SP4}-\text{SP5})C_{22}^{(5)}(m_{H^\pm}^2)X_{dd}$

$-(2\text{SP2}(\text{SP4}-\text{SP5})+\text{SP1}t)C_0^{(5)}(m_{H^\pm}^2)X_{du}$

$+C_2^{(5)}(m_{H^\pm}^2)(\text{SP1}m_t^2X_{dd}$

$-2\text{SP2}(\text{SP4}-\text{SP5})(X_{dd}+X_{du})))$

$+2\text{SP2}((C_{12}^{(5)}(m_W^2)$

$+C_{22}^{(5)}(m_W^2))(\text{SP5}m_b^2-2(\text{SP4}-\text{SP5})m_W^2)$

$-m_b^2(\text{SP4}C_{12}^{(5)}(m_W^2)$

$+(\text{SP4}-\text{SP5})C_{12}^{(5)}(m_{H^\pm}^2)X_{dd})$

$-\text{SP1}(-m_b^2(C_0^{(5)}(m_{H^\pm}^2)X_{du}m_t^2$

$+B_0^{(4)}(m_{H^\pm}^2)X_{dd}$

$+(4C_{00}^{(5)}(m_W^2)+1)m_W^2-B_0^{(4)}(m_W^2)(m_b^2+2m_W^2))))),$

$\qquad\qquad (A.4)$

$R_4^{\text{vertex}}=F_{16}((-2B_0^{(4)}(m_W^2)+4C_{00}^{(4)}(m_W^2)$

$+2tC_2^{(4)}(m_W^2)+1)m_W^2-m_b^2((C_0^{(4)}(m_W^2)$

$+C_0^{(4)}(m_{H^\pm}^2)X_{du})m_t^2+B_0^{(4)}(m_W^2)$

$+B_0^{(4)}(m_{H^\pm}^2)X_{dd}-2(C_{00}^{(4)}(m_W^2)$

$+C_{00}^{(4)}(m_{H^\pm}^2)X_{dd}))$

$+\text{SP1}\,F_5(m_W^2(1-2(B_0^{(4)}(m_W^2)-2C_{00}^{(4)}(m_W^2)$

$-tC_2^{(4)}(m_W^2)))$

$-m_b^2((C_0^{(4)}(m_W^2)+C_0^{(4)}(m_{H^\pm}^2)X_{du})m_t^2$

$+B_0^{(4)}(m_W^2)+B_0^{(4)}(m_{H^\pm}^2)X_{dd}$

$-2(C_{00}^{(4)}(m_W^2)+C_{00}^{(4)}(m_{H^\pm}^2)X_{dd}))$

$+m_t(((s_{23}\text{SP1}+t_{12}\text{SP1}+4\text{SP2}\,\text{SP5})F_1$

$+(s_{23}+t_{12})F_{12}-2\text{SP5}\,F_{13})(C_0^{(4)}(m_W^2)$

$+C_0^{(4)}(m_{H^\pm}^2)X_{du})m_b^2+2\text{SP5}(2\text{SP2}\,F_1$

$-F_{13})(-m_b^2(C_{12}^{(4)}(m_{H^\pm}^2)X_{dd}-C_2^{(4)}(m_{H^\pm}^2)X_{du})$

$-C_{12}^{(4)}(m_W^2)(m_b^2+2m_W^2)$

$+C_2^{(4)}(m_W^2)(m_b^2-2m_W^2)))+\text{SP2}\,F_4(m_b^2(4(C_{00}^{(4)}(m_W^2)$

$+C_{00}^{(4)}(m_{H^\pm}^2)X_{dd})$

$-2((C_0^{(4)}(m_W^2)+C_0^{(4)}(m_{H^\pm}^2)X_{du})m_t^2$

$$+B_0^{(4)}(m_W^2) + B_0^{(4)}(m_{H^\pm}^2)X_{dd}))$$
$$+(-4B_0^{(4)}(m_W^2) + 8C_{00}^{(4)}(m_W^2) + 4tC_2^{(4)}(m_W^2) + 2)m_W^2)$$
$$-F_3(-(SP4(B_0^{(4)}(m_W^2)$$
$$-2C_{00}^{(4)}(m_W^2)) + (SP4 - SP5)((C_0^{(4)}(m_W^2)$$
$$+C_0^{(4)}(m_{H^\pm}^2)X_{du})m_t^2 + (B_0^{(4)}(m_{H^\pm}^2)$$
$$-2C_{00}^{(4)}(m_{H^\pm}^2))X_{dd})m_b^2$$
$$+(SP4 - SP5 + 2(SP4 + SP5)tC_2^{(4)}(m_W^2))m_W^2$$
$$+(B_0^{(4)}(m_W^2) - 2C_{00}^{(4)}(m_W^2))(SP5\,m_b^2 - 2(SP4 - SP5)m_W^2)$$
$$-SP5(4C_2^{(4)}(m_W^2)m_t^2 m_W^2$$
$$+2(s_{23}+t_{12})(C_{12}^{(4)}(m_{H^\pm}^2)X_{dd}m_b^2$$
$$+C_{12}^{(4)}(m_W^2)(m_b^2 + 2m_W^2)))), \tag{A.5}$$

$$R_5^{\text{vertex}} = X_{dd}m_b^2(2C_{00}^{(6)}(m_{H^\pm}^2)$$
$$\times(2(SP4 - SP5)F_3 + 2(SP3 - SP2)F_4 - 2SP1\,F_5$$
$$+SP1\,F_1 m_t)$$
$$+C_0^{(6)}(m_{H^\pm}^2)(m_b^2 - m_{H^\pm}^2)(2(SP4 - SP5)F_3$$
$$+2(SP3 - SP2)F_4 - 2SP1\,F_5$$
$$+SP1\,F_1 m_t + m_t(C_{12}^{(6)}(m_{H^\pm}^2)F_1(SP1\,m_t^2 - 4SP3\,SP4$$
$$+4SP2\,SP5 - SP1(2t + t_{12}))$$
$$+C_1^{(6)}(m_{H^\pm}^2)m_t(2(SP5 - SP4)F_3$$
$$+2(SP2 - SP3)F_4$$
$$+SP1(2F_5 - F_1 m_t))))$$
$$+m_t(F_1(SP1\,m_t^2 - 4SP3\,SP4$$
$$+4SP2\,SP5 - SP1(2t + t_{12}))(C_{12}^{(6)}(m_W^2) - C_2^{(6)}(m_W^2))$$
$$+m_t(2C_0^{(6)}(m_W^2)((SP2 - SP3)F_4$$
$$+SP1(F_5 - F_1 m_t)) + C_1^{(6)}(m_W^2)(2(SP5 - SP4)F_3$$
$$+2(SP2 - SP3)F_4 + SP1(2F_5 - F_1 m_t)))$$
$$+(-SP1(2C_0^{(6)}(m_{H^\pm}^2) + C_2^{(6)}(m_{H^\pm}^2))F_1 m_t^2$$
$$+2C_0^{(6)}(m_{H^\pm}^2)((SP5 - SP4)F_3$$
$$+(SP2 - SP3)F_4 + SP1\,F_5)m_t + (4SP3\,SP4$$
$$-4SP2\,SP5 + 2SP1t + SP1t_{12})(C_0^{(6)}(m_{H^\pm}^2)$$
$$+C_2^{(6)}(m_{H^\pm}^2))F_1)X_{du}m_b^2$$
$$+(2SP1\,m_t^3(-C_1^{(6)}(m_W^2) + C_{12}^{(6)}(m_W^2)$$
$$+2C_2^{(6)}(m_W^2))F_1 - 4(C_2^{(6)}(m_W^2) - C_1^{(6)}(m_W^2))$$
$$\times((SP5 - SP4)F_3 + (SP2 - SP3)F_4 + SP1\,F_5)m_t^2$$
$$+F_1 m_t(SP1\,C_0^{(6)}(m_W^2)m_b^2 + SP1$$
$$-2(4SP3\,SP4 - 4SP2\,SP5 + 2SP1t$$
$$+SP1t_{12})C_{12}^{(6)}(m_W^2) + (-4m_t^2 SP1 + 4s_{23}SP1$$
$$-8SP3\,SP4 + 8SP2\,SP5)C_2^{(6)}(m_W^2))$$
$$-2((SP4 - SP5)F_3 + (SP3 - SP2)F_4$$
$$-SP1\,F_5)(-C_0^{(6)}(m_W^2)m_b^2 + 2t_{12}C_2^{(6)}(m_W^2) - 1))m_W^2$$
$$+C_0^{(6)}(m_W^2)(-2m_b^4((SP2$$
$$-SP3)F_4 + SP1\,F_5) + F_1(SP1\,m_b^2 + 4SP3\,SP4$$
$$-4SP2\,SP5 + 2SP1t + SP1t_{12})m_t m_b^2$$
$$+2(2(SP2 - SP3)F_4 + SP1(2F_5 - F_1 m_t))m_W^4$$
$$+2(SP4 - SP5)F_3(m_b^4 - m_t^2 m_b^2$$
$$-2m_W^4)) + (2(SP4 - SP5)F_3 + 2(SP3$$

$$-SP2)F_4 - 2SP1\,F_5 + SP1\,F_1 m_t)$$
$$\times(2C_{00}^{(6)}(m_W^2)(m_b^2 + 2m_W^2)$$
$$-B_0^{(5)}(m_b^2)((X_{dd} + 1)m_b^2 + 2m_W^2)). \tag{A.6}$$

For the box part (cf. Eqs. (3.13)), we obtain

$$R_1^{\text{box}} = m_b^2(2(SP3(SP4 - SP5)T_d D_0^{(1)}(m_W^2)$$
$$+(2SP2\,SP5 - SP3(SP4 + SP5))T_e D_0^{(2)}(m_W^2)$$
$$-SP1\,T_d D_{00}^{(1)}(m_W^2)) + ((SP4 - SP5)$$
$$\times(T_d(2(SP2 - SP3)(D_{12}^{(1)}(m_{H^\pm}^2)$$
$$+2D_{122}^{(1)}(m_{H^\pm}^2))$$
$$-2SP3D_{13}^{(1)}(m_{H^\pm}^2))+4(SP2-SP3)(T_d D_{222}^{(1)}(m_{H^\pm}^2)$$
$$+T_e D_{222}^{(2)}(m_{H^\pm}^2)))$$
$$-4(SP3\,SP4 + SP2\,SP5)T_d D_{223}^{(1)}(m_{H^\pm}^2) - (4SP2$$
$$-6SP3)SP5\,T_e D_{23}^{(2)}(m_{H^\pm}^2)$$
$$-SP3(T_d(4(SP4 - SP5)D_{123}^{(1)}(m_{H^\pm}^2)$$
$$-8SP5D_{223}^{(1)}(m_{H^\pm}^2) + 6(SP4 - SP5)D_{23}^{(1)}(m_{H^\pm}^2))$$
$$+2SP4\,T_e(2(D_{123}^{(2)}(m_{H^\pm}^2) + D_{223}^{(2)}(m_{H^\pm}^2))$$
$$+D_{23}^{(2)}(m_{H^\pm}^2))) + 4SP3\,SP5(T_d D_{233}^{(1)}(m_{H^\pm}^2)$$
$$+T_e D_{233}^{(2)}(m_{H^\pm}^2)) + (T_d D_{22}^{(1)}(m_{H^\pm}^2)$$
$$+T_e D_{22}^{(2)}(m_{H^\pm}^2))(6(SP2 - SP3)(SP4 - SP5)$$
$$-SP1\,m_t^2) + T_e((SP2 - SP3)(4SP4D_{112}^{(2)}(m_{H^\pm}^2)$$
$$+2(SP4 - SP5)(4D_{122}^{(2)}(m_{H^\pm}^2)$$
$$+D_2^{(2)}(m_{H^\pm}^2)))-4SP5((2SP2-3SP3)D_{123}^{(2)}(m_{H^\pm}^2)$$
$$+(SP2 - SP3)(D_{112}^{(2)}(m_{H^\pm}^2)$$
$$+D_{113}^{(2)}(m_{H^\pm}^2) + D_{13}^{(2)}(m_{H^\pm}^2))$$
$$-SP3D_{133}^{(2)}(m_{H^\pm}^2) + (SP2 - 2SP3)D_{223}^{(2)}(m_{H^\pm}^2))$$
$$-SP1t(D_{11}^{(2)}(m_{H^\pm}^2) + D_{12}^{(2)}(m_{H^\pm}^2)$$
$$-D_{13}^{(2)}(m_{H^\pm}^2) - D_{23}^{(2)}(m_{H^\pm}^2))$$
$$+D_{12}^{(2)}(m_{H^\pm}^2)(6(SP2 - SP3)$$
$$\times(SP4 - SP5) - SP1\,m_t^2)))X_{dd}$$
$$-(4(SP1(T_d D_{00}^{(1)}(m_{H^\pm}^2)$$
$$+T_e D_{00}^{(2)}(m_{H^\pm}^2)) + (SP2 - SP3)$$
$$\times(SP4 - SP5)(T_d(D_{12}^{(1)}(m_{H^\pm}^2) + D_{22}^{(1)}(m_{H^\pm}^2))$$
$$+T_e(D_{12}^{(2)}(m_{H^\pm}^2) + D_{22}^{(2)}(m_{H^\pm}^2))))$$
$$-4(SP3\,SP4 + SP2\,SP5)T_d D_{23}^{(1)}(m_{H^\pm}^2)$$
$$-2T_e((2SP2\,SP5 - SP3(SP4$$
$$+SP5))D_0^{(2)}(m_{H^\pm}^2) + (SP2 - SP3)(SP4 + SP5)$$
$$\times D_1^{(2)}(m_{H^\pm}^2) + 2SP5((SP2 - SP3)D_{13}^{(2)}(m_{H^\pm}^2)$$
$$+(SP2 - 2SP3)D_{23}^{(2)}(m_{H^\pm}^2)))$$

$-(4\text{SP2} - 6\text{SP3})\text{SP5}T_e D_3^{(2)}(m_{H^\pm}^2)$

$+\text{SP1}(s_{23}T_d(D_0^{(1)}(m_{H^\pm}^2) - D_1^{(1)}(m_{H^\pm}^2)$

$+D_3^{(1)}(m_{H^\pm}^2)) + t T_e(D_0^{(2)}(m_{H^\pm}^2)$

$-D_1^{(2)}(m_{H^\pm}^2) + D_3^{(2)}(m_{H^\pm}^2)))$

$-\text{SP3}(T_d(2(\text{SP4} - \text{SP5})(D_0^{(1)}(m_{H^\pm}^2)$

$+2D_{13}^{(1)}(m_{H^\pm}^2)) - 8\text{SP5}D_{23}^{(1)}(m_{H^\pm}^2)$

$+2(\text{SP4} - 3\text{SP5})D_3^{(1)}(m_{H^\pm}^2))$

$+\text{SP4}T_e(4D_{23}^{(2)}(m_{H^\pm}^2) - 2D_3^{(2)}(m_{H^\pm}^2)))$

$+4\text{SP3 SP5}(T_d D_{33}^{(1)}(m_{H^\pm}^2)$

$+T_e D_{33}^{(2)}(m_{H^\pm}^2)) + (T_d D_2^{(1)}(m_{H^\pm}^2)$

$+T_e D_2^{(2)}(m_{H^\pm}^2))(2(\text{SP2} - \text{SP3})(\text{SP4} - 3\text{SP5})$

$-\text{SP1}m_t^2))X_{du} - (T_d D_{22}^{(1)}(m_W^2)$

$+T_e D_{22}^{(2)}(m_W^2))(\text{SP1}m_t^2(m_b^2 + 2m_W^2)$

$-2(\text{SP2} - \text{SP3})(\text{SP4} - \text{SP5})(m_b^2 + 6m_W^2))$

$-\text{SP5}(2T_e D_{23}^{(2)}(m_W^2)(\text{SP3}m_b^2$

$+2(4\text{SP2} - 5\text{SP3})m_W^2) - 4(\text{SP3}(T_d D_{233}^{(1)}(m_W^2)$

$+T_e D_{233}^{(2)}(m_W^2))(m_b^2 + 2m_W^2) + \text{SP2}T_e D_3^{(2)}$

$(m_W^2)(m_b^2 - 2m_W^2))$

$+\text{SP3}(4(T_d D_{33}^{(1)}(m_W^2) + T_e D_{33}^{(2)}(m_W^2))(m_b^2 - 2m_W^2)$

$+T_e D_3^{(2)}(m_W^2)(6m_b^2 - 4m_W^2)))$

$+T_e((2(\text{SP2} - \text{SP3})(\text{SP4} + \text{SP5})D_1^{(2)}(m_W^2)$

$+4\text{SP2 SP4}D_{112}^{(2)}(m_W^2))m_b^2 - 8(\text{SP3 SP4}$

$-\text{SP2}(\text{SP4} - \text{SP5}))D_{122}^{(2)}(m_W^2)(m_b^2 + 2m_W^2)$

$+4(\text{SP2} - \text{SP3})D_2^{(2)}(m_W^2)(\text{SP5}m_b^2$

$+(\text{SP4} - \text{SP5})m_W^2) - 4\text{SP4}D_{112}^{(2)}(m_W^2)$

$\times(\text{SP3}m_b^2 - 2(\text{SP2} - \text{SP3})m_W^2)$

$-D_{12}^{(2)}(m_W^2)(\text{SP1}m_t^2(m_b^2 + 2m_W^2) - 2$

$\times(\text{SP2} - \text{SP3})(\text{SP4} - \text{SP5})(m_b^2 + 6m_W^2))$

$-4((\text{SP3 SP4} - \text{SP2}(\text{SP4} - \text{SP5}))$

$\times D_{222}^{(2)}(m_W^2)(m_b^2 + 2m_W^2)$

$+\text{SP5}(4(\text{SP2} - \text{SP3})D_{13}^{(2)}(m_W^2)m_W^2$

$+((\text{SP2} - \text{SP3})(D_{112}^{(2)}(m_W^2) + D_{113}^{(2)}(m_W^2))$

$+2\text{SP2}D_{123}^{(2)}(m_W^2) - \text{SP3}D_{133}^{(2)}(m_W^2)$

$+\text{SP2}D_{223}^{(2)}(m_W^2))(m_b^2 + 2m_W^2))))$

$+\text{SP3}(T_e(2\text{SP4}(D_{23}^{(2)}(m_W^2) - D_3^{(2)}$

$(m_W^2))(m_b^2 - 2m_W^2)$

$-(4\text{SP4}(D_{123}^{(2)}(m_W^2)$

$+D_{223}^{(2)}(m_W^2)) - 4\text{SP5}(2D_{122}^{(2)}(m_W^2)$

$+3D_{123}^{(2)}(m_W^2) + D_{222}^{(2)}(m_W^2)$

$+2D_{223}^{(2)}(m_W^2)))(m_b^2 + 2m_W^2))$

$-T_d(4(\text{SP4} - 2\text{SP5})D_{223}^{(1)}(m_W^2)(m_b^2 + 2m_W^2)$

$+2D_{23}^{(1)}(m_W^2)((\text{SP4} + \text{SP5})m_b^2$

$+2(3\text{SP4} - 5\text{SP5})m_W^2) - 2D_3^{(1)}(m_W^2)((\text{SP4}$

$-3\text{SP5})m_b^2 - 2(\text{SP4} - \text{SP5})m_W^2)$

$-(\text{SP4} - \text{SP5})(2D_{13}^{(1)}(m_W^2)(m_b^2 - 2m_W^2)$

$-4D_{123}^{(1)}(m_W^2)(m_b^2 + 2m_W^2))))$

$-(\text{SP1}m_b^2(T_d C_0^{(1)}(m_b^2) + T_e C_1^{(1)}(m_b^2)$

$+(T_d + T_e)C_2^{(1)}(m_b^2) - T_d(2D_{00}^{(1)}(m_{H^\pm}^2)$

$+4D_{002}^{(1)}(m_{H^\pm}^2) + D_0^{(1)}(m_{H^\pm}^2)(m_b^2 - m_{H^\pm}^2))$

$-T_e(4(D_{001}^{(2)}(m_{H^\pm}^2) + D_{002}^{(2)}(m_{H^\pm}^2))$

$+(D_1^{(2)}(m_{H^\pm}^2) + D_2^{(2)}(m_{H^\pm}^2))(m_b^2 - m_{H^\pm}^2)))$

$-T_d D_2^{(1)}(m_{H^\pm}^2)(2(\text{SP2} - \text{SP3})$

$\times(\text{SP4} - \text{SP5})m_b^2 + \text{SP1}(m_b^4 - m_b^2(m_{H^\pm}^2 + m_t^2))))$

$X_{dd} - T_d(s_{23}\text{SP1}(D_1^{(1)}(m_{H^\pm}^2)$

$+D_{12}^{(1)}(m_{H^\pm}^2) - D_{23}^{(1)}(m_{H^\pm}^2))X_{dd}m_b^2$

$+(\text{SP2}-\text{SP3})(\text{SP4}-\text{SP5})(2D_{12}^{(1)}(m_W^2)(m_b^2 - 2m_W^2)$

$-4(D_{122}^{(1)}(m_W^2) + D_{222}^{(1)}(m_W^2))(m_b^2 + 2m_W^2))$

$-4\text{SP2 SP5}(D_{23}^{(1)}(m_W^2)(m_b^2 - 2m_W^2)$

$-D_{223}^{(1)}(m_W^2)(m_b^2 + 2m_W^2)) - D_2^{(1)}(m_W^2)$

$\times(4(\text{SP2} - \text{SP3})(\text{SP5}m_b^2 + (\text{SP4} - \text{SP5})m_W^2)$

$+\text{SP1}(m_b^4 - 2m_W^4 + (m_b^2 + 4m_t^2)m_W^2)))$

$-\text{SP1}(-((T_d + T_e)C_0^{(1)}(m_b^2)$

$-T_d D_0^{(1)}(m_{H^\pm}^2)(m_b^2 - m_{H^\pm}^2) + T_e D_0^{(2)}(m_{H^\pm}^2)$

$\times(-m_b^2 + m_{H^\pm}^2 + m_t^2))X_{du}m_b^2$

$+(T_e C_1^{(1)}(m_b^2) + (T_d + T_e)C_2^{(1)}(m_b^2))$

$\times(m_b^2 + 2m_W^2) - C_0^{(1)}(m_b^2)(T_e m_b^2 - 2T_d m_W^2)$

$-T_d((4D_{00}^{(1)}(m_W^2) - 6t_{12}D_2^{(1)}(m_W^2)$

$+2D_0^{(1)}(m_W^2)(m_b^2 - m_W^2))m_W^2$

$+4D_{002}^{(1)}(m_W^2)(m_b^2 + 2m_W^2)) - T_e(-(4(D_{00}^{(2)}(m_W^2)$

$-D_{001}^{(2)}(m_W^2))$

$-D_0^{(2)}(m_W^2)(-m_b^2 + m_W^2 + m_t^2))m_b^2$

$+8D_{001}^{(2)}(m_W^2)m_W^2 + 4D_{002}^{(2)}(m_W^2)(m_b^2 + 2m_W^2)$

$+D_1^{(2)}(m_W^2)(m_b^4 + m_W^2 m_b^2 - 2m_W^4) + D_2^{(2)}(m_W^2)$

$\times(m_b^4 + (m_t^2 + m_W^2)m_b^2 - 2m_W^4))$

$+s_{23}(2T_e D_3^{(2)}(m_W^2)m_W^2 + T_d(D_0^{(1)}(m_W^2)m_b^2$

$+2(D_1^{(1)}(m_W^2) + 3D_2^{(1)}(m_W^2))m_W^2$

$+(D_{12}^{(1)}(m_W^2) - D_{23}^{(1)}(m_W^2))(m_b^2 + 2m_W^2)$

$+D_3^{(1)}(m_W^2)(m_b^2 - 2m_W^2)))$

$+t(6T_d D_2^{(1)}(m_W^2)m_W^2 + T_e((D_0^{(2)}(m_W^2) - D_1^{(2)}(m_W^2)$

$+D_{11}^{(2)}(m_W^2) + D_3^{(2)}(m_W^2))m_b^2$

$+2D_{11}^{(2)}(m_W^2)m_W^2 + (D_{12}^{(2)}(m_W^2)$

$-D_{13}^{(2)}(m_W^2) - D_{23}^{(2)}(m_W^2))(m_b^2 + 2m_W^2)))),$ (A.7)

$R_2^{\text{box}} = m_b^2((\text{SP4} - \text{SP5})(T_d D_0^{(1)}(m_{H^\pm}^2)$

$-T_e D_0^{(2)}(m_{H^\pm}^2))X_{du}m_t^2$

$+(((\text{SP4} - \text{SP5})T_d D_{12}^{(1)}(m_{H^\pm}^2)$

$+T_e((3\text{SP4} - \text{SP5})D_{12}^{(2)}(m_{H^\pm}^2)$

$-2\text{SP5}D_{13}^{(2)}(m_{H^\pm}^2))$

$+\text{SP4}T_d D_2^{(1)}(m_{H^\pm}^2)$

$+T_e((4\text{SP4} - 2\text{SP5})D_{22}^{(2)}(m_{H^\pm}^2)$

$-\text{SP5}D_2^{(2)}(m_{H^\pm}^2))$

$-2\text{SP5}(T_d(D_{22}^{(1)}(m_{H^\pm}^2) + D_{23}^{(1)}(m_{H^\pm}^2))$

$+T_e D_{23}^{(2)}(m_{H^\pm}^2)))m_t^2 + (\text{SP4}(T_d - T_e)$

$-\text{SP5}(3T_d - T_e))C_0^{(1)}(m_b^2)$

$-(\text{SP5}(T_d - T_e) - \text{SP4}(T_d + T_e))C_1^{(1)}(m_b^2)$

$-2(\text{SP5}T_d - \text{SP4}T_e)C_2^{(1)}(m_b^2)$

$+T_e(2(3\text{SP4} + \text{SP5})D_{00}^{(2)}(m_{H^\pm}^2)$

$-4(\text{SP4} - 2\text{SP5})D_{002}^{(2)}(m_{H^\pm}^2))$

$-T_d(2(\text{SP4} - 5\text{SP5})D_{00}^{(1)}(m_{H^\pm}^2)$

$+4(\text{SP4} - \text{SP5})(D_{001}^{(1)}(m_{H^\pm}^2)$

$+D_{002}^{(1)}(m_{H^\pm}^2)) - 4\text{SP5}D_{003}^{(1)}(m_{H^\pm}^2)$

$+((\text{SP4} - 3\text{SP5})D_0^{(1)}(m_{H^\pm}^2)$

$+(\text{SP4} - \text{SP5})D_1^{(1)}(m_{H^\pm}^2))(m_b^2 - m_{H^\pm}^2))$

$+T_e(((\text{SP4} - \text{SP5})D_0^{(2)}(m_{H^\pm}^2)$

$-(\text{SP4} + \text{SP5})D_1^{(2)}(m_{H^\pm}^2))(m_b^2 - m_{H^\pm}^2)$

$+\text{SP4}D_2^{(2)}(m_{H^\pm}^2)(-2m_b^2 + 2m_{H^\pm}^2 + m_t^2))$

$+\text{SP5}T_d(2D_3^{(1)}(m_{H^\pm}^2)(m_b^2 - m_{H^\pm}^2)$

$+D_2^{(1)}(m_{H^\pm}^2)(2m_b^2 - 2m_{H^\pm}^2 - 3m_t^2)))X_{dd})$

$+2m_W^2((\text{SP4} - \text{SP5})t_{12}T_d D_3^{(1)}(m_W^2)$

$+T_e D_3^{(2)}(m_W^2)(2\text{SP5}m_b^2 + (\text{SP4} - \text{SP5})m_t^2))$

$+C_0^{(1)}(m_b^2)(m_b^2((\text{SP4} - 3\text{SP5})T_d$

$+(\text{SP5} - \text{SP4})T_e) - 2(\text{SP5}(T_d - T_e)$

$-\text{SP4}(3T_d - T_e)m_W^2)$

$-C_2^{(1)}(m_b^2)(m_b^2(2\text{SP5}T_d - 2\text{SP4}T_e)$

$-4(\text{SP4}T_d - \text{SP5}T_e)m_W^2)$

$+C_1^{(1)}(m_b^2)((\text{SP4} - \text{SP5})T_d(m_b^2 + 2m_W^2)$

$+(\text{SP4} + \text{SP5})T_e(m_b^2 - 2m_W^2))$

$+\text{SP5}(4(2T_e D_{002}^{(2)}(m_W^2) + T_d D_{003}^{(1)}$

$(m_W^2))(m_b^2 + 2m_W^2)$

$+2T_d D_3^{(1)}(m_W^2)(m_b^4$

$-(m_b^2 - m_t^2 m_W^2)) - T_d(2D_{00}^{(1)}(m_W^2)((\text{SP4}$

$-5\text{SP5})m_b^2 + 2(3\text{SP4} - \text{SP5})m_W^2)$

$+(\text{SP4} - \text{SP5})(m_b^2 + 2m_W^2)(4(D_{001}^{(1)}(m_W^2)$

$+D_{002}^{(1)}(m_W^2))$

$+D_1^{(1)}(m_W^2)(m_b^2 - m_W^2)) - D_2^{(1)}(m_W^2)(4\text{SP4}m_W^4$

$+2(\text{SP4} + \text{SP5})(3(s_{23} + t)$

$+t_{12})m_W^2 + m_b^2(\text{SP5}(2m_b^2 - 3m_t^2) - 2(2\text{SP4}$

$+\text{SP5})m_W^2)) + D_0^{(1)}(m_W^2)((\text{SP4}$

$-3\text{SP5})m_b^4 - ((\text{SP4} - \text{SP5})m_t^2 - (5\text{SP4}$

$+\text{SP5})m_W^2)m_b^2 - 2(3\text{SP4} - \text{SP5})m_W^4))$

$-T_e(2D_3^{(2)}(m_W^2)(2\text{SP5}m_W^2 + (\text{SP4}$

$+\text{SP5})t_{12})m_W^2 + 4\text{SP4}D_{002}^{(2)}(m_W^2)(m_b^2 + 2m_W^2)$

$-2D_{00}^{(2)}(m_W^2)((3\text{SP4} + \text{SP5})m_b^2 - 2(\text{SP4}$

$+\text{SP5})m_W^2) - (\text{SP4} - \text{SP5})D_0^{(2)}(m_W^2)(m_b^4$

$-(m_t^2 - m_W^2)m_b^2 - 2m_W^4) + D_2^{(2)}(m_W^2)$

$\times(2\text{SP4}m_b^4 - ((\text{SP4} - \text{SP5})m_t^2$

$+2(\text{SP4} + 2\text{SP5})m_W^2)m_b^2 - 2m_W^2$

$\times(-3(\text{SP4} - \text{SP5})m_t^2 - 2\text{SP5}m_W^2 + (2\text{SP4}$

$-2\text{SP5})t_{12})) + D_1^{(2)}(m_W^2)$

$(4(\text{SP4} - \text{SP5})(s_{23} + t)m_W^2 + (\text{SP4}$

$+\text{SP5})(2m_W^4$

$+m_b^2(m_b^2 - 3m_W^2)))) + m_t^2$

$\times(-2\text{SP5}(T_e D_{23}^{(2)}(m_W^2)(m_b^2 + 2m_W^2)$

$+T_d D_{23}^{(1)}(m_W^2)(m_b^2 - 2m_W^2))$

$+T_d(((\text{SP4} - \text{SP5})D_{12}^{(1)}(m_W^2)$

$-2\text{SP5}D_{22}^{(1)}(m_W^2))(m_b^2 - 2m_W^2)$

$+\text{SP4}(D_2^{(1)}(m_W^2)m_b^2 - 2D_3^{(1)}(m_W^2)m_W^2))$

$+T_e(D_{12}^{(2)}(m_W^2)((3\text{SP4} - \text{SP5})m_b^2 - 2(\text{SP4}$

$+\text{SP5})m_W^2) - 2(\text{SP5}D_{13}^{(2)}(m_W^2)m_b^2$

$-D_{22}^{(2)}(m_W^2)((2\text{SP4} - \text{SP5})m_b^2 - 2\text{SP5}m_W^2))))$

$+s_{23}(T_e(4(\text{SP4} - \text{SP5})(D_1^{(2)}(m_W^2)$

$-D_{22}^{(2)}(m_W^2)) - 4(\text{SP4} - 2\text{SP5})D_{23}^{(2)}(m_W^2)$

$+4\text{SP5}(D_{12}^{(2)}(m_W^2) + D_{33}^{(2)}(m_W^2))m_W^2$

$-4(\text{SP5}T_d D_{12}^{(1)}(m_W^2)m_b^2 + \text{SP4}T_e D_{12}^{(2)}(m_W^2)m_W^2)$

$+\text{SP5}(4T_e D_{13}^{(2)}(m_W^2)m_W^2$

$$-T_d D_{13}^{(1)}(m_W^2)(3m_b^2 - 2m_W^2))$$
$$+T_d(((SP4 - SP5)D_{11}^{(1)}(m_{H^\pm}^2)$$
$$+2(SP4 - 2SP5)D_{12}^{(1)}(m_{H^\pm}^2)$$
$$+(SP4 - 3SP5)(D_1^{(1)}(m_{H^\pm}^2) + D_{13}^{(1)}(m_{H^\pm}^2))$$
$$+2(SP4 - SP5)(D_2^{(1)}(m_{H^\pm}^2) + D_{22}^{(1)}(m_{H^\pm}^2)$$
$$+D_{23}^{(1)}(m_{H^\pm}^2)))X_{dd}m_b^2$$
$$+(SP4 - SP5)D_{11}^{(1)}(m_W^2)$$
$$\times(m_b^2 + 2m_W^2) + D_1^{(1)}(m_W^2)((SP4 - 3SP5)m_b^2$$
$$+2(3SP4 - SP5)m_W^2) + 2D_{23}^{(1)}(m_W^2)$$
$$\times((SP4 - SP5)m_b^2 - 2SP4m_W^2)$$
$$+SP4(2D_{12}^{(1)}(m_W^2)(m_b^2 + 2m_W^2)$$
$$+D_{13}^{(1)}(m_W^2)(m_b^2 - 2m_W^2)) + 2((SP4 - SP5)$$
$$\times D_{22}^{(1)}(m_W^2)m_b^2 + D_2^{(1)}(m_W^2)$$
$$\times((SP4 - SP5)m_b^2 - 2(SP4 + SP5)m_W^2))))$$
$$+t(T_d(4(SP4 - SP5)(D_{12}^{(1)}(m_W^2)$$
$$+D_{22}^{(1)}(m_W^2)) - 4SP5(2D_2^{(1)}(m_W^2)$$
$$+D_{23}^{(1)}(m_W^2)))m_W^2 + T_e(-(2(SP4 - SP5)$$
$$\times(D_{22}^{(2)}(m_W^2) + D_{23}^{(2)}(m_W^2))$$
$$-((SP4 + SP5)D_{11}^{(2)}(m_{H^\pm}^2)$$
$$+2SP5D_{12}^{(2)}(m_{H^\pm}^2)$$
$$-(SP4 - SP5)(D_1^{(2)}(m_{H^\pm}^2)$$
$$+D_{13}^{(2)}(m_{H^\pm}^2) + 2(D_2^{(2)}(m_{H^\pm}^2)$$
$$+D_{22}^{(2)}(m_{H^\pm}^2) + D_{23}^{(2)}(m_{H^\pm}^2))))X_{dd}m_b^2$$
$$+(-(SP4 - SP5)D_1^{(2)}(m_W^2) + (SP4$$
$$+SP5)D_{11}^{(2)}(m_W^2) - SP4D_{13}^{(2)}(m_W^2)$$
$$+SP5D_{13}^{(2)}(m_W^2) - 2(SP4 - SP5)D_2^{(2)}$$
$$(m_W^2))(m_b^2 - 2m_W^2)$$
$$+SP5(4(D_{23}^{(2)}(m_W^2)$$
$$+D_{33}^{(2)}(m_W^2))m_W^2 + 2D_{12}^{(2)}(m_W^2)$$
$$(m_b^2 - 2m_W^2)))), \tag{A.8}$$
$$R_3^{\text{box}} = -m_b^2((4T_d((SP2 - SP3)D_{002}^{(1)}(m_{H^\pm}^2)$$
$$-SP3D_{003}^{(1)}(m_{H^\pm}^2)) + SP3(4T_dD_{00}^{(1)}(m_{H^\pm}^2)$$
$$-2T_e(D_0^{(2)}(m_{H^\pm}^2) + D_1^{(2)}(m_{H^\pm}^2)$$
$$+D_3^{(2)}(m_{H^\pm}^2))(m_b^2 - m_{H^\pm}^2))$$
$$+T_e((8SP2 - 4SP3)D_{00}^{(2)}(m_{H^\pm}^2)$$
$$+4((SP2 - SP3)D_{001}^{(2)}(m_{H^\pm}^2)$$
$$+(SP2 - 2SP3)D_{002}^{(2)}(m_{H^\pm}^2))$$
$$+2SP3(D_2^{(2)}(m_{H^\pm}^2)m_{H^\pm}^2 + C_0^{(1)}(m_b^2)$$

$$+C_1^{(1)}(m_b^2))) - 2(SP3T_eD_2^{(2)}(m_{H^\pm}^2)m_b^2$$
$$+SP2(T_dD_{22}^{(1)}(m_{H^\pm}^2) - T_eD_{22}^{(2)}(m_{H^\pm}^2))m_t^2$$
$$+(SP3T_d + SP2T_e)C_0^{(1)}(m_b^2)$$
$$+(SP2T_d - SP3T_e)C_2^{(1)}(m_b^2)$$
$$+T_dD_2^{(1)}(m_{H^\pm}^2)$$
$$\times(SP2m_{H^\pm}^2 + SP3m_t^2))$$
$$+2((SP3T_dD_0^{(1)}(m_{H^\pm}^2)$$
$$+SP2T_eD_0^{(2)}(m_{H^\pm}^2))(m_b^2 - m_{H^\pm}^2)$$
$$+SP2(T_dD_2^{(1)}(m_{H^\pm}^2)m_b^2 + T_eD_{12}^{(2)}$$
$$\times(m_{H^\pm}^2)m_t^2)))X_{dd} - 2m_t^2((SP2$$
$$-SP3)(T_dD_2^{(1)}(m_{H^\pm}^2) + T_e(D_0^{(2)}(m_{H^\pm}^2)$$
$$+D_1^{(2)}(m_{H^\pm}^2) + D_2^{(2)}(m_{H^\pm}^2)))$$
$$-SP3(T_dD_3^{(1)}(m_{H^\pm}^2) + T_eD_3^{(2)}$$
$$\times(m_{H^\pm}^2))X_{du} - 4m_W^2(SP3T_dD_3^{(1)}(m_W^2)m_W^2$$
$$+(s_{23} + t)(SP2T_eD_3^{(2)}(m_W^2) - SP3T_dD_{33}^{(1)}(m_W^2)))$$
$$+2C_2^{(1)}(m_b^2)((SP2T_d - SP3T_e)m_b^2$$
$$-2(SP3T_d - SP2T_e)m_W^2) + SP3(4(2T_eD_{002}^{(2)}(m_W^2)$$
$$+T_dD_{003}^{(1)}(m_W^2))(m_b^2 + 2m_W^2)$$
$$+2T_eD_3^{(2)}(m_W^2)(m_b^4 - (m_t^2 + m_W^2)m_b^2$$
$$+2m_t^2m_W^2) + m_t^2(2T_dD_{22}^{(1)}(m_W^2)(SP2m_b^2$$
$$+s2(SP2 - 2SP3)m_W^2) - 2(2(SP2$$
$$+SP3)T_dD_{23}^{(1)}(m_W^2)m_W^2 + SP2T_eD_{22}^{(2)}(m_W^2)(m_b^2$$
$$-2m_W^2))) - T_e(2C_1^{(1)}(m_b^2)(SP3m_b^2 - 2SP2m_W^2)$$
$$+SP2(2D_{12}^{(2)}(m_W^2)(m_b^2 - 2m_W^2)m_t^2$$
$$+4D_{002}^{(2)}(m_W^2)(m_b^2 + 2m_W^2))$$
$$+4((SP2 - SP3)D_{001}^{(2)}(m_W^2)(m_b^2 + 2m_W^2)$$
$$+D_{00}^{(2)}(m_W^2)((2SP2 - SP3)m_b^2 - 4SP3m_W^2))$$
$$-D_1^{(2)}(m_W^2)(2SP3m_b^4 + 2(m_t^2(SP2$$
$$-SP3) - (2SP2 + SP3)m_W^2)m_b^2 + 4SP2m_W^4)$$
$$-D_2^{(2)}(m_W^2)(2SP3m_b^4 + (2(SP2$$
$$-SP3)m_t^2 - 2(2SP2 + SP3)m_W^2)m_b^2$$
$$-4m_W^2((SP2 + SP3)t_{12} + SP2(-2m_t^2 - m_W^2)))$$
$$-(SP2 - SP3)(2C_0^{(1)}(m_b^2)$$
$$\times(m_b^2 + 2m_W^2) - 2D_0^{(2)}(m_W^2)(m_b^4 - (m_t^2 - m_W^2)m_b^2$$
$$-2m_W^4))) + T_d(4(SP2 - SP3)t_{12}(D_{12}^{(1)}(m_W^2)$$
$$+D_{23}^{(1)}(m_W^2))m_W^2 + 2C_0^{(1)}(m_b^2)(SP3m_b^2$$
$$-2SP2m_W^2) - D_{00}^{(1)}(m_W^2)(4SP3m_b^2$$
$$-8(SP2 + SP3)m_W^2) - 4(SP3t_{12}D_{13}^{(1)}(m_W^2)m_W^2$$

$$+ (\text{SP2} - \text{SP3})D_{002}^{(1)}(m_W^2)(m_b^2 + 2m_W^2))$$
$$- 2(\text{SP3}D_3^{(1)}(m_W^2)(m_t^2 - 2m_W^2)m_b^2$$
$$+ D_0^{(1)}(m_W^2)(m_b^2 - m_W^2)(\text{SP3}m_b^2 - 2\text{SP2}m_W^2))$$
$$- D_2^{(1)}(m_W^2)(4\text{SP3}m_W^2(-m_b^2$$
$$+ m_W^2 + m_t^2) + \text{SP2}(2m_b^4 - 2(m_t^2 + m_W^2)m_b^2$$
$$+ 4(s_{23} + t)m_W^2)))$$
$$- t(4T_d((\text{SP2} - \text{SP3})D_{22}^{(1)}(m_W^2)$$
$$- \text{SP3}(D_2^{(1)}(m_W^2) + D_{23}^{(1)}(m_W^2)))m_W^2$$
$$+ 2T_e((2\text{SP3}D_{12}^{(2)}(m_W^2) - \text{SP2}D_{13}^{(2)}(m_W^2)$$
$$- (\text{SP2} - \text{SP3})D_{22}^{(2)}(m_W^2))m_b^2$$
$$+ (\text{SP3}D_{11}^{(2)}(m_{H^\pm}^2) - (\text{SP2} - 2\text{SP3})D_{12}^{(2)}(m_{H^\pm}^2)$$
$$- (\text{SP2} - \text{SP3})(D_1^{(2)}(m_{H^\pm}^2)$$
$$+ D_{13}^{(2)}(m_{H^\pm}^2) + D_2^{(2)}(m_{H^\pm}^2) + D_{22}^{(2)}(m_{H^\pm}^2)$$
$$+ D_{23}^{(2)}(m_{H^\pm}^2)))\text{X}_{dd}m_b^2 - ((\text{SP2}$$
$$- \text{SP3})D_1^{(2)}(m_W^2) + \text{SP2}D_{12}^{(2)}(m_W^2))$$
$$\times (m_b^2 + 2m_W^2) + D_{13}^{(2)}(m_W^2)(\text{SP3}m_b^2 + 2\text{SP2}m_W^2)$$
$$- D_{23}^{(2)}(m_W^2)((\text{SP2} - \text{SP3})m_b^2$$
$$- 2\text{SP2}m_W^2) + D_{11}^{(2)}(m_W^2)$$
$$\times (\text{SP3}m_b^2 - 2\text{SP2}m_W^2)$$
$$- D_2^{(2)}(m_W^2)((\text{SP2} - \text{SP3})m_b^2 - 2(\text{SP2}$$
$$+ \text{SP3})m_W^2))) + s_{23}(4(\text{SP2} - \text{SP3})T_em_W^2$$
$$\times (D_{12}^{(2)}(m_W^2) + D_{22}^{(2)}(m_W^2))$$
$$+ \text{SP3}(2T_d(D_2^{(1)}(m_W^2) + D_{23}^{(1)}(m_W^2))m_b^2$$
$$- 4T_em_W^2(2D_2^{(2)}(m_W^2) + D_{23}^{(2)}(m_W^2)))$$
$$- 2T_d((\text{SP2} - \text{SP3})(D_{22}^{(1)}(m_W^2)$$
$$+ (D_2^{(1)}(m_{H^\pm}^2) + D_{22}^{(1)}(m_{H^\pm}^2)$$
$$+ D_{23}^{(1)}(m_{H^\pm}^2))\text{X}_{dd})m_b^2 - D_{12}^{(1)}(m_W^2)(\text{SP3}m_b^2$$
$$+ 2(\text{SP2} - 2\text{SP3})m_W^2) + \text{SP2}(D_2^{(1)}(m_W^2)$$
$$+ D_{23}^{(1)}(m_W^2))(m_b^2 - 2m_W^2)$$
$$- D_1^{(1)}(m_W^2)(\text{SP3}m_b^2 - 2\text{SP2}m_W^2)$$
$$- \text{SP3}((D_1^{(1)}(m_{H^\pm}^2) + D_{12}^{(1)}(m_{H^\pm}^2)$$
$$+ D_{13}^{(1)}(m_{H^\pm}^2))\text{X}_{dd}m_b^2 + D_{13}^{(1)}$$
$$(m_W^2)(m_b^2 - 4m_W^2)))), \tag{A.9}$$

$$R_4^{\text{box}} = -(4(2\text{SP3 SP5}T_d D_{123}^{(1)}(m_{H^\pm}^2)$$
$$+ (\text{SP3 SP4} + (\text{SP2} - 2\text{SP3})\text{SP5})T_e D_{123}^{(2)}(m_{H^\pm}^2)$$
$$+ \text{SP3 SP5}(T_d D_{13}^{(1)}(m_{H^\pm}^2) - T_e D_{13}^{(2)}(m_{H^\pm}^2)$$
$$+ T_d D_{133}^{(1)}(m_{H^\pm}^2) - T_e D_{133}^{(2)}(m_{H^\pm}^2)))$$
$$+ (4\text{SP3 SP4} - 4\text{SP2 SP5})(T_d(D_{22}^{(1)}(m_{H^\pm}^2)$$

$$+ D_{23}^{(1)}(m_{H^\pm}^2)) + T_e(D_{22}^{(2)}(m_{H^\pm}^2)$$
$$+ D_{23}^{(2)}(m_{H^\pm}^2))) + \text{SP1}((T_d - T_e)(C_0^{(1)}(m_b^2)$$
$$- C_1^{(1)}(m_b^2))$$
$$- 2T_d(D_{00}^{(1)}(m_{H^\pm}^2)$$
$$- 2D_{001}^{(2)}(m_{H^\pm}^2)) + 2T_e(D_{00}^{(2)}(m_{H^\pm}^2)$$
$$- 2D_{001}^{(2)}(m_{H^\pm}^2)) - (T_d D_0^{(1)}(m_{H^\pm}^2)$$
$$- T_e D_0^{(2)}(m_{H^\pm}^2) - T_d D_1^{(1)}(m_{H^\pm}^2)$$
$$+ T_e D_1^{(2)}(m_{H^\pm}^2))(m_b^2 - m_{H^\pm}^2))$$
$$- T_d((\text{SP4} - \text{SP5})(4\text{SP3}D_{113}^{(1)}(m_{H^\pm}^2)$$
$$- 4(\text{SP2} - \text{SP3})(D_{112}^{(1)}(m_{H^\pm}^2)$$
$$+ D_{122}^{(1)}(m_{H^\pm}^2))) + 4(\text{SP3 SP4}$$
$$+ \text{SP2 SP5})D_{123}^{(1)}(m_{H^\pm}^2)$$
$$- D_2^{(1)}(m_{H^\pm}^2)(\text{SP1}m_t^2$$
$$+ 4\text{SP3 SP4} - 4\text{SP2 SP5}) - D_{12}^{(1)}(m_{H^\pm}^2)$$
$$\times (-\text{SP1}m_t^2 + 4\text{SP3 SP5} + \text{SP2}(4\text{SP4}$$
$$- 8\text{SP5}))) + T_e((\text{SP2} - \text{SP3})(4\text{SP5}D_{113}^{(2)}(m_{H^\pm}^2)$$
$$- 4(\text{SP4} - \text{SP5})(D_{112}^{(2)}(m_{H^\pm}^2)$$
$$+ D_{122}^{(2)}(m_{H^\pm}^2))) - D_{12}^{(2)}(m_{H^\pm}^2)$$
$$\times (-\text{SP1}m_t^2 + (4\text{SP2} - 8\text{SP3})\text{SP4} + 4\text{SP3 SP5})$$
$$+ D_2^{(2)}(m_{H^\pm}^2)(-\text{SP1}m_t^2 + 4\text{SP3 SP4}$$
$$- 4\text{SP2 SP5}))\text{X}_{dd}m_b^2$$
$$- T_d(4(\text{SP2} - \text{SP3})(\text{SP4} - \text{SP5})$$
$$\times (D_{112}^{(1)}(m_W^2) + D_{122}^{(1)}(m_W^2))(m_b^2 + 2m_W^2)$$
$$- 4D_{22}^{(1)}(m_W^2)(\text{SP2 SP5}m_b^2$$
$$+ 2(\text{SP3 SP4} - \text{SP2 SP5})m_W^2)$$
$$+ D_{12}^{(1)}(m_W^2)((-\text{SP1}m_t^2$$
$$+ 4\text{SP3 SP5} + \text{SP2}(4\text{SP4}$$
$$- 8\text{SP5}))m_b^2 + 2m_W^2(-\text{SP1}m_t^2$$
$$+ (4\text{SP2} - 8\text{SP3})\text{SP4}$$
$$+ 4\text{SP3 SP5})) + s D_2^{(1)}(m_W^2)(\text{SP1}(m_b^2 + 2m_W^2)m_t^2$$
$$+ 4(\text{SP3 SP4} - \text{SP2 SP5})(m_b^2$$
$$- 2m_W^2))) - 4(\text{SP3 SP4}T_d D_{22}^{(1)}(m_W^2)m_b^2$$
$$+ \text{SP1}t_{12}T_e D_2^{(2)}(m_W^2)m_W^2$$
$$+ (\text{SP3 SP4} - \text{SP2 SP5})(T_e D_{22}^{(2)}(m_W^2)$$
$$+ T_d D_{23}^{(1)}(m_W^2) + T_e D_{23}^{(2)}(m_W^2))(m_b^2 - 2m_W^2)$$
$$+ \text{SP5}(\text{SP3}(T_d D_{133}^{(1)}(m_W^2) - T_e D_{133}^{(2)}(m_W^2))$$
$$\times (m_b^2 + 2m_W^2) - T_e D_{13}^{(2)}(m_W^2)(\text{SP3}m_b^2$$
$$- 2(2\text{SP2} - \text{SP3})m_W^2))) + 4((m_b^2 + 2m_W^2)$$
$$\times (\text{SP3 SP5}T_e D_{122}^{(2)}(m_W^2) + (\text{SP3 SP4}$$

$$+\mathrm{SP2\,SP5}\,T_d D_{123}^{(1)}(m_W^2))$$
$$+\mathrm{SP3}((\mathrm{SP5}\,T_e D_{112}^{(1)}(m_W^2)$$
$$+T_d((\mathrm{SP4}-\mathrm{SP5})D_{113}^{(1)}(m_W^2)$$
$$-2\mathrm{SP5}\,D_{123}^{(1)}(m_W^2))-(\mathrm{SP4}$$
$$-2\mathrm{SP5})T_e D_{123}^{(2)}(m_W^2))(m_b^2+2m_W^2)$$
$$-T_d D_{13}^{(1)}(m_W^2)(\mathrm{SP5}\,m_b^2-2(2\mathrm{SP4}$$
$$-\mathrm{SP5})m_W^2)))-T_e(4((\mathrm{SP3\,SP4}-\mathrm{SP2(SP4}$$
$$-\mathrm{SP5}))(D_{112}^{(2)}(m_W^2)+D_{122}^{(2)}(m_W^2))$$
$$+\mathrm{SP5}((\mathrm{SP2}-\mathrm{SP3})D_{113}^{(2)}(m_W^2)$$
$$+\mathrm{SP2}\,D_{123}^{(2)}(m_W^2)))(m_b^2+2m_W^2)$$
$$-D_{12}^{(2)}(m_W^2)((-\mathrm{SP1}\,m_t^2+(4\mathrm{SP2}-8\mathrm{SP3})\mathrm{SP4}$$
$$+4\mathrm{SP3\,SP5})m_b^2+2(-\mathrm{SP1}\,m_t^2$$
$$+4\mathrm{SP3\,SP5}+\mathrm{SP2(4SP4}-8\mathrm{SP5}))m_W^2)$$
$$+D_2^{(2)}(m_W^2)(4(\mathrm{SP3\,SP4}$$
$$-\mathrm{SP2\,SP5})(m_b^2-2m_W^2)-\mathrm{SP1}\,m_t^2(m_b^2+6m_W^2))$$
$$+\mathrm{SP1}\,t(-(D_1^{(2)}(m_{H^\pm}^2)-D_{11}^{(2)}(m_{H^\pm}^2)$$
$$+D_{13}^{(2)}(m_{H^\pm}^2))\mathrm{X}_{dd}\,m_b^2+4D_2^{(2)}(m_W^2)m_W^2$$
$$+(D_{11}^{(2)}(m_W^2)-D_{13}^{(2)}(m_W^2))(m_b^2+2m_W^2)$$
$$-D_1^{(2)}(m_W^2)(m_b^2-2m_W^2)))$$
$$+\mathrm{SP1}(2(s_{23}+t)(T_d D_3^{(1)}(m_W^2)$$
$$-T_e D_3^{(2)}(m_W^2))m_W^2-s_{23}(4T_e(D_1^{(2)}(m_W^2)$$
$$+D_2^{(2)}(m_W^2))m_W^2+T_d((D_1^{(1)}(m_{H^\pm}^2)-D_{11}^{(1)}(m_{H^\pm}^2)$$
$$+D_{13}^{(1)}(m_{H^\pm}^2))\mathrm{X}_{dd}\,m_b^2$$
$$+(D_1^{(1)}(m_W^2)-D_{11}^{(1)}(m_W^2)+D_{13}^{(1)}(m_W^2))$$
$$(m_b^2+2m_W^2))))$$
$$-\mathrm{SP1}((T_d D_0^{(1)}(m_{H^\pm}^2)$$
$$-T_e D_0^{(2)}(m_{H^\pm}^2))m_b^2\mathrm{X}_{du}\,m_t^2$$
$$+((T_d-T_e)C_0^{(1)}(m_b^2)-T_d C_1^{(1)}(m_b^2))(m_b^2+2m_W^2)$$
$$-T_d((m_b^2+2m_W^2)(2D_{00}^{(1)}(m_W^2)-4D_{001}^{(1)}(m_W^2)$$
$$-D_1^{(1)}(m_W^2)(m_b^2-m_W^2))$$
$$+D_0^{(1)}(m_W^2)(m_b^4-(m_t^2-m_W^2)m_b^2-2m_W^4))$$
$$+T_e((C_1^{(1)}(m_b^2)+2D_{00}^{(2)}(m_W^2)$$
$$-4D_{001}^{(2)}(m_W^2))(m_b^2+2m_W^2)+D_0^{(2)}(m_W^2)$$
$$\times(m_b^4-(m_t^2-m_W^2)m_b^2-2m_W^4)$$
$$-D_1^{(2)}(m_W^2)(m_b^4+m_W^2(m_b^2-2m_W^2$$
$$+4(s_{23}+t)))))),\qquad(\mathrm{A}.10)$$
$$R_5^{\mathrm{box}}=m_t((-(T_d D_2^{(1)}(m_{H^\pm}^2)$$
$$-T_e D_2^{(2)}(m_{H^\pm}^2))m_t^2+T_d D_0^{(1)}$$
$$\times(m_{H^\pm}^2)(m_b^2-m_{H^\pm}^2)$$

$$+T_e D_0^{(2)}(m_{H^\pm}^2)(-m_b^2+m_{H^\pm}^2+m_t^2))$$
$$\times\mathrm{X}_{du}\,m_b^2+((T_d D_{22}^{(1)}(m_W^2)$$
$$-T_e D_{22}^{(2)}(m_W^2))m_t^2$$
$$+(T_d-T_e)C_2^{(1)}(m_b^2))(m_b^2-2m_W^2)$$
$$+T_e((C_0^{(1)}(m_b^2)-C_1^{(1)}(m_b^2))m_b^2$$
$$+D_0^{(2)}(m_W^2)(-m_b^2+m_W^2+m_t^2)m_b^2$$
$$+2C_1^{(1)}(m_b^2)m_W^2-(D_{12}^{(2)}(m_W^2)m_t^2$$
$$+4D_{00}^{(2)}(m_W^2))(m_b^2-2m_W^2)$$
$$+D_1^{(2)}(m_W^2)(m_b^4-3m_W^2 m_b^2+2m_W^4)$$
$$+D_2^{(2)}(m_W^2)(m_b^4+(m_t^2-3m_W^2)m_b^2+2m_W^4))$$
$$-T_d(-2D_0^{(1)}(m_W^2)(m_b^2-m_W^2)m_W^2$$
$$+2D_{00}^{(1)}(m_W^2)(m_b^2-2m_W^2)$$
$$+D_2^{(1)}(m_W^2)(m_b^4-m_W^2(3m_b^2-2(m_W^2$$
$$+4(s_{23}+t)+t_{12}))))+(((T_d D_{22}^{(1)}(m_{H^\pm}^2)$$
$$-T_e D_{22}^{(2)}(m_{H^\pm}^2))m_t^2+T_d C_0^{(1)}(m_b^2)$$
$$-T_e C_1^{(1)}(m_b^2)+(T_d-T_e)C_2^{(1)}(m_b^2)$$
$$+s_{23}T_d(D_1^{(1)}(m_{H^\pm}^2)$$
$$+D_{12}^{(1)}(m_{H^\pm}^2)-D_{23}^{(1)}(m_{H^\pm}^2))$$
$$+T_e((D_1^{(2)}(m_{H^\pm}^2)+D_2^{(2)}(m_{H^\pm}^2))$$
$$\times(m_b^2-m_{H^\pm}^2)-t(D_{11}^{(2)}(m_{H^\pm}^2)+D_{12}^{(2)}(m_{H^\pm}^2)$$
$$-D_{13}^{(2)}(m_{H^\pm}^2)-D_{23}^{(2)}(m_{H^\pm}^2)))m_b^2$$
$$-(T_d(2D_{00}^{(1)}(m_{H^\pm}^2)+D_0^{(1)}(m_{H^\pm}^2)(m_b^2-m_{H^\pm}^2))$$
$$+T_e(D_{12}^{(2)}(m_{H^\pm}^2)m_t^2$$
$$+4D_{00}^{(2)}(m_{H^\pm}^2)))m_b^2-T_d D_2^{(1)}(m_{H^\pm}^2)$$
$$\times(m_b^4-m_b^2(m_{H^\pm}^2$$
$$+m_t^2)))\mathrm{X}_{dd}-C_0^{(1)}(m_b^2)((T_d-T_e)$$
$$\times\mathrm{X}_{du}\,m_b^2+2T_d m_W^2)$$
$$-s_{23}(2T_e D_3^{(2)}(m_W^2)m_W^2$$
$$+T_d(-(D_0^{(1)}(m_W^2)+(D_0^{(1)}(m_{H^\pm}^2)-D_1^{(1)}$$
$$\times(m_{H^\pm}^2)+D_3^{(1)}(m_{H^\pm}^2))\mathrm{X}_{du})m_b^2$$
$$+2(D_1^{(1)}(m_W^2)-3D_2^{(1)}(m_W^2))m_W^2$$
$$-(D_{12}^{(1)}(m_W^2)-D_{23}^{(1)}(m_W^2)$$
$$+D_3^{(1)}(m_W^2))(m_b^2-2m_W^2)))$$
$$+t(6T_d D_2^{(1)}(m_W^2)m_W^2$$
$$+T_e(-(D_0^{(2)}(m_W^2)-D_1^{(2)}(m_W^2)$$
$$+D_{11}^{(2)}(m_W^2)+D_3^{(2)}(m_W^2)$$
$$+(D_0^{(2)}(m_{H^\pm}^2)-D_1^{(2)}(m_{H^\pm}^2)$$
$$+D_3^{(2)}(m_{H^\pm}^2))\mathrm{X}_{du})m_b^2$$

$$+2D_{11}^{(2)}(m_W^2)m_W^2 - (D_{12}^{(2)}(m_W^2)$$
$$-D_{13}^{(2)}(m_W^2) - D_{23}^{(2)}(m_W^2))(m_b^2 - 2m_W^2)))), \quad (A.11)$$

$$R_6^{\text{box}} = m_b^2(-\text{SP5}(X_{du}(T_d(D_0^{(1)}(m_{H^\pm}^2)$$
$$+D_3^{(1)}(m_{H^\pm}^2)) + T_e(D_0^{(2)}(m_{H^\pm}^2) + D_3^{(2)}(m_{H^\pm}^2)))$$
$$+T_dD_0^{(1)}(m_W^2) + T_eD_0^{(2)}(m_W^2)) + X_{du}$$
$$\times(\text{SP4} - \text{SP5})(T_d(D_1^{(1)}(m_{H^\pm}^2) + D_2^{(1)}(m_{H^\pm}^2))$$
$$+T_eD_2^{(2)}(m_{H^\pm}^2))$$
$$-X_{dd}((\text{SP4} - \text{SP5})(T_d(D_{12}^{(1)}(m_{H^\pm}^2)$$
$$+D_2^{(1)}(m_{H^\pm}^2) + D_{22}^{(1)}(m_{H^\pm}^2))$$
$$+T_e(D_2^{(2)}(m_{H^\pm}^2) + D_{22}^{(2)}(m_{H^\pm}^2)))$$
$$-\text{SP5}(T_dD_{23}^{(1)}(m_{H^\pm}^2) + T_eD_{23}^{(2)}(m_{H^\pm}^2))$$
$$+T_e((\text{SP4} - \text{SP5})D_{12}^{(2)}(m_{H^\pm}^2)$$
$$-\text{SP5}D_{13}^{(2)}(m_{H^\pm}^2)))$$
$$+T_d((\text{SP4} - \text{SP5})D_1^{(1)}(m_W^2)$$
$$-\text{SP4}D_{12}^{(1)}(m_W^2)))$$
$$+(m_b^2 - 2m_W^2)(\text{SP5}(T_d(D_{23}^{(1)}(m_W^2) - D_3^{(1)}(m_W^2))$$
$$+T_e(D_{22}^{(2)}(m_W^2) + D_{23}^{(2)}(m_W^2)$$
$$-D_3^{(2)}(m_W^2))) + T_e(\text{SP5}(D_{12}^{(2)}(m_W^2)$$
$$+D_{13}^{(2)}(m_W^2))$$
$$-\text{SP4}(D_{12}^{(2)}(m_W^2) + D_{22}^{(2)}(m_W^2))))$$
$$+T_dD_{12}^{(1)}(m_W^2)(\text{SP5}m_b^2$$
$$+2m_W^2(\text{SP4} - \text{SP5}))$$
$$+(\text{SP4} - \text{SP5})(2m_W^2(T_dD_2^{(1)}(m_W^2)$$
$$+T_eD_2^{(2)}(m_W^2))-T_d(m_b^2-2m_W^2)D_{22}^{(1)}(m_W^2)), \quad (A.12)$$

$$R_7^{\text{box}} = m_b^2(\text{SP3}(X_{du}(T_d(D_0^{(1)}(m_{H^\pm}^2)$$
$$+D_3^{(1)}(m_{H^\pm}^2)) + T_e(D_0^{(2)}(m_{H^\pm}^2)$$
$$+D_3^{(2)}(m_{H^\pm}^2)))$$
$$-X_{dd}(T_dD_{23}^{(1)}(m_{H^\pm}^2)$$
$$+T_eD_{23}^{(2)}(m_{H^\pm}^2)))$$
$$+\text{SP3}(T_dD_0^{(1)}(m_W^2) + T_eD_0^{(2)}(m_W^2))$$
$$+(\text{SP2} - \text{SP3})(X_{dd}(T_dD_{22}^{(1)}(m_{H^\pm}^2)$$
$$+T_e(D_{12}^{(2)}(m_{H^\pm}^2) + D_2^{(2)}(m_{H^\pm}^2)$$
$$+D_{22}^{(2)}(m_{H^\pm}^2)))$$
$$-X_{du}(T_dD_2^{(1)}(m_{H^\pm}^2)$$
$$+T_eD_1^{(2)}(m_{H^\pm}^2) + T_eD_2^{(2)}(m_{H^\pm}^2)))$$
$$+T_d(X_{dd}((\text{SP2} - \text{SP3})D_{12}^{(1)}(m_{H^\pm}^2)$$
$$-\text{SP3}D_{13}^{(1)}(m_{H^\pm}^2) + (\text{SP2} - \text{SP3})D_2^{(1)}(m_{H^\pm}^2))$$
$$+\text{SP2}D_{12}^{(1)}(m_W^2)) - T_e(\text{SP2} - \text{SP3})D_1^{(2)}(m_W^2))$$

$$+(m_b^2 - 2m_W^2)(\text{SP3}(-T_d(D_{13}^{(1)}(m_W^2)$$
$$+D_{23}^{(1)}(m_W^2)) + T_dD_3^{(1)}(m_W^2) - T_e(D_{12}^{(2)}(m_W^2)$$
$$+D_{22}^{(2)}(m_W^2) + D_{23}^{(2)}(m_W^2))$$
$$+T_eD_3^{(2)}(m_W^2)) + \text{SP2}T_e(D_{12}^{(2)}(m_W^2)$$
$$+D_{22}^{(2)}(m_W^2))) - T_dD_{12}^{(1)}(m_W^2)(\text{SP3}m_b^2$$
$$+2m_W^2(\text{SP2} - \text{SP3})) - (\text{SP2} - \text{SP3})$$
$$\times(2m_W^2(T_dD_2^{(1)}(m_W^2) + T_eD_2^{(2)}(m_W^2))$$
$$-T_d(m_b^2 - 2m_W^2)D_{22}^{(1)}(m_W^2)), \quad (A.13)$$

$$R_8^{\text{box}} = m_b^2X_{dd}(-((T_d + T_e)(C_0^{(1)}(m_b^2)$$
$$-C_1^{(1)}(m_b^2)) - (m_b^2 - m_{H^\pm}^2)(T_dD_0^{(1)}(m_{H^\pm}^2)$$
$$-T_dD_1^{(1)}(m_{H^\pm}^2) + T_eD_0^{(2)}(m_{H^\pm}^2)$$
$$-T_eD_1^{(2)}(m_{H^\pm}^2)) - 6(T_dD_{00}^{(1)}(m_{H^\pm}^2)$$
$$+T_eD_{00}^{(2)}(m_{H^\pm}^2)) + m_t^2(-(T_dD_{12}^{(1)}(m_{H^\pm}^2)$$
$$-T_dD_2^{(1)}(m_{H^\pm}^2) + T_eD_{12}^{(2)}(m_{H^\pm}^2)$$
$$-T_eD_2^{(2)}(m_{H^\pm}^2))))) - (m_b^2 - 2m_W^2)$$
$$\times((T_d + T_e)(C_0^{(1)}(m_b^2) - C_1^{(1)}(m_b^2))$$
$$-6(T_dD_{00}^{(1)}(m_W^2) + T_eD_{00}^{(2)}(m_W^2)))$$
$$-m_b^2X_{du}m_t^2(T_dD_0^{(1)}(m_{H^\pm}^2)$$
$$+T_eD_0^{(2)}(m_{H^\pm}^2))$$
$$+(-m_b^2(m_t^2 + 3m_W^2) + m_b^4 + 2m_W^4)(T_dD_0^{(1)}(m_W^2)$$
$$+T_eD_0^{(2)}(m_W^2))$$
$$-T_d(-3m_b^2m_W^2 + m_b^4 + 2m_W^4)D_1^{(1)}(m_W^2)$$
$$+s_{23}(4T_em_W^2D_1^{(2)}(m_W^2)$$
$$-T_d(m_b^2X_{dd}(D_1^{(1)}(m_{H^\pm}^2)$$
$$-D_{11}^{(1)}(m_{H^\pm}^2) + D_{13}^{(1)}(m_{H^\pm}^2))$$
$$+(m_b^2 - 2m_W^2)(D_1^{(1)}(m_W^2)$$
$$-D_{11}^{(1)}(m_W^2) + D_{13}^{(1)}(m_W^2))))$$
$$+m_t^2((m_b^2 - 2m_W^2)(T_dD_{12}^{(1)}(m_W^2) - T_dD_2^{(1)}(m_W^2)$$
$$+T_eD_{12}^{(2)}(m_W^2) - T_eD_2^{(2)}(m_W^2))$$
$$+2T_dm_W^2D_3^{(1)}(m_W^2))$$
$$-m_W^2(2t_{12}T_dD_3^{(1)}(m_W^2)$$
$$-2T_e(s_{23} + t)D_3^{(2)}(m_W^2))$$
$$-tT_e(m_b^2X_{dd}(D_1^{(2)}(m_{H^\pm}^2)$$
$$-D_{11}^{(2)}(m_{H^\pm}^2) + D_{13}^{(2)}(m_{H^\pm}^2))$$
$$+(m_b^2 - 6m_W^2)D_1^{(2)}(m_W^2) - (m_b^2 - 2m_W^2)$$
$$\times(D_{11}^{(2)}(m_W^2) - D_{13}^{(2)}(m_W^2)))$$
$$-T_eD_1^{(2)}(m_W^2)(m_W^2(-3m_b^2 + 2m_W^2$$
$$+4(s_{23} + t)) + m_b^4). \quad (A.14)$$

Finally, for the self-energy part (cf. Eqs. (3.14)), we get

$$R_1^{\text{self}} = -((\text{SP4} - \text{SP5})F_3 + 2\text{SP3}\,F_4$$
$$-\text{SP1}\,F_5 + F_{16})((B_0^{(2)}(m_W^2) + B_1^{(2)}(m_W^2)$$
$$+B_1^{(2)}(m_{H^\pm}^2)\text{X}_{dd}$$
$$+B_0^{(2)}(m_{H^\pm}^2)\text{X}_{du})m_b^2 + (2B_1^{(2)}(m_W^2) + 1)m_W^2), \quad (A.15)$$

$$R_2^{\text{self}} = ((\text{SP4} - \text{SP5})F_3 + 2\text{SP3}\,F_4 - \text{SP1}\,F_5$$
$$+F_{16} + (\text{SP1}\,F_1 - F_{12})m_t)(B_0^{(1)}(m_W^2)$$
$$+B_0^{(1)}(m_{H^\pm}^2)\text{X}_{du}), \quad (A.16)$$

$$R_3^{\text{self}} = ((\text{SP4} - \text{SP5})F_3 - 2\text{SP2}\,F_4$$
$$-\text{SP1}\,F_5 - F_{16} + (\text{SP1}\,F_1 + F_{12})m_t)((B_0^{(2)}(m_W^2)$$
$$+B_1^{(2)}(m_W^2) + B_1^{(2)}(m_{H^\pm}^2)\text{X}_{dd} + B_0^{(2)}(m_{H^\pm}^2)\text{X}_{du})m_b^2$$
$$+(2B_1^{(2)}(m_W^2) + 1)m_W^2), \quad (A.17)$$

$$R_4^{\text{self}} = -((\text{SP4} - \text{SP5})F_3 - 2\text{SP2}\,F_4$$
$$-\text{SP1}\,F_5 - F_{16})(B_0^{(1)}(m_W^2) + B_0^{(1)}(m_{H^\pm}^2)\text{X}_{du}), \quad (A.18)$$

$$R_5^{\text{self}} = -(2(\text{SP4} - \text{SP5})F_3 - 2((\text{SP2} - \text{SP3})F_4$$
$$+\text{SP1}\,F_5) + \text{SP1}\,F_1 m_t)((2B_1^{(2)}$$
$$\times(m_W^2) + 1)m_W^2 - m_b^2(B_0^{(1)}(m_W^2) - B_0^{(2)}(m_W^2))$$
$$-B_1^{(2)}(m_W^2)$$
$$-B_1^{(2)}(m_{H^\pm}^2)\text{X}_{dd}$$
$$+(B_0^{(1)}(m_{H^\pm}^2)$$
$$-B_0^{(2)}(m_{H^\pm}^2))\text{X}_{du})), \quad (A.19)$$

$$R_6^{\text{self}} = -(t + t_{12})((\text{SP4} - \text{SP5})F_3$$
$$+2\text{SP3}\,F_4 - \text{SP1}\,F_5 + F_{16})(B_0^{(3)}(m_W^2)$$
$$+B_0^{(3)}(m_{H^\pm}^2)\text{X}_{du})m_b^2 - s_{23}((\text{SP4} - \text{SP5})F_3$$
$$+2\text{SP3}\,F_4 - \text{SP1}\,F_5 + F_{16}$$
$$+(\text{SP1}\,F_1 - F_{12})m_t)((B_0^{(3)}(m_W^2) + B_1^{(3)}(m_W^2)$$
$$+B_1^{(3)}(m_{H^\pm}^2)\text{X}_{dd}$$
$$+B_0^{(3)}(m_{H^\pm}^2)\text{X}_{du})m_b^2 + (2B_1^{(3)}(m_W^2) + 1)m_W^2), \quad (A.20)$$

$$R_7^{\text{self}} = m_b^2 m_t^2((\text{SP4} - \text{SP5})F_3 - 2\text{SP2}\,F_4$$
$$-\text{SP1}\,F_5 - F_{16} + (\text{SP1}\,F_1 + F_{12})m_t)$$
$$\times(B_0^{(4)}(m_W^2) + B_0^{(4)}(m_{H^\pm}^2)\text{X}_{du})$$
$$+t(((\text{SP4} - \text{SP5})F_3 - 2\text{SP2}\,F_4 - \text{SP1}\,F_5 - F_{16})$$
$$\times(B_1^{(4)}(m_{H^\pm}^2)\text{X}_{dd}m_b^2 + m_W^2$$
$$+B_1^{(4)}(m_W^2)(m_b^2 + 2m_W^2))$$
$$-(\text{SP1}\,F_1 + F_{12})m_b^2 m_t(B_0^{(4)}(m_W^2)$$
$$+B_0^{(4)}(m_{H^\pm}^2)\text{X}_{du})). \quad (A.21)$$

Here the scalar functions $B_\alpha^{(k)}$, $C_\beta^{(k)}$, and $D_\lambda^{(k)}$ are defined, respectively, as

$$B_\alpha^{(1)}(m^2) = B_\alpha(0, m_b^2, m^2),$$
$$B_\alpha^{(2)}(m^2) = B_\alpha(m_t^2, m_b^2, m^2),$$
$$B_\alpha^{(3)}(m^2) = B_\alpha(s_{23}, m_b^2, m^2),$$
$$B_\alpha^{(4)}(m^2) = B_\alpha(t, m_b^2, m^2),$$

$$B_\alpha^{(5)}(m^2) = B_\alpha(t_{12}, m_b^2, m^2), \quad (A.22)$$
$$C_\beta^{(1)}(m^2) = C_\beta(0, 0, t_{12}, m_b^2, m_b^2, m^2),$$
$$C_\beta^{(2)}(m^2) = C_\beta(0, s_{23}, 0, m_b^2, m_b^2, m^2),$$
$$C_\beta^{(3)}(m^2) = C_\beta(0, s_{23}, m_t^2, m_b^2, m_b^2, m^2),$$
$$C_\beta^{(4)}(m^2) = C_\beta(0, t, 0, m_b^2, m_b^2, m^2),$$
$$C_\beta^{(5)}(m^2) = C_\beta(0, t, m_t^2, m_b^2, m_b^2, m^2),$$
$$C_\beta^{(6)}(m^2) = C_\beta(t_{12}, m_t^2, 0, m_b^2, m_b^2, m^2), \quad (A.23)$$
$$D_\lambda^{(1)}(m^2) = D_\lambda(0, 0, m_t^2, 0, t_{12}, s_{23}, m_b^2, m_b^2, m_b^2, m^2),$$
$$D_\lambda^{(2)}(m^2) = D_\lambda(0, 0, m_t^2, 0, t_{12}, t, m_b^2, m_b^2, m_b^2, m^2), (A.24)$$

where

$$\alpha = 0, 1,$$
$$\beta = 0, 00, 1, 12, 2, 22,$$
$$\lambda = 0, 00, 001, 002, 003, 1, 11, 112, 113, 12, 122, 123,$$
$$13, 133, 2, 22, 222, 223, 23, 233, 3, 33.$$

These functions can be further decomposed into the basic scalar one-loop integrals A_0, B_0, C_0, and D_0; see Refs. [147–150] for details.

References

1. S.L. Glashow, J. Iliopoulos, L. Maiani, Weak interactions with lepton-hadron symmetry. Phys. Rev. D 2, 1285–1292 (1970).
2. G. Eilam, J.L. Hewett, A. Soni, Rare decays of the top quark in the standard and two Higgs doublet models. Phys. Rev. D **44** (1991) 1473–1484 [Erratum: Phys. Rev D 59, 039901 (1999)]
3. N.G. Deshpande, B. Margolis, H.D. Trottier, Gluon mediated rare decays of the top quark: anomalous threshold and its phenomenological consequences. Phys. Rev. D 45, 178–186 (1992).
4. W.-S. Hou, Tree level $t \to ch$ or $h \to t\bar{c}$ decays. Phys. Lett. B 296, 179–184 (1992).
5. M.E. Luke, M.J. Savage, Flavor changing neutral currents in the Higgs sector and rare top decays. Phys. Lett. B **307**, 387–393 (1993). (**[hep-ph/9303249]**)
6. D. Atwood, L. Reina, A. Soni, Phenomenology of two Higgs doublet models with flavor changing neutral currents. Phys. Rev. D **55**, 3156–3176 (1997). (**[hep-ph/9609279]**)
7. S. Bejar, J. Guasch, J. Sola, Loop induced flavor changing neutral decays of the top quark in a general two Higgs doublet model. Nucl. Phys. B **600**, 21–38 (2001). (**[hep-ph/0011091]**)
8. R.A. Diaz, R. Martinez, J. Alexis Rodriguez, The rare decay $t \to c\gamma$ in the general 2 HDM type III. arXiv:hep-ph/0103307
9. E.O. Iltan, $t \to cH^0$ decay in the general two Higgs doublet model. Phys. Rev. D 65, 075017 (2002). arXiv:hep-ph/0111318.
10. A. Arhrib, Top and Higgs flavor changing neutral couplings in two Higgs doublets model. Phys. Rev. D 72, 075016 (2005). arXiv:hep-ph/0510107.
11. S. Bar-Shalom, G. Eilam, M. Frank, I. Turan, Width effects on near threshold decays of the top quark $t \to cWW$, cZZ and of neutral Higgs bosons. Phys. Rev. D 72, 055018 (2005). arXiv:hep-ph/0506167.

12. G. Abbas, A. Celis, X.-Q. Li, J. Lu, A. Pich, Flavour-changing top decays in the aligned two-Higgs-doublet model. JHEP **06**, 005 (2015). arXiv:1503.06423

13. W.-S. Hou, T.-H. Hsu, T. Modak, Constraining the $t \to u$ flavor changing neutral Higgs coupling at the LHC. Phys. Rev. D **102**(5), 055006 (2020). arXiv:2008.02573

14. S. Balaji, CP asymmetries in the rare top decays $t \to c\gamma$ and $t \to cg$. Phys. Rev. D **102**(11), 113010 (2020). arXiv:2009.03315

15. C.S. Li, R.J. Oakes, J.M. Yang, Rare decay of the top quark in the minimal supersymmetric model. Phys. Rev. D **49** (1994) 293–298 [Erratum: Phys. Rev. D 56, 3156 (1997)]

16. G.M. de Divitiis, R. Petronzio, L. Silvestrini, Flavor changing top decays in supersymmetric extensions of the standard model. Nucl. Phys. B 504, 45–60 (1997). arXiv:hep-ph/9704244.

17. J. Guasch, J. Sola, FCNC top quark decays: a door to SUSY physics in high luminosity colliders? Nucl. Phys. B 562, 3–28 (1999). arXiv:hep-ph/9906268.

18. G. Eilam, A. Gemintern, T. Han, J.M. Yang, X. Zhang, Top quark rare decay $t \to ch$ in R-parity violating SUSY. Phys. Lett. B 510, 227–235 (2001). arXiv:hep-ph/0102037.

19. J.J. Liu, C.S. Li, L.L. Yang, L.G. Jin, $t \to cV$ via SUSY FCNC couplings in the unconstrained MSSM. Phys. Lett. B 599, 92–101 (2004). arXiv:hep-ph/0406155.

20. M. Frank, I. Turan, $t \to cg$, $c\gamma$, cZ in the left-right supersymmetric model. Phys. Rev. D 72, 035008 (2005). arXiv:hep-ph/0506197.

21. G. Eilam, M. Frank, I. Turan, Single top production via gluon fusion at LHC. Phys. Rev. D 74, 035012 (2006). arXiv:hep-ph/0601253.

22. J.J. Cao, G. Eilam, M. Frank, K. Hikasa, G.L. Liu, I. Turan, J.M. Yang, SUSY-induced FCNC top-quark processes at the large hadron collider. Phys. Rev. D 75, 075021 (2007). arXiv:hep-ph/0702264.

23. Z.-X. Heng, G.-R. Lu, L. Wu, J.M. Yang, Top quark three-body decays in R-violating MSSM. Phys. Rev. D 79, 094029 (2009). arXiv:0904.0597.

24. J. Cao, C. Han, L. Wu, J.M. Yang, M. Zhang, SUSY induced top quark FCNC decay $t \to ch$ after Run I of LHC. Eur. Phys. J. C 74(9), 3058 (2014). arXiv:1404.1241.

25. A. Dedes, M. Paraskevas, J. Rosiek, K. Suxho, K. Tamvakis, Rare top-quark decays to Higgs boson in MSSM. JHEP 11, 137 (2014). arXiv:1409.6546.

26. G. Eilam, B. Haeri, A. Soni, Flavor changing Higgs transitions. Phys. Rev. D 41, 875 (1990).

27. J.A. Aguilar-Saavedra, B.M. Nobre, Rare top decays $t \to c\gamma$, $t \to cg$ and CKM unitarity. Phys. Lett. B 553, 251–260 (2003). arXiv:hep-ph/0210360.

28. J. Han, B. Li, X. Wang, Top quark rare three-body decays in the littlest Higgs model with T-parity. Phys. Rev. D 83, 034032 (2011). arXiv:1102.4402.

29. T.-J. Gao, T.-F. Feng, J.-B. Chen, $t \to c\gamma$ and $t \to cg$ in warped extra dimensions. JHEP 02, 029 (2013). arXiv:1303.0082.

30. U.K. Dey, T. Jha, Rare top decays in minimal and nonminimal universal extra dimension models. Phys. Rev. D **94**(5), 056011 (2016). arXiv:1602.03286.

31. A. Diaz-Furlong, M. Frank, N. Pourtolami, M. Toharia, R. Xoxocotzi, Flavor-changing decays of the top quark in 5D warped models. Phys. Rev. D **94**(3), 036001 (2016). arXiv:1603.08929

32. C.-W. Chiang, U.K. Dey, T. Jha, $t \to cg$ and $t \to cZ$ in universal extra-dimensional models. Eur. Phys. J. Plus **134**(5), 210 (2019). arXiv:1807.01481

33. W. Altmannshofer, B. Maddock, D. Tuckler, Rare top decays as probes of flavorful Higgs bosons. Phys. Rev. D **100**(1), 015003 (2019). arXiv:1904.10956

34. Y. Liu, B. Yan, R. Zhang, Loop induced top quark FCNC through top quark and dark matter interactions. arXiv:2103.07859

35. J.A. Aguilar-Saavedra, Top flavor-changing neutral interactions: theoretical expectations and experimental detection. Acta Phys. Polon. B 35, 2695–2710 (2004). arXiv:hep-ph/0409342.

36. Top Quark Working Group Collaboration, K. Agashe et al., Working group report: top quark, in community summer study 2013: snowmass on the Mississippi, 11, 2013. arXiv:1311.2028

37. J.L. Diaz-Cruz, M.A. Perez, G. Tavares-Velasco, J.J. Toscano, Testing flavor changing neutral currents in the rare top quark decays $t \to c$ V(i) V(j). Phys. Rev. D 60, 115014 (1999). arXiv:hep-ph/9903299.

38. A. Cordero-Cid, J.M. Hernandez, G. Tavares-Velasco, J.J. Toscano, Rare top quark decay $t \to u_1\bar{u}_2u_2$ in the standard model. Phys. Rev. D 73, 094005 (2006). arXiv:hep-ph/0411188.

39. G. Eilam, M. Frank, I. Turan, Rare decay of the top $t \to cgg$ in the standard model. Phys. Rev. D 73, 053011 (2006). arXiv:hep-ph/0601151.

40. W.-S. Hou, QCD induced charmless B decays. Nucl. Phys. B 308, 561–588 (1988).

41. J. Liu, Y.-P. Yao, An extension of the low-energy theorem and its implications on the decay $b \to sgg$ in the standard model. Phys. Rev. D 41, 2147–2159 (1990).

42. H. Simma, D. Wyler, Hadronic rare B decays: the case $b \to sgg$. Nucl. Phys. B 344, 283–316 (1990).

43. W.-S. Hou, A. Soni, H. Steger, Charmless decays of bottom mesons and a fourth generation. Phys. Rev. Lett. 59, 1521 (1987).

44. W.-S. Hou, R.G. Stuart, Higher order dominance in the standard model. Phys. Lett. B 242, 467–473 (1990).

45. C. Greub, P. Liniger, Calculation of next-to-leading QCD corrections to $b \to sg$. Phys. Rev. D 63, 054025 (2001). arXiv:hep-ph/0009144.

46. C. Greub, T. Hurth, M. Misiak, D. Wyler, The $c \to u\gamma$ contribution to weak radiative charm decay. Phys. Lett. B 382, 415–420 (1996). arXiv:hep-ph/9603417.

47. T.D. Lee, A theory of spontaneous T violation. Phys. Rev. D 8, 1226–1239 (1973).

48. J.F. Gunion, H.E. Haber, G.L. Kane, S. Dawson, The Higgs hunter's guide, Front. Phys. **80** (2000)

49. G.C. Branco, P.M. Ferreira, L. Lavoura, M.N. Rebelo, M. Sher, J.P. Silva, Theory and phenomenology of two-Higgs-doublet models. Phys. Rep. 516, 1–102 (2012). arXiv:1106.0034.

50. S.L. Glashow, S. Weinberg, Natural conservation laws for neutral currents. Phys. Rev. D 15, 1958 (1977).

51. A. Pich, P. Tuzon, Yukawa alignment in the two-Higgs-doublet model. Phys. Rev. D 80, 091702 (2009). arXiv:0908.1554.

52. N. Cabibbo, Unitary symmetry and leptonic decays. Phys. Rev. Lett. 10, 531–533 (1963).

53. M. Kobayashi, T. Maskawa, CP violation in the renormalizable theory of weak interaction. Prog. Theor. Phys. 49, 652–657 (1973).

54. P.M. Ferreira, L. Lavoura, J.P. Silva, Renormalization-group constraints on Yukawa alignment in multi-Higgs-doublet models. Phys. Lett. B 688, 341–344 (2010). arXiv:1001.2561.

55. J. Bijnens, J. Lu, J. Rathsman, Constraining general two Higgs doublet models by the evolution of Yukawa couplings. JHEP 05, 118 (2012). arXiv:1111.5760.

56. P. Ferreira, H.E. Haber, E. Santos, Preserving the validity of the Two-Higgs Doublet Model up to the Planck scale. Phys. Rev. D **92**, 033003 (2015). arXiv:1505.04001 [Erratum: Phys. Rev. D 94, 059903 (2016)]

57. F.J. Botella, G.C. Branco, A.M. Coutinho, M.N. Rebelo, J.I. Silva-Marcos, Natural quasi-alignment with two Higgs doublets and RGE stability. Eur. Phys. J. C **75**, 286 (2015). arXiv:1501.07435

58. A. Peñuelas, A. Pich, Flavour alignment in multi-Higgs-doublet models. JHEP 12, 084 (2017). arXiv:1710.02040.

59. S. Gori, H.E. Haber, E. Santos, High scale flavor alignment in two-Higgs doublet models and its phenomenology. JHEP **06**, 110 (2017). arXiv:1703.05873

60. M. Jung, A. Pich, P. Tuzon, Charged-Higgs phenomenology in the Aligned two-Higgs-doublet model. JHEP 11, 003 (2010). arXiv:1006.0470.

61. M. Jung, A. Pich, P. Tuzon, The $B \to X_s \gamma$ Rate and CP asymmetry within the aligned two-Higgs-doublet model. Phys. Rev. D 83, 074011 (2011). arXiv:1011.5154.

62. M. Jung, X.-Q. Li, A. Pich, Exclusive radiative B-meson decays within the aligned two-Higgs-doublet model. JHEP 10, 063 (2012). arXiv:1208.1251.

63. Q. Chang, P.-F. Li, X.-Q. Li, B_s^0 - $\bar{B}_s^0$ mixing within minimal flavor-violating two-Higgs-doublet models. Eur. Phys. J. C **75**(12), 594 (2015). arXiv:1505.03650

64. N. Cho, X.-Q. Li, F. Su, X. Zhang, $K^0 - \overline{K}^0$ mixing in the minimal flavor-violating two-Higgs-doublet models. Adv. High Energy Phys. **2017**, 2863647 (2017). arXiv:1705.07638

65. G. Cree, H.E. Logan, Yukawa alignment from natural flavor conservation. Phys. Rev. D 84, 055021 (2011). arXiv:1106.4039.

66. A. Celis, M. Jung, X.-Q. Li, A. Pich, Sensitivity to charged scalars in $B \to D^{(*)}\tau\nu_\tau$ and $B \to \tau\nu_\tau$ decays. JHEP 01, 054 (2013). arXiv:1210.8443.

67. X.-Q. Li, J. Lu, A. Pich, $B_{s,d}^0 \to \ell^+\ell^-$ decays in the aligned two-Higgs-doublet model. JHEP 06, 022 (2014). arXiv:1404.5865.

68. T. Enomoto, R. Watanabe, Flavor constraints on the two Higgs doublet models of Z_2 symmetric and aligned types. JHEP **05**, 002 (2016). arXiv:1511.05066

69. L. Wang, J.M. Yang, Y. Zhang, Probing a pseudoscalar at the LHC in light of $R(D^{(*)})$ and muon g-2 excesses. Nucl. Phys. B 924, 47–62 (2017).

70. Q.-Y. Hu, X.-Q. Li, Y.-D. Yang, $B^0 \to K^{*0}\mu^+\mu^-$ decay in the aligned two-Higgs-doublet model. Eur. Phys. J. C **77**(3), 190 (2017). arXiv:1612.08867

71. Q.-Y. Hu, X.-Q. Li, Y.-D. Yang, The $\Lambda_b \to \Lambda(\to p\pi^-)\mu^+\mu^-$ decay in the aligned two-Higgs-doublet model. Eur. Phys. J. C **77**(4), 228 (2017). arXiv:1701.04029

72. P. Arnan, D. Bečirević, F. Mescia, O. Sumensari, Two Higgs doublet models and $b \to s$ exclusive decays. Eur. Phys. J. C **77**(11), 796 (2017). arXiv:1703.03426

73. L. Delle Rose, S. Khalil, S.J.D. King, S. Moretti, R_K and R_{K^*} in an aligned 2HDM with right-handed neutrinos. Phys. Rev. D **101**(11), 115009 (2020). arXiv:1903.11146

74. S.-W. Wang, Probing the effects of some new physics models in $B_s \to D_s\tau\bar{\nu}$ decay. Nucl. Phys. B 954, 114997 (2020).

75. O. Eberhardt, A.P. Martnez, A. Pich, Global fits in the aligned two-Higgs-doublet model. JHEP **05**, 005 (2021). arXiv:2012.09200

76. W. Dekens, J. de Vries, J. Bsaisou, W. Bernreuther, C. Hanhart, U.-G. Meißner, A. Nogga, A. Wirzba, Unraveling models of CP violation through electric dipole moments of light nuclei. JHEP 07, 069 (2014). arXiv:1404.6082.

77. M. Jung, A. Pich, Electric dipole moments in two-Higgs-doublet models. JHEP 04, 076 (2014). arXiv:1308.6283.

78. H. Gisbert, J. Ruiz Vidal, Improved bounds on heavy quark electric dipole moments. Phys. Rev. D **101**(11), 115010 (2020). arXiv:1905.02513

79. K. Enomoto, S. Kanemura, Y. Mura, Electroweak baryogenesis in aligned two Higgs doublet models. JHEP **01**, 104 (2022). arXiv:2111.13079

80. T. Han, S.K. Kang, J. Sayre, Muon $g-2$ in the aligned two Higgs doublet model. JHEP **02**, 097 (2016). arXiv:1511.05162

81. V. Ilisie, New Barr–Zee contributions to $(g-2)_\mu$ in two-Higgs-doublet models. JHEP **04**, 077 (2015). arXiv:1502.04199

82. X.-F. Han, L. Wang, J.M. Yang, An extension of two-Higgs-doublet model and the excesses of 750 GeV diphoton, muon g-2 and $h \to \mu\tau$. Phys. Lett. B **757**, 537–547 (2016). arXiv:1601.04954

83. A. Cherchiglia, P. Kneschke, D. Stöckinger, H. Stöckinger-Kim, The muon magnetic moment in the 2HDM: complete two-loop result. JHEP **01**, 007 (2017). arXiv:1607.06292 [Erratum: JHEP 10, 242 (2021)]

84. A. Cherchiglia, D. Stöckinger, H. Stöckinger-Kim, Muon g-2 in the 2HDM: maximum results and detailed phenomenology. Phys. Rev. D **98**, 035001 (2018). arXiv:1711.11567

85. L. DelleRose, S. Khalil, S. Moretti, Explaining electron and muon $g - 2$ anomalies in an aligned 2-Higgs doublet model with right-handed neutrinos. Phys. Lett. B **816**, 136216 (2021). arXiv:2012.06911

86. M. Carena, S. Gori, A. Juste, A. Menon, C.E.M. Wagner, L.-T. Wang, LHC discovery potential for non-standard Higgs bosons in the 3b channel. JHEP 07, 091 (2012). arXiv:1203.1041.

87. W. Altmannshofer, S. Gori, G.D. Kribs, A minimal flavor violating 2HDM at the LHC. Phys. Rev. D 86, 115009 (2012). arXiv:1210.2465.

88. Y. Bai, V. Barger, L.L. Everett, G. Shaughnessy, General two Higgs doublet model (2HDM-G) and Large Hadron Collider data. Phys. Rev. D 87, 115013 (2013). arXiv:1210.4922.

89. V. Barger, L.L. Everett, H.E. Logan, G. Shaughnessy, Scrutinizing the 125 GeV Higgs boson in two Higgs doublet models at the LHC, ILC, and Muon Collider. Phys. Rev. D 88(11), 115003 (2013). arXiv:1308.0052.

90. D. López-Val, T. Plehn, M. Rauch, Measuring extended Higgs sectors as a consistent free couplings model. JHEP 10, 134 (2013). arXiv:1308.1979.

91. L. Wang, X.-F. Han, Status of the aligned two-Higgs-doublet model confronted with the Higgs data. JHEP 04, 128 (2014). arXiv:1312.4759.

92. A. Celis, V. Ilisie, A. Pich, LHC constraints on two-Higgs doublet models. JHEP 07, 053 (2013). arXiv:1302.4022.

93. A. Celis, V. Ilisie, A. Pich, Towards a general analysis of LHC data within two-Higgs-doublet models. JHEP 12, 095 (2013). arXiv:1310.7941.

94. L. Duarte, G.A. González-Sprinberg, J. Vidal, Top quark anomalous tensor couplings in the two-Higgs-doublet models. JHEP 11, 114 (2013). arXiv:1308.3652.

95. V. Ilisie, A. Pich, Low-mass fermiophobic charged Higgs phenomenology in two-Higgs-doublet models. JHEP 09, 089 (2014). arXiv:1405.6639.

96. S. Berge, W. Bernreuther, S. Kirchner, Prospects of constraining the Higgs boson's CP nature in the tau decay channel at the LHC. Phys. Rev. D 92, 096012 (2015). arXiv:1510.03850

97. L. Wang, S. Yang, X.-F. Han, $h \to \mu\tau$ and muon g-2 in the alignment limit of two-Higgs-doublet model. Nucl. Phys. B **919**, 123–141 (2017). arXiv:1606.04408

98. C. Ayala, G.A. González-Sprinberg, R. Martinez, J. Vidal, The top right coupling in the aligned two-Higgs-doublet model. JHEP **03**, 128 (2017). arXiv:1611.07756

99. G. Abbas, D. Das, M. Patra, Loop induced $H^\pm \to W^\pm Z$ decays in the aligned two-Higgs-doublet model. Phys. Rev. D **98**(11), 115013 (2018). arXiv:1806.11035

100. S. Kanemura, M. Kubota, K. Yagyu, Testing aligned CP-violating Higgs sector at future lepton colliders. JHEP **04**, 144 (2021). arXiv:2101.03702

101. V. Ilisie, Fingerprinting the presence of extra scalars in the $h \to Vff'$ forward–backward asymmetry. arXiv:2103.04444

102. ATLAS Collaboration, G. Aad et al., Search for single top-quark production via flavour-changing neutral currents at 8 TeV with the ATLAS detector. Eur. Phys. J. C **76**(2), 55 (2016). arXiv:1509.00294

103. C.M.S. Collaboration, V. Khachatryan et al., Search for anomalous Wtb couplings and flavour-changing neutral currents in t-

channel single top quark production in pp collisions at $\sqrt{s} = 7$ and 8 TeV. JHEP **02**, 028 (2017). arXiv:1610.03545

104. P. Azzi et al., Report from working group 1: standard model physics at the HL-LHC and HE-LHC. CERN Yellow Rep. Monogr. **7**, 1–220 (2019). arXiv:1902.04070

105. M. Cepeda et al., Report from working group 2: Higgs physics at the HL-LHC and HE-LHC. CERN Yellow Rep. Monogr. **7**, 221–584 (2019). arXiv:1902.00134

106. X. Cid Vidal et al., Report from working group 3: beyond the standard model physics at the HL-LHC and HE-LHC. CERN Yellow Rep. Monogr. **7**, 585–865 (2019). arXiv:1812.07831

107. A. Cerri et al., Report from working group 4: opportunities in flavour physics at the HL-LHC and HE-LHC. CERN Yellow Rep. Monogr. **7**, 867–1158 (2019). arXiv:1812.07638

108. ATLAS, CMS Collaboration, Report on the physics at the HL-LHC, and perspectives for the HE-LHC: Collection of notes from ATLAS and CMS. CERN Yellow Rep. Monogr. **7** (2019). arXiv:1902.10229

109. FCC Collaboration, A. Abada et al., FCC physics opportunities: future circular collider conceptual design report volume 1. Eur. Phys. J. C **79**(6), 474 (2019).

110. F.C.C. Collaboration, A. Abada et al., FCC-ee: The lepton collider: future circular collider conceptual design report volume 2. Eur. Phys. J. ST **228**(2), 261–623 (2019).

111. F.C.C. Collaboration, A. Abada et al., FCC-hh: the hadron collider: future circular collider conceptual design report volume 3. Eur. Phys. J. ST **228**(4), 755–1107 (2019).

112. F.C.C. Collaboration, A. Abada et al., HE-LHC: the high-energy large hadron collider: future circular collider conceptual design report volume 4. Eur. Phys. J. ST **228**(5), 1109–1382 (2019).

113. K.Y. Oyulmaz, A. Senol, H. Denizli, O. Cakir, Top quark anomalous FCNC production via tqg couplings at FCC-hh. Phys. Rev. D **99**(11), 115023 (2019). arXiv:1902.03037

114. H. Khanpour, Probing top quark FCNC couplings in the triple-top signal at the high energy LHC and future circular collider. Nucl. Phys. B **958**, 115141 (2020). arXiv:1909.03998

115. I.F. Ginzburg, M. Krawczyk, Symmetries of two Higgs doublet model and CP violation. Phys. Rev. D **72**, 115013 (2005). arXiv:hep-ph/0408011.

116. S. Davidson, H.E. Haber, Basis-independent methods for the two-Higgs-doublet model. Phys. Rev. D **72**, 035004 (2005). arXiv:hep-ph/0504050 [Erratum: Phys. Rev. D 72, 099902 (2005)]

117. H.E. Haber, D. O'Neil, Basis-independent methods for the two-Higgs-doublet model. II. The Significance of tanβ. Phys. Rev. D **74**, 015018 (2006). arXiv:hep-ph/0602242 [Erratum: Phys. Rev. D 74, no. 5, 059905 (2006)]

118. H.E. Haber, D. O'Neil, Basis-independent methods for the two-Higgs-doublet model III: the CP-conserving limit, custodial symmetry, and the oblique parameters S, T, U. Phys. Rev. D **83**, 055017 (2011). arXiv:1011.6188.

119. F.J. Botella, J.P. Silva, Jarlskog–like invariants for theories with scalars and fermions. Phys. Rev. D **51**, 3870–3875 (1995). arXiv:hep-ph/9411288.

120. D. O'Neil, Phenomenology of the basis-independent CP-violating two-Higgs doublet model [Dissertation]. Ph.D. thesis, UC, Santa Cruz, Phys. Dept., 6, 2009. arXiv:0908.1363

121. M. Jezabek, J.H. Kuhn, QCD corrections to semileptonic decays of heavy quarks. Nucl. Phys. B **314**, 1–6 (1989).

122. A. Czarnecki, QCD corrections to the decay $t \to Wb$ in dimensional regularization. Phys. Lett. B **252**, 467–470 (1990).

123. C.S. Li, R.J. Oakes, T.C. Yuan, QCD corrections to $t \to W^+b$. Phys. Rev. D **43**, 3759–3762 (1991).

124. A. Denner, T. Sack, The top width. Nucl. Phys. B **358**, 46–58 (1991).

125. G. Eilam, R.R. Mendel, R. Migneron, A. Soni, Radiative corrections to top quark decay. Phys. Rev. Lett. 66, 3105–3108 (1991).

126. M. Brucherseifer, F. Caola, K. Melnikov, $\mathcal{O}(\alpha_s^2)$ corrections to fully-differential top quark decays. JHEP 04, 059 (2013). arXiv:1301.7133.

127. J. Gao, C.S. Li, H.X. Zhu, Top quark decay at next-to-next-to leading order in QCD. Phys. Rev. Lett. 110(4), 042001 (2013). arXiv:1210.2808.

128. I.R. Blokland, A. Czarnecki, M. Slusarczyk, F. Tkachov, Heavy to light decays with a two loop accuracy. Phys. Rev. Lett. 93, 062001 (2004). arXiv:hep-ph/0403221.

129. K.G. Chetyrkin, R. Harlander, T. Seidensticker, M. Steinhauser, Second order QCD corrections to $\Gamma(t \to Wb)$. Phys. Rev. D 60, 114015 (1999). arXiv:hep-ph/9906273.

130. A. Czarnecki, K. Melnikov, Two loop QCD corrections to top quark width. Nucl. Phys. B 544, 520–531 (1999). arXiv:hep-ph/9806244.

131. N.D. Christensen, C. Duhr, FeynRules–Feynman rules made easy. Comput. Phys. Commun. 180, 1614–1641 (2009). arXiv:0806.4194.

132. A. Alloul, N.D. Christensen, C. Degrande, C. Duhr, B. Fuks, FeynRules 2.0—a complete toolbox for tree-level phenomenology. Comput. Phys. Commun. **185**, 2250–2300 (2014). arXiv:1310.1921

133. J. Kublbeck, M. Bohm, A. Denner, Feyn Arts: computer algebraic generation of Feynman graphs and amplitudes. Comput. Phys. Commun. 60, 165–180 (1990).

134. T. Hahn, Generating Feynman diagrams and amplitudes with FeynArts 3. Comput. Phys. Commun. 140, 418–431 (2001). arXiv:hep-ph/0012260.

135. T. Hahn, M. Perez-Victoria, Automatized one loop calculations in four-dimensions and D-dimensions. Comput. Phys. Commun. 118, 153–165 (1999). arXiv:hep-ph/9807565.

136. T. Hahn, Loop calculations with FeynArts, FormCalc, and LoopTools. Acta Phys. Polon. B 30, 3469–3475 (1999). arXiv:hep-ph/9910227.

137. R. Mertig, M. Bohm, A. Denner, FEYN CALC: computer algebraic calculation of Feynman amplitudes. Comput. Phys. Commun. 64, 345–359 (1991).

138. V. Shtabovenko, R. Mertig, F. Orellana, New developments in FeynCalc 9.0. Comput. Phys. Commun. **207**, 432–444 (2016). arXiv:1601.01167

139. V. Shtabovenko, R. Mertig, F. Orellana, FeynCalc 9.3: new features and improvements. Comput. Phys. Commun. **256**, 107478 (2020). arXiv:2001.04407

140. G. 't Hooft, M.J.G. Veltman, Regularization and renormalization of gauge fields. Nucl. Phys. B **44**, 189–213 (1972)

141. C.G. Bollini, J.J. Giambiagi, Dimensional renormalization: the number of dimensions as a regularizing parameter. Nuovo Cim. B 12, 20–26 (1972).

142. G.M. Cicuta, E. Montaldi, Analytic renormalization via continuous space dimension. Lett. Nuovo Cim. 4, 329–332 (1972).

143. J.F. Ashmore, A method of gauge invariant regularization. Lett. Nuovo Cim. 4, 289–290 (1972).

144. T. Kinoshita, Mass singularities of Feynman amplitudes. J. Math. Phys. 3, 650–677 (1962).

145. T.D. Lee, M. Nauenberg, Degenerate systems and mass singularities. Phys. Rev. 133, B1549–B1562 (1964).

146. H.E. Logan, U. Nierste, $B_{s,d} \to \ell^+\ell^-$ in a two Higgs doublet model. Nucl. Phys. B 586, 39–55 (2000). arXiv:hep-ph/0004139.

147. A. Denner, S. Dittmaier, Electroweak radiative corrections for collider physics. Phys. Rep. **864**, 1–163 (2020). arXiv:1912.06823

148. A. Denner, Techniques for calculation of electroweak radiative corrections at the one loop level and results for W physics at LEP-200. Fortsch. Phys. 41, 307–420 (1993). [arXiv:0709.1075].

149. G. 't Hooft, M.J.G. Veltman, Scalar one loop integrals. Nucl. Phys. B **153**, 365–401 (1979)
150. G. Passarino, M.J.G. Veltman, One loop corrections for e+ e-annihilation into mu+ mu- in the Weinberg model. Nucl. Phys. B 160, 151–207 (1979).
151. Particle Data Group Collaboration, P. Zyla et al., Review of particle physics. PTEP **2020**(8) 083C01 (2020) and 2021 update
152. L. Wolfenstein, Parametrization of the Kobayashi-Maskawa matrix. Phys. Rev. Lett. 51, 1945 (1983).
153. A.J. Buras, M.E. Lautenbacher, G. Ostermaier, Waiting for the top quark mass, $K^+ \rightarrow \pi^+ \nu \bar{\nu}$, $B_s^0 - \bar{B}_s^0$ mixing and CP asymmetries in B decays. Phys. Rev. D 50, 3433–3446 (1994). arXiv:hep-ph/9403384.
154. K.G. Chetyrkin, J.H. Kuhn, M. Steinhauser, RunDec: a mathematica package for running and decoupling of the strong coupling and quark masses. Comput. Phys. Commun. 133, 43–65 (2000). arXiv:hep-ph/0004189.
155. F. Herren, M. Steinhauser, Version 3 of RunDec and CRunDec. Comput. Phys. Commun. **224**, 333–345 (2018). arXiv:1703.03751
156. ALEPH, DELPHI, L3, OPAL, LEP Collaboration, G. Abbiendi et al., Search for charged Higgs bosons: combined results using LEP data. Eur. Phys. J. C **73**, 2463 (2013). arXiv:1301.6065
157. ATLAS Collaboration, M. Aaboud et al., Search for charged Higgs bosons decaying via $H^\pm \rightarrow \tau^\pm \nu_\tau$ in the τ+jets and τ+lepton final states with 36 fb^{-1} of pp collision data recorded at $\sqrt{s} = 13$ TeV with the ATLAS . JHEP **09**, 139 (2018). arXiv:1807.07915
158. ATLAS Collaboration, G. Aad et al., Search for charged Higgs bosons decaying into a top quark and a bottom quark at $\sqrt{s}$ = 13 TeV with the ATLAS detector. JHEP **06**, 145 (2021). arXiv:2102.10076
159. C.M.S. Collaboration, A.M. Sirunyan et al., Search for charged Higgs bosons in the H$^\pm \rightarrow \tau^\pm \nu_\tau$ decay channel in proton–proton collisions at $\sqrt{s} = 13$ TeV. JHEP **07**, 142 (2019). arXiv:1903.04560
160. C.M.S. Collaboration, A.M. Sirunyan et al., Search for a charged Higgs boson decaying into top and bottom quarks in events with electrons or muons in proton-proton collisions at $\sqrt{s} = 13$ TeV. JHEP **01**, 096 (2020). arXiv:1908.09206
161. A.G. Akeroyd et al., Prospects for charged Higgs searches at the LHC. Eur. Phys. J. C **77**(5), 276 (2017). arXiv:1607.01320
162. A. Arbey, F. Mahmoudi, O. Stal, T. Stefaniak, Status of the charged Higgs boson in two Higgs doublet models. Eur. Phys. J. C **78**(3), 182 (2018). arXiv:1706.07414
163. D. Chowdhury, O. Eberhardt, Update of global two-Higgs-doublet model fits. JHEP **05**, 161 (2018). arXiv:1711.02095
164. J. Haller, A. Hoecker, R. Kogler, K. Mönig, T. Peiffer, J. Stelzer, Update of the global electroweak fit and constraints on two-Higgs-doublet models. Eur. Phys. J. C **78**(8), 675 (2018). arXiv:1803.01853
165. M. Misiak, A. Rehman, M. Steinhauser, Towards $\bar{B} \rightarrow X_s \gamma$ at the NNLO in QCD without interpolation in m$_c$. JHEP **06**, 175 (2020). arXiv:2002.01548
166. O. Atkinson, M. Black, A. Lenz, A. Rusov, J. Wynne, Cornering the two Higgs doublet model type II. arXiv:2107.05650
167. T. Hermann, M. Misiak, M. Steinhauser, $\bar{B} \rightarrow X_s \gamma$ in the two Higgs doublet model up to next-to-next-to-leading order in QCD. JHEP 11, 036 (2012). arXiv:1208.2788.